UDK 66:54(05) CODEN HMIDA 8 ISSN 0367–598X

4

Hemijska industrija

Vol. 76

Časopis Saveza hemijskih inženjera Srbije

Chemical Industry

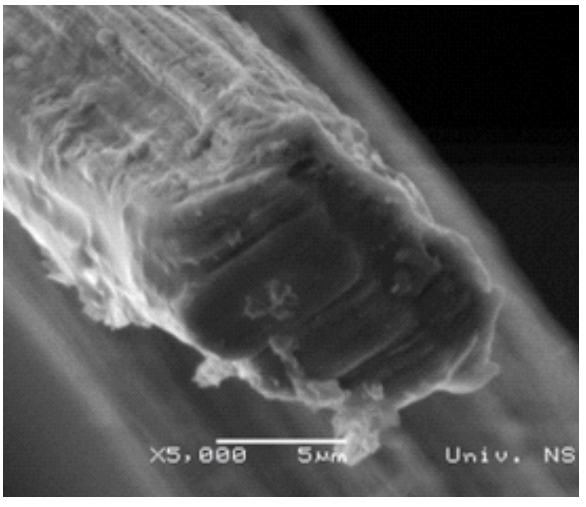

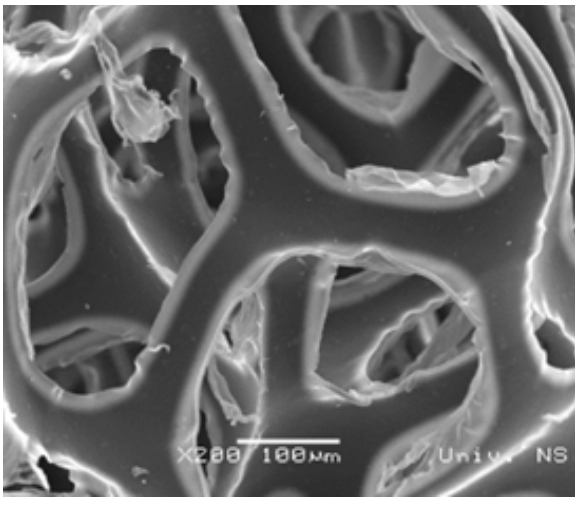

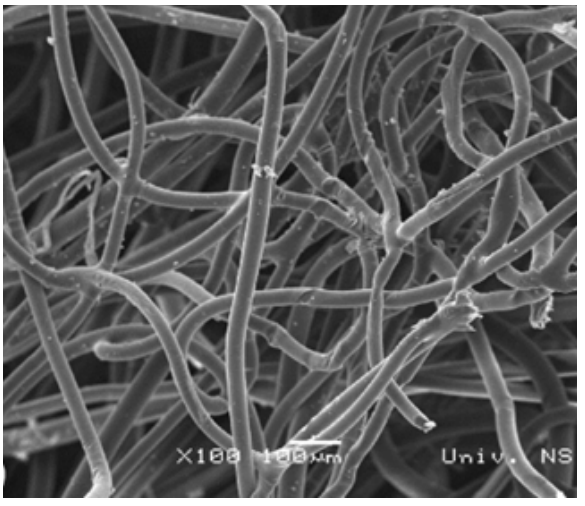

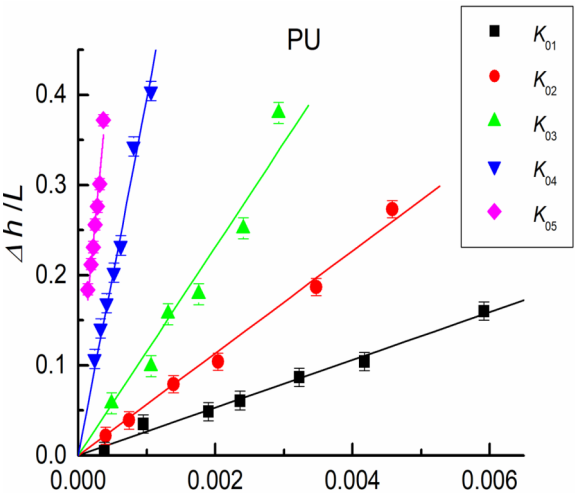

BEOGRAD, JULI-DECEMBAR 2022. HMIDA 8, 76 (4) 183-269 (2022)

Aktivnosti Saveza hemijskih inženjera Srbije pomažu:

**MINISTARSTVO NAUKE,
TEHNOLOŠKOG RAZVOJA
I INOVACIJA
REPUBLIKE SRBIJE**

Tehnološko-metalurški fakultet
Univerziteta u Beogradu

Prirodno-matematički fakultet
Univerziteta u Novom Sadu

Institut za tehnologiju nuklearnih i
drugih mineralnih sirovina, Beograd

Tehnološki fakultet
Univerziteta u Novom Sadu

Institut za hemiju, tehnologiju i metalurgiju
Univerziteta u Beogradu

Fakultet tehničkih nauka
Univerziteta u Novom Sadu

Tehnološki fakultet
Univerziteta u Nišu, Leskovac

Fakultet tehničkih nauka
Univerziteta u Prištini
Kosovska Mitrovica

Institut IMS, Beograd

DCP HEMIGAL
Leskovac

Elixir Prahovo

Chemical Industry
Химическая промышленность

Hemijska industrija

Časopis Saveza hemijskih inženjera Srbije
Journal of the Association of Chemical Engineers of Serbia
Журнал Союза химических инженеров Сербии

VOL. 76 **Beograd, juli-decembar 2022.** **Broj 4**

Izdavač
Savez hemijskih inženjera Srbije
Beograd, Kneza Miloša 9/I

Glavni urednik
Bojana Obradović

Zamenica glavnog i odgovornog urednika
Emila Živković

Pomoćnik glavnog i odgovornog urednika
Ivana Drvenica

Urednici
Jelena Bajat, Dejan Bezbradica, Ivana Banković-Ilić, Dušan Mijin, Marija Nikolić, Đorđe Veljović, Tatjana Volkov-Husović

Članovi uredništva
Nikolaj Ostrovski, Milorad Cakić, Željko Čupić, Miodrag Lazić, Slobodan Petrović, Milovan Purenović, Aleksandar Spasić, Dragoslav Stoiljković, Radmila Šećerov-Sokolović, Slobodan Šerbanović, Nikola Nikačević, Svetomir Milojević

Članovi uredništva iz inostranstva
Dragomir Bukur (SAD), Jiri Hanika (Češka Republika), Valerij Meshalkin (Rusija), Ljubiša Radović (SAD), Constantinos Vayenas (Grčka)

Likovno-grafičko rešenje naslovne strane
Milan Jovanović

Redakcija
11000 Beograd, Kneza Miloša 9/I
Tel/fax: 011/3240-018
E-pošta: shi@ache.org.rs
www.ache.org.rs

Izlazi kvartalno, rukopisi se ne vraćaju

Za izdavača: Ivana T. Drvenica

Sekretar redakcije: Slavica Desnica

Izdavanje časopisa pomaže
Republika Srbija, Ministarstvo nauke, tehnološkog razvoja i inovacija

Uplata pretplate i oglasnog prostora vrši se na tekući račun Saveza hemijskih inženjera Srbije, Beograd, broj 205-2172-71, Komercijalna banka a.d., Beograd

Menadžer časopisa i kompjuterska priprema
Aleksandar Dekanski

Štampa
Razvojno-istraživački centar grafičkog inženjerstva, Tehnološko-metalurški fakultet, Univerzitet u Beogradu, Karnegijeva 4, 11000 Beograd

Indeksiranje
Radovi koji se publikuju u časopisu *Hemijska Industrija* ideksiraju se preko *Thompson Reuters Scietific®* servisa *Science Citation Index - Expanded™* i *Journal Citation Report (JCR)*

SADRŽAJ/CONTENTS

Development of an analytical model for copper heap leaching from secondary sulfides in chloride media in an industrial environment

Manuel Saldaña[1,2], Eleazar Salinas-Rodríguez[3], Jonathan Castillo[4], Felipe Peña-Graf[5] and Francisca Roldán[6]

[1]*Faculty of Engineering and Architecture, Universidad Arturo Prat, Iquique 1110939, Chile*
[2]*Departamento de Ingeniería Química y Procesos de Minerales, Facultad de Ingeniería, Universidad de Antofagasta, Antofagasta 1240000, Chile*
[3]*Área Académica de Ciencias de la Tierra y Materiales, Universidad Autónoma del Estado de Hidalgo, Carretera Pachuca—Tulancingo km. 4.5, C.P. 42184, Mineral de la Reforma, Hidalgo C.P. 42184, Mexico*
[4]*Departamento de Ingeniería en Metalurgia, Universidad de Atacama, Copiapó 1531772, Chile*
[5]*Escuela de Ingeniería, Universidad Católica del Norte, Coquimbo 1531772, Chile*
[6]*Centro de Investigación para la Gestión Integrada del Riesgo de Desastres (CIGIDEN), Departamento de Ciencias Geológicas. Universidad Católica del Norte (UCN), Antofagasta, Chile*

Abstract

In multivariate analysis, a predictive model is a mathematical/statistical model that relates a set of independent variables to dependent or response variable(s). This work presents a descriptive model that explains copper recovery from secondary sulfide minerals (chalcocite) taking into account the effects of time, heap height, superficial velocity of leaching flow, chloride concentration, particle size, porosity, and effective diffusivity of the solute within particle pores. Copper recovery is then modelled by a system of first-order differential equations. The results indicated that the heap height and superficial velocity of leaching flow are the most critical independent variables while the others are less influential under operational conditions applied. In the present study representative adjustment parameters are obtained, so that the model could be used to explore copper recovery in chloride media as a part of the extended value chain of the copper sulfides processing.

Keywords: copper extraction, phenomenological modeling, chloride leaching, modelling, hydrometallurgy.

Available on-line at the Journal web address: http://www.ache.org.rs/HI/

TECHNICAL PAPER

UDC: 669.3.053: 549.331.21:303.094

Hem. Ind. **76(4)** 183-195 (2022)

1. INTRODUCTION

Copper mining is an industry in constant growth [1]. Currently, 19.7 million tons of copper are produced world-wide [2], 75 % of which are processed by pyrometallurgical processes, while the rest is processed by hydrometallurgical routes [3–5]. Pyrometallurgical processes generate large environmental liabilities, such as tailings dams [6–8] produced by flotation processes, which can affect acid rains and increase local pollution [9,10]. Hydrometallurgical processes, together with copper bioleaching processes [11–13], have proven to be more environmentally friendly.

Leaching processes in recent years have been used to treat oxidized copper ores, being a useful technological alternative to treat low-medium grade ores [14–17]. However, oxides available for treatment are becoming scarce mainly due to overexploitation [18]. In Chile, for example, copper oxides that are processed by this route currently represent 30.8 % of the country's production and are projected to decline to 12 % of the production by 2027 [2]. Despite the problem, this option is currently being used not only for oxides, but also for secondary sulfides, especially low-grade minerals [19,20], or copper sulfide minerals [21–26], like chalcocite or covellite, ores that are processed in acidic environments with the addition of chlorides [27], found naturally in seawater. This resource has begun to be exploited in recent decades in Chilean mining [28], mainly due to the situation of water scarcity in the country. It is worth highlighting the rise in copper leaching in chloride media, finding applications, as stated in the literature, from processing of secondary copper sulfide minerals [22,23,29,30], to copper smelting slag leaching [31,32]. On the other hand, though

Corresponding authors: Manuel Saldaña, Faculty of Engineering and Architecture, Universidad Arturo Prat, Iquique 1110939, Chile; Tel. +56 9 5383 4174
E-mail: masaldana@unap.cl
Paper received: 14 February 2022; Paper accepted: 16 August; Paper published: 2 September 2022.
https://doi.org/10.2298/HEMIND220214015S

leaching of primary copper sulfides, such as chalcopyrite [33,34], is also possible, it is economically infeasible at industrial scale.

In line with the above, considerable pressure is currently exerted on water resources required for population, urban and economic growth [35]. Due to water scarcity and the lack of surface and subsurface water recharge, it has become a priority focus for decision makers in the world [36]. Chile, for its part, has 1,251 rivers, which are in 101 main basins of the country whose recharge comes mainly from rains. However, it is a country highly vulnerable to climate change [37]. Reports indicate that there is an increase in temperature [38–40], increase in wind intensity [38,41], appearance of flow-type landslides [42] and a decrease in rainfall [38,39,41]. Considering that a large part of the Chilean economy is based on the economic contribution of the mining sector [43] and flotation metallurgical processes being the ones that consume the most water in the country, promoting hydrometallurgy can help in this regard [44]. In turn, the mining nucleus of Chile is located in the Atacama Desert, characterized as the driest desert in the world. This extreme aridity is due to the fact that in the western regions there is a combination of the barrier effect of the high Andes Mountain Range, permanence of the Southeast Pacific anticyclone and the existence of the Humboldt Current-coastal upwelling system that prevents this region from receiving the moist Atlantic air masses. Its scant rainfall is due to climatic anomalies, the main one being the ocean-climatic anomaly ENSO (El Niño-Southem Oscillation) [45,46]. On the other hand, in the eastern highland regions, recharge is due to summer rainfall, fed by moisture of Amazonian origin, which became, in certain years, very abundant [45]. The groundwater recharge comes from precipitation, melting ice or lacustrine origin from the Andes Mountains and surrounding areas [47].

Mean annual rainfall in the Atacama Desert is less than 20 mm and has been a desert for 12000 ± 1000 years shifting between arid and hyper-arid periods [48]. Accordingly, fluvial run-off is minimal and erosion rates are extremely low ranging from 0.2 to 0.4 m Ma^{-1} [49]. Therefore, more environmentally friendly forms of copper extraction should be sought in Chilean mining, providing water reuse, such as hydrometallurgical processes used in the country today.

Leaching processes include several stages. First, the ore (chalcocite) is crushed until it reaches a size under 1 in [14]. Then, the crushed ore is transported to the pile, having a height between 4 to 10 m [50]. Finally, the ore is irrigated by a leaching solution distributed by sprinklers or drip emitters, flowing down through the heap by gravity [14]. At the end of the process, cupric ions are obtained together with other ions dissolved in the PLS (Pregnant Liquid Solution), which is deposited in leaching pools, and subsequently advanced to the solvent extraction stage [51].

In this work, an analytical model for estimation of copper recovery from chalcocite in the heap leaching process is derived. Creation of analytical models (theoretical and/or empirical) representing dynamics of mining processes such as heap leaching are of vital importance for study of the process performance at the operational level [52], since such models can support development, verification, testing and application of new specialized technologies related to process innovation, different modes of operation, or operational efficiency. This work presents the theoretical framework supporting the analytical model for copper recovery estimation, fundamentals of the uncertainty analysis and the model optimization process followed by application of the optimized analytical model, the uncertainty analysis, and discussion of the model results.

2. MATERIALS AND METHODS

2. 1. Chalcocite Heap Leaching

Heap leaching data at the operational level were recovered from a mine with the copper ore grade of 0.6 % approximately, located in the Antofagasta region, Chile. Samples of copper recovery were recorded for a period of two years approximately, in processes with different levels of the factors: heap height (300 - 840 cm), particle size (15 - 33 mm), porosity (1 -5.5), effective diffusivity of the solute within the particle pores (0.06 - 0.108 cm^2 day^{-1}), superficial velocity of leaching flow (9 - 54 cm day^{-1}) and chloride concentrations (20 - 50 g dm^{-3}).

2. 2. Analytical models for heap leaching

There are several copper recovery models in literature [53,54], while the analytical model used in this work is given by Eq. (1) [55–58], which is based on the hypothesis that the leaching process could be modelled by using a system of first-order differential equation (1).

$$\frac{\partial y}{\partial \tau} = -k_{\tau} e^{n_{\tau}} \tag{1}$$

where *y* is a dynamic quantity, such as concentration or recovery R_τ, k_τ is the kinetic constant and n_τ is the order of the reaction and τ represent a time scale that depends on the phenomenon to model. To solve Eq. (1), an initial condition is required, introducing a delay parameter ω. Then, the general solution for this problem is known, as $n_\tau = 1$, and the solution is given by the Eq. (2).

$$R_\tau = R_\tau^{\infty}(1 - e^{-k_\tau(\tau-\omega)}) \tag{2}$$

R_τ^{∞} is the maximum expected recovery depending on the experimental conditions, and ω is a factor of reaction delay (associated with the activation time; generally, this period is minimal or is considered as 0). Dixon and Hendrix [59–61] considered that the leaching process occurs at different scales of size and time with participation of different phenomena [58]. It is possible to represent these phenomena by using Eq. (2) in conjunction with expressions associated with the particle properties and the heap height in the leaching process. At the particle level τ (see Eq. 3), the authors considered that the process was dominated by the porosity ε_0 of the feeding material, the effective diffusivity of solute within the particle pores D_{Ae}, particle size (radius, *r*) and *t* is time.

$$\tau = \frac{D_{Ae} t}{\varepsilon_0 r^2} \tag{3}$$

At the bulk level θ, the authors considered that the heap is porous, formed by particles through which the leaching solution flows at a constant rate. Recovery can be defined based on the heap height as is presented in Eq. (4).

$$\theta = \frac{\mu_s t}{\varepsilon_b Z} \tag{4}$$

Where μ_s is the superficial velocity of the leaching flow, ε_b is the volumetric fraction of the leaching solution in the bed and *Z* is the pile height. Eq. (2) could be rewritten to include both dependences of the reaction.

Then, considering the evident proportional relation between the copper recovery from secondary sulfides and chloride concentration [20,26,27,62,63], the term δ^{ρ} is incorporated into the analytical model as factors of both scales, as shown in Equations (5) and (6). The term δ^{ρ_i} (chloride concentration, c_{Cl}) is defined as the potency of the fraction of the sampled chloride concentration (x_i) over the average concentration (x) raised to a mathematical adjustment constant ρ_i, where *i* are the particle levels and heap height.

$$R_\tau = R_\tau^{\infty}\left(1 - e^{-k_\tau \delta^{\rho_1}\left(\frac{D_{Ae}}{\varepsilon_0 r^2} t - \hat{\omega}\right)}\right) \tag{5}$$

$$R_\theta = R_\theta^{\infty}\left(1 - e^{-k_\theta \delta^{\rho_2}\left(\frac{\mu_s}{\varepsilon_b Z} t - \omega\right)}\right) \tag{6}$$

Including both scales in an aggregate model, Mellado *et al*. [58] assumed that the total recovery is the sum of both recoveries (, $R^{\infty} = R_\tau + R_\theta$, see Eq. 7), which shows asymptotic behaviour over time.

$$R = R^{\infty}\left(1 - \lambda e^{-k_\theta \delta^{\rho_2}\left(\frac{\mu_s}{\varepsilon_b Z} t - \omega\right)} - (1-\lambda) e^{-k_\tau \delta^{\rho_1}\left(\frac{D_{Ae}}{\varepsilon_0 r^2} t - \hat{\omega}\right)}\right) \tag{7}$$

where $\hat{\omega}$ represents the delay on the scale of τ, and its relation to ω is given by Eq. (8) [58], and λ represents the kinetic weight factor. The analytical model for R^{∞} used by Mellado *et al*. [58] is presented by Eq. (9).

$$\hat{\omega} = \frac{D_{Ae}}{\varepsilon_0 r^2} \frac{\varepsilon_b Z}{\mu_s} \omega \tag{8}$$

$$R^{\infty} = \frac{\alpha}{Z^{\gamma} + \beta} \tag{9}$$

Where α, γ and β are mathematical adjustment coefficients, and Z is the heap height. Finally, the model for copper heap leaching for copper sulfide minerals is given by Eq. (10).

$$R = \frac{\alpha}{Z^{\gamma} + \beta} \left(1 - \lambda e^{-k_0 \delta^{\rho_2} \frac{\mu_s}{\varepsilon_b Z} \left(t - \frac{\varepsilon_b Z}{\mu_s} \omega \right)} - (1 - \lambda) e^{-k_r \delta^{\rho_1} \frac{D_{Ae}}{\varepsilon_0 r^2} \left(t - \frac{\varepsilon_b Z}{\mu_s} \omega \right)} \right) \tag{10}$$

2. 3. Uncertainty analysis

The uncertainly analysis (UA) determines the uncertainty of output variables due to the uncertainty of input variables [64]. It is generally performed by using the probability theory [65], where uncertainty is represented by probability distribution functions (PDF) and can be realized in four steps. First, the PDF type and the uncertainty magnitude for each input variable are determined, *i.e.* the input uncertainty is characterized. Second, for each input variable, a sample of the PDF is generated. Third, output variable values are determined for each element sampled. Finally, the results are analysed by using graphs, descriptive statistics, and statistical tests to characterize the behaviour of the output variables.

When the input variables have epistemic uncertainties, the uncertainty can be represented by a uniform distribution. Design and operation variables present this type of uncertainty. When the input variables have stochastic uncertainties, normal distribution is generally used to represent this type of uncertainty [66].

2. 4. Optimization of the experimental model

A multivariate function of seven independent variables and one dependent variable is defined from an inverse exponential model, a statistical analysis, and the multiple regression adjustment is presented in Eq. (11).

$$R(X) = f(X) \tag{11}$$

Formalizing the optimization model, the objective is to maximize copper recovery considering the range of sampled values as domain of the input variables [67] expressed in Eq. (12).

$$\text{Max } \{R(X)\} \tag{12}$$

The operational constraints for the n independent variables are shown in Eq. 13:

$$x_i^{min} \leq x_i \leq x_i^{max} \; \forall \; i \in X \mid X = \{x_1, x_2 \ldots, x_n\} \tag{13}$$

Considering the nature of the analytical model developed, it is proposed to optimize it using the Lagrange multipliers technique, which provides determination of the optimal values of a multivariate function when there are one or more restrictions on the input parameters.

3. RESULTS AND DISCUSSIONS

3. 1. Analysis of the effects of main independent variables

Analysis of the data generated by the factorial model, also used for the fit of the analytical model presented by Eq. (7), indicated only four factors that have main effects on the response variable: the heap height, superficial velocity of leaching flow and chloride concentration. It is corroborated that the superficial velocity of leaching flow in the bed is the variable with the greatest impact (of the analyzed variables) on the copper recovery as shown in Figure 1.

Figure 2 shows that copper recovery increases as superficial velocity of lixiviant flow and chloride concentration are increased, while decreases at higher heap heights.

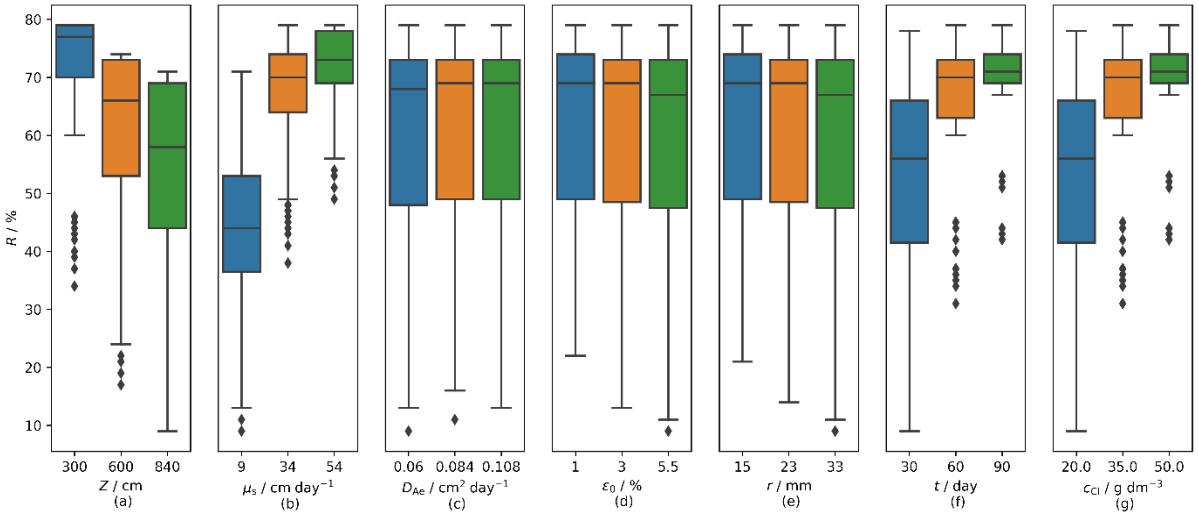

Figure 1. Main effects of independent variables heap height Z (a), superficial velocity of lixiviant flow μ_s (b), effective diffusivity D_{Ae} (c), porosity e ε_0 (d), particle ratio r (e), leaching time t (f) and Cl concentration c_{Cl} (g), in copper extraction R from sulfide minerals

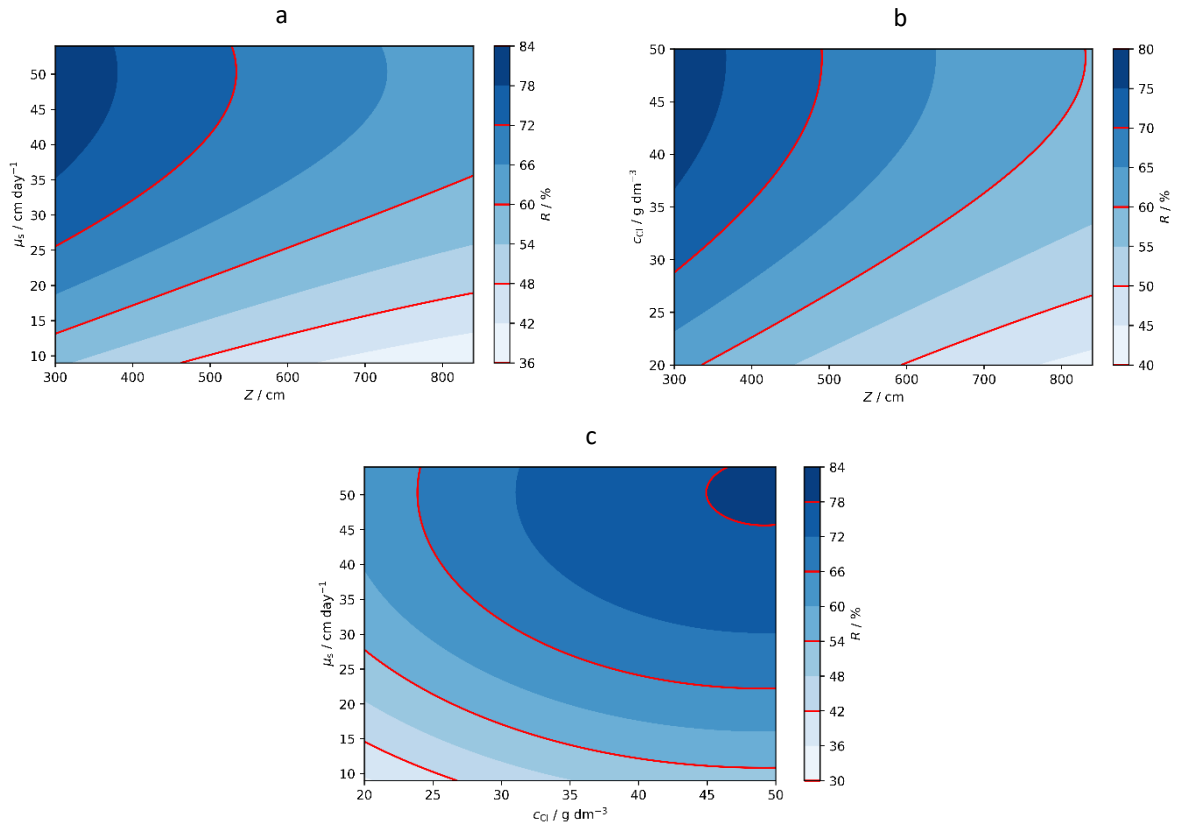

Figure 2. Contour plot of copper recovery versus the heap height and superficial velocity (a); heap height and chloride concentration (b); and, chloride concentration and superficial velocity (c).

3. 2. Uncertainty analysis

Eq. (10) included the copper recovery dependence on the following operational variables: leaching time, particle size, heap height, particle porosity, superficial velocity of the leaching flow and effective diffusivity of the solute through particle pores. A proper distribution function to represent epistemic uncertainties is the uniform PDF, taking the values of x_1, x_2…, x_n, as the central tendency values of the parameters p_1, p_2…, p_n, respectively. The sensitivity analysis was performed 3 times for leaching times of 30, 60 and 90 days (see Fig. 3).

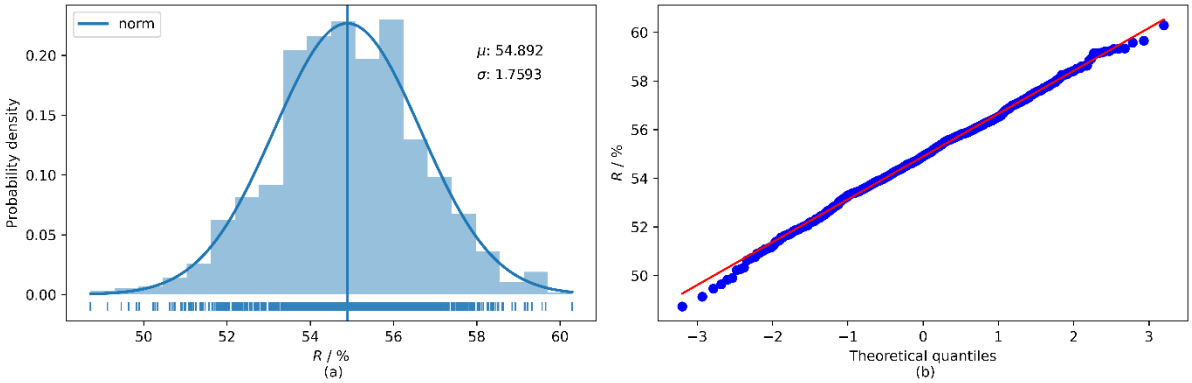

Figure 3. Probability density (a) and normal Q-Q plot (b) of UA at 30 days of leaching

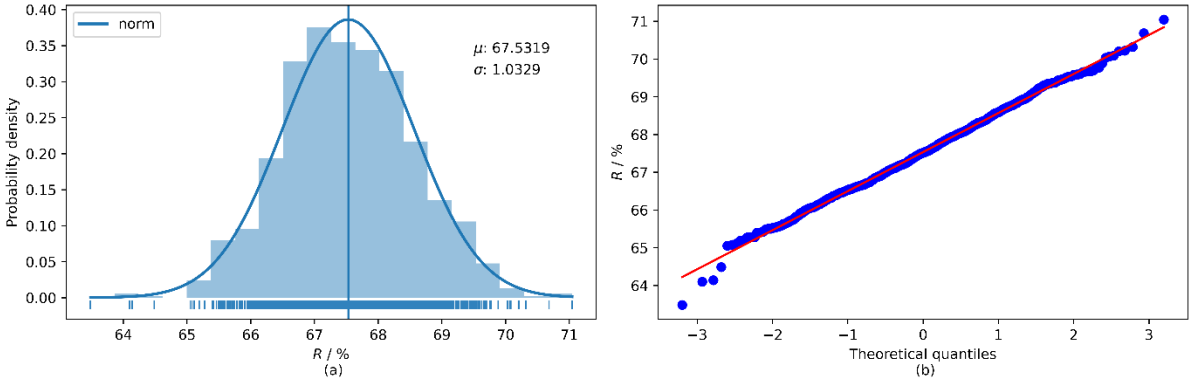

Figure 4. Probability density (a) and normal Q-Q plot (b) of UA at 60 days of leaching

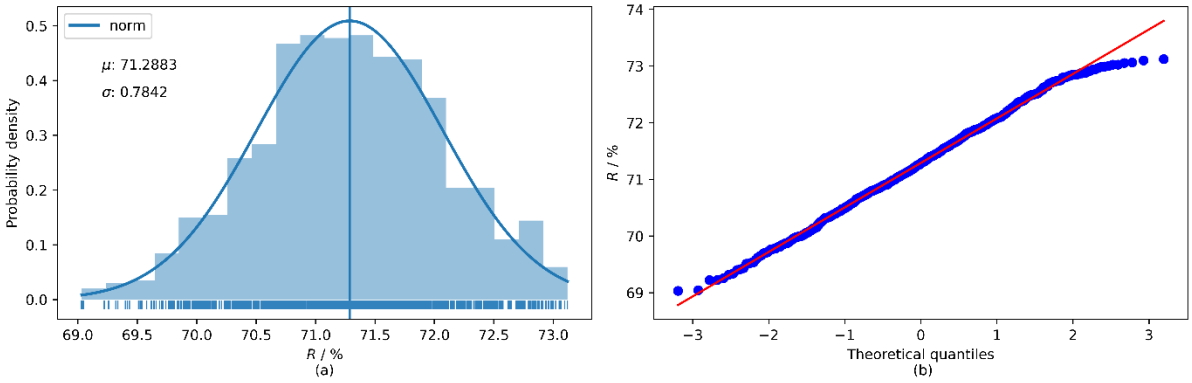

Figure 5. Probability density (a) and normal Q-Q plot (b) of UA at 90 days of leaching

UA shows that leaching time affects the kinetic uncertainty of the heap leaching phase. Histograms show that uncertainty in the input variables produces lower uncertainty in recovery as the leaching time is increased from 30 to 90 days. The normal distribution plots (Q-Q plot) indicate that copper recovery normally behaves for all investigated leaching times. The recovery presents a normal PDF with averages of 54.89 ± 1.76, 67.53 ± 1.03, and 71.29 ± 0.78 %. On the other hand, the normal probability plot indicates that for the leaching time of 90 days the recovery has a tail that deviates from the normal behaviour. The change in the recovery behaviour as a function of the time factor is due to the tendency to asymptotic behaviour.

3. 3. Analytical model adjustment

The fit of the analytical model developed by Mellado *et al.* [57] by optimization algorithms [67] indicates that the copper recovery from sulfide minerals can be explained by Eq. (14), where the volumetric fraction of the solution in the bed is assumed as $\varepsilon_b = 0.015$, while the delay of the reaction is assumed as $\omega = 1$.

$$R = \frac{138.83}{Z^{0.042}+0.038}\left(1-0.705\,e^{-0.027\delta^{1.81}\frac{\mu_s}{0.015Z}\left(t-\frac{0.015Z}{\mu_s}\right)}-0.295\,e^{-2.3\delta^{2.081}\frac{D_{Ae}}{\varepsilon_0 r^2}\left(t-\frac{0.015Z}{\mu_s}\right)}\right) \quad (14)$$

The analytical model presented by this equation is validated by the goodness-of-fit statistics Mean Absolute Error (MAD), Mean Squared Error (MSE) and Mean Absolute Percent Error (MAPE), with values of 1.147×10^{-2}, 2.475×10^{-4} and 0.793 %, respectively. The error statistics indicates that the fitted model explains the system under the set of sampled values. The Sensitivity analysis of the dependent variables that model the copper recovery for low, medium, and high levels operational conditions, check again that the variables that influence the copper recovery are the heap height (see Fig. 6a), chloride concentration (see Fig. 6b), and superficial velocity of lixiviant flow (see Fig. 6c). The impact of the other variables at different levels is considered are negligible (see Figures 6d, 6e, and 6f).

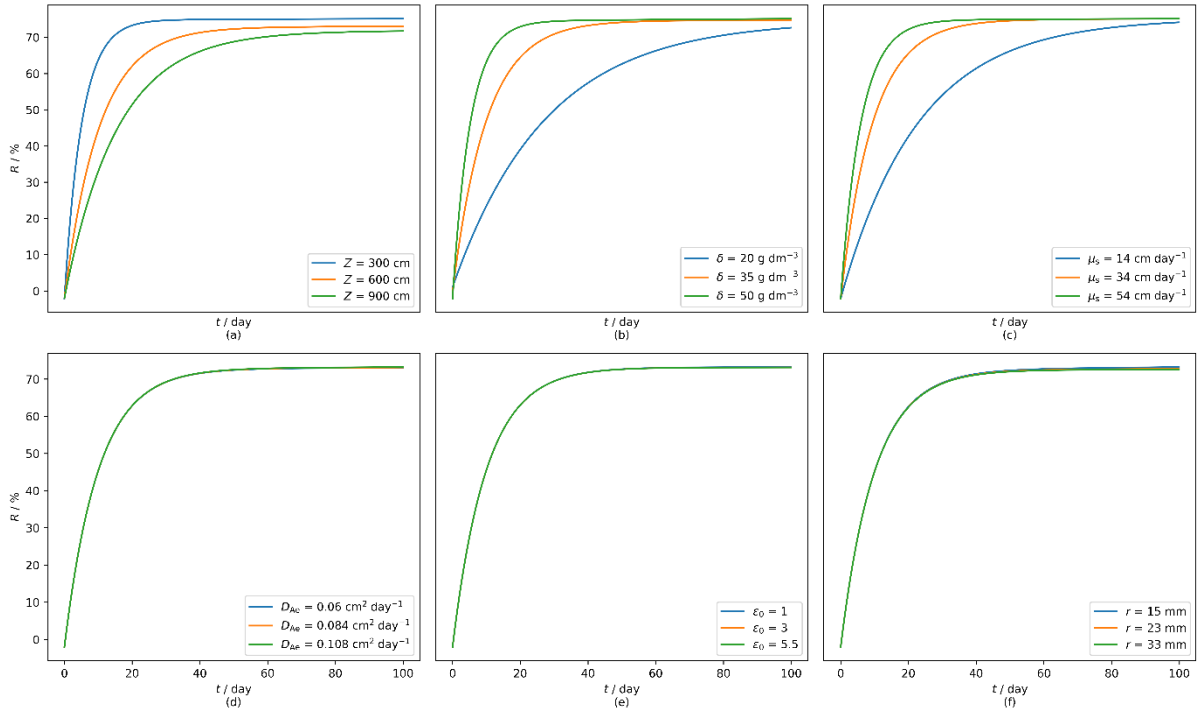

Figure 6. Sensitivity analysis of copper recovery for low, medium, and high levels of the factors: heap height (a), chloride concentration (b), superficial velocity of lixiviant flow (c), effective diffusivity within particle pores (d), porosity (e), and particle size (f)

Finally, comparison of the theoretical results in the literature and industrial heap processes, shows that despite the fact that the heap height is inversely proportional to the recovery, the heights of industrial heaps are at high levels. The increase in the height of commercial heaps is due to economic efficiency, which is the function of the available surface area [14]. The factors that influence the process kinetics the most are the percolation rate and chloride concentration as the leaching agent, of which, the percolation rate is directly related with the heap height and its permeability [51]. Also, the time factor has a strong impact on the copper recovery, being initially rapid recovery and showing asymptotic behaviour as time increases.

The current low ore grades reduce profitability of other recovery technologies due to requirements of greater comminution, temperature [68], or operating times. Those variables may change depending on the working material and the recovery standards of a mining company [66] severely impacting the projected profits. Therefore, mathematical models that provide optimization of the process would be an added value to the study and improvement of ore recovery in industrial contexts.

3. 4. Optimization of the analytical model

Optimization of the analytical model adjusted in the previous section for the set of sampled values was performed by using the Python library "SciPy Optimize" (Version 3.7.0). This library provides several methods to minimize/maximize objective functions subject to constraints.

Table 1 presents the operational restrictions associated with the independent variables in the form of lower and upper limit values. Optimal values for each variable are also presented.

The graphical analysis of the copper recovery response surface (see Fig. 7), model the recovery over time in the form of an inverse exponential function tending to become asymptotic between 80 and 100 days of leaching.

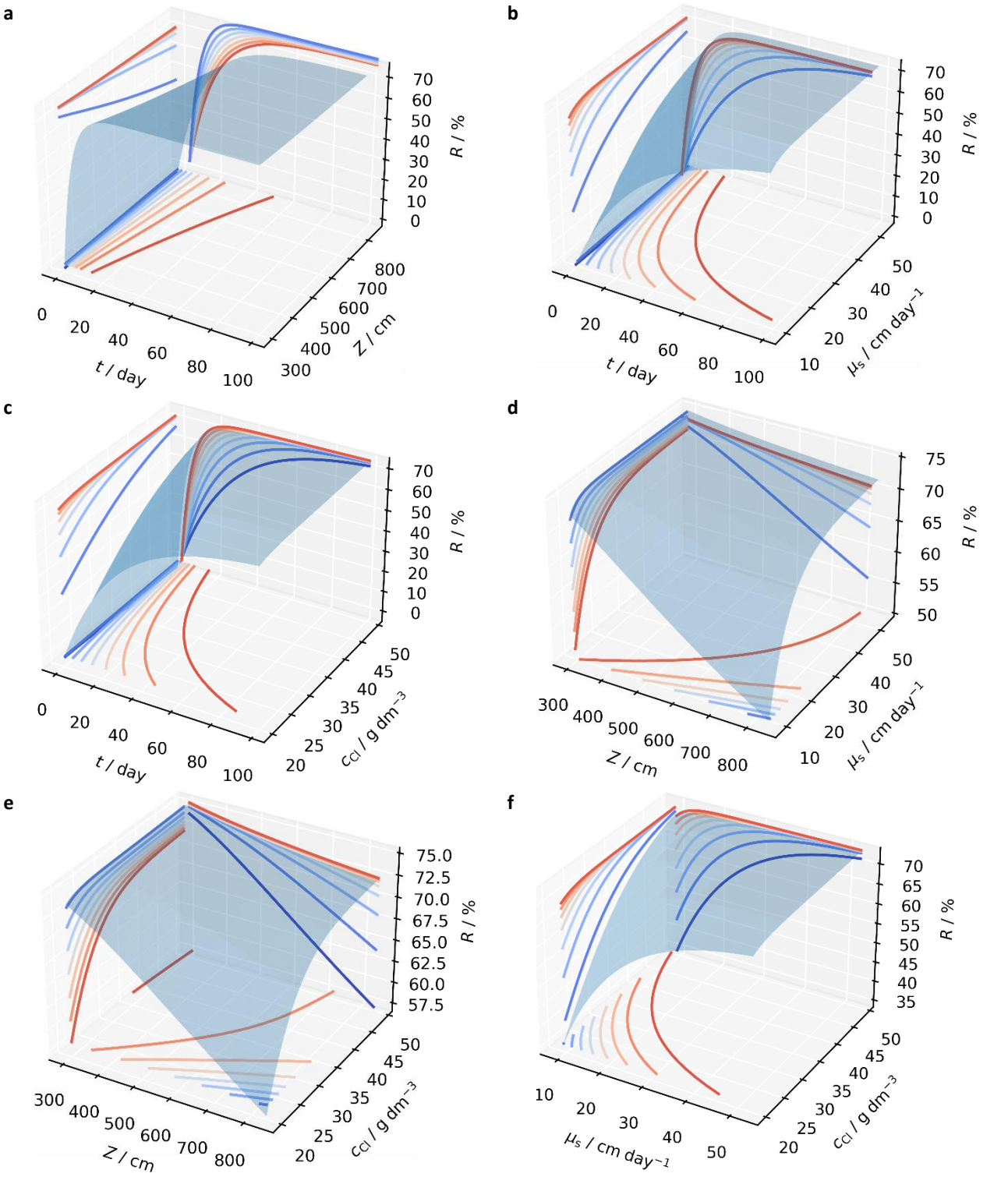

Figure 7. Response surface of copper recovery from sulfide minerals versus: time and the heap height (a); time and the superficial velocity of the leaching flow (b); time and the chloride concentration (c); heap height and the superficial velocity (d); heap height and the chloride concentration (e); superficial velocity and the chloride concentration (f)

Table 1 Limits and optimal values of the independent variables

Variable	Lower limit	Upper limit	Optimal value
Z / cm	300	900	900
μ_s/ cm^3 cm^{-2} d^{-1}	9	54	54
D_{Ae}/ cm^3 cm^{-1} d^{-1}	0.06	0.108	0.108
ε_0 / %	1	5.5	1
r / mm	15	33	15
t / day	0	90	90
c_{Cl}/ g dm^{-3}	20	50	50
R / %	-	-	72.12

This value for leaching time is common in hydrometallurgical processes in the Chilean mining industry. On the other hand, at the lower heap height, a greater recovery is observed, which is due to the improvement in the efficiency of the percolation of the leaching flow through the heap. And finally, additional surface plots in Figure 7 model the dynamics of response variable as functions of significant independent variables.

Additionally, future works could incorporate machine learning techniques for process modelling, simulation and optimization [69]. Also, integration of the model presented here along with discrete events simulation models, (*e.g*. [63,70]), aimed to optimize the mineral recovery, while incorporating the feeding mineralogical variation, different process operation modes by variation of reagents or the levels of the variables and/or other operational parameters, has the potential to add value to the study of leaching dynamics of sulfide copper minerals.

4. CONCLUSIONS

The present investigation presents the results of an analytical model of copper extraction from a sulfide mineral (chalcocite) as a system of first-order differential equations through an inverse exponential function. The main findings in this study are summarized below.

The behavior of heap leaching process of copper sulfide minerals (secondary sulfides), like chalcocite, can be modelled as a system of first-order differential equations, which is validated by the goodness-of-fit statistics.

Particle size, porosity, and effective diffusivity of the solute within the particle pores are not as significant in the copper extraction, as is leaching time, heap height, superficial velocity of the leaching flow and chloride concentration in the leaching solution.

The best result predicted by optimizing the generated analytical model would be obtained by working at high chloride concentration and a high leaching flow rate.

On the other hand, the fit of this type of analytical models can be extended to other variable levels or factors, such as inclusion of different leaching agents. The model would be modified then according to the kinetics that describe or dominate the operation.

Generation of analytical models to represent complex processes, such as mineral leaching, has the potential to be used for analysis, generalization, and optimization tasks, since these models capture the essence of the modelled process and could be used to predict the response under operational conditions, identifying the conditions that maximize the aggregate process productivity.

Acknowledgements: Manuel Saldaña acknowledges the infrastructure and support of Doctorado en Ingeniería de Procesos de Minerales of the Universidad de Antofagasta. Francisca Roldán acknowledges the support of ANID/FONDAP/15110017 project.

REFERENCES

[1] Flanagan DM. Copper. In Mineral Commodity Summaries 2021. Reston, VA, USA: U.S. Geological Survey; 2021; 52–3. ISBN 9781411343986.

[2] Villela D, Kutscher C, Castillo E. Sulfuros primarios: desafíos y oportunidades. Comisión Chilena del Cobre (COCHILCO). Santiago, Chile: 2017.

[3] ICSG. Copper: Preliminary Data for January 2020. International Copper Study Group (ICSG): Lisbon, Portugal: 2020.
[4] Pérez K, Toro N, Gálvez E, Robles P, Wilson R, Navarra A. Environmental, economic and technological factors affecting Chilean copper smelters – A critical review. *J Mat Res Technol.* 2021; 15: 213–25. https: //doi.org/10.1016/j.jmrt.2021.08.007
[5] Navarra A, Wilson R, Parra R, Toro N, Ross A, Nave JC, Mackey PJ. Quantitative methods to support data acquisition modernization within copper smelters. *Processes* 2020; 8(11): 1–22. https: //doi.org/10.3390/pr8111478
[6] Lazo A, Lazo P, Urtubia A, Lobos MG, Gutiérrez C, Hansen HK. Copper Analysis by Two Different Procedures of Sequential Extraction after Electrodialytic Remediation of Mine Tailings. *Int J Environ Res Public Health* 2019; 16(20): 3957. https: //doi.org/10.3390/ijerph16203957
[7] Rodríguez F, Moraga C, Castillo J, Gálvez E, Robles P, Toro N. Submarine tailings in chile—a review. *Metals (Basel)* 2021; 11(5): 1–17. https: //doi.org/10.3390/met11050780
[8] Toro N, Rodríguez F, Rojas A, Robles P, Ghorbani Y. Leaching manganese nodules with iron-reducing agents – A critical review. *Min Eng.* 2021; 163: 106748. https: //doi.org/10.1016/J.MINENG.2020.106748
[9] Dijkstra R. Economical abatement of high-strength SO2 off-gas from a smelter. *J South Afr Inst Min Metall.* 2017; 117(11): 1003–7. https: //doi.org/10.17159/2411-9717/2017/v117n11a2
[10] Daibova EB, Lushchaeva I v, Sachkov VI, Karakchieva NI, Orlov V v, Medvedev RO, Nefedov RA, Shplis ON, Sodnam NI. Bioleaching of Au-Containing Ore Slates and Pyrite Wastes. *Minerals* 2019; 9(10): 1–11. https: //doi.org/10.3390/min9100643
[11] Conić V, Stanković S, Marković B, Božić D, Stojanović J, Sokić M. Investigation of the optimal technology for copper leaching from old flotation tailings of the copper mine bor (Serbia). *Metal Mat Eng.* 2020; 26(2): 209–22. https: //doi.org/10.30544/514
[12] Casas JM, Martinez J, Moreno L, Vargas T. Bioleaching model of a copper-sulfide ore bed in heap and dump configurations. *Metal Mat Trans B.* 1998; 29(4): 899–909. https: //doi.org/10.1007/s11663-998-0149-0
[13] Behrad Vakylabad A, Nazari S, Darezereshki E. Bioleaching of copper from chalcopyrite ore at higher NaCl concentrations. *Min Eng.* 2022; 175: 107281. https: //doi.org/10.1016/J.MINENG.2021.107281
[14] Ghorbani Y, Franzidis J-P, Petersen J. Heap leaching technology – current state, innovations and future directions: A review. *Mineral Proces Extract Metal Rev.* 2015: 08827508.2015.1115990. https: //doi.org/10.1080/08827508.2015.1115990
[15] Kevin Pérez , Norman Toro, Eduardo Campos AN and MHR. Extraction of Mn from Black Copper Using Iron Acid Medium. *Metals (Basel)* 2019; 9(10): 1–10. https: //doi.org/https: //doi.org/10.3390/met9101112
[16] Hernández PC, Taboada ME, Herreros OO, Graber TA, Ghorbani Y. Leaching of chalcopyrite in acidified nitrate using seawater-based media. *Minerals* 2018; 8(6). https: //doi.org/10.3390/min8060238
[17] Toro N, Ghorbani Y, Turan MD, Robles P, Gálvez E. Gangues and Clays Minerals as Rate-Limiting Factors in Copper Heap Leaching: A Review. *Metals 2021, Vol 11, Page 1539* 2021; 11(10): 1539. https: //doi.org/10.3390/MET11101539
[18] Cerda CP, Taboada ME, Jamett NE, Ghorbani Y, Hernández PC. Effect of pretreatment on leaching primary copper sulfide in acid-chloride media. *Minerals* 2018; 8(1): 1–14. https: //doi.org/10.3390/min8010001
[19] Pradhan N, Nathsarma KC, Srinivasa Rao K, Sukla LB, Mishra BK. Heap bioleaching of chalcopyrite: A review. *Min Eng.* 2008; 21(5): 355–65. https: //doi.org/10.1016/j.mineng.2007.10.018
[20] Castillo J, Sepúlveda R, Araya G, Guzmán D, Toro N, Pérez K, Rodríguez M, Navarra A. Leaching of white metal in a NaCl-H2SO4 system under environmental conditions. *Minerals* 2019; 9(5). https: //doi.org/10.3390/min9050319
[21] Velásquez-Yévenes L. The kinetics of the dissolution of chalcopyrite in chloride media: PhD Thesis, Murdoch University, Australia. 2009.
[22] Velásquez-Yévenes L, Nicol M, Miki H. The dissolution of chalcopyrite in chloride solutions Part 1. The effect of solution potential. *Hydrometallury.* 2010; 103(1–4): 108–13. https: //doi.org/10.1016/j.hydromet.2010.03.001
[23] Nicol M, Miki H, Velásquez-Yévenes L. The dissolution of chalcopyrite in chloride solutions Part 3. Mechanisms. *Hydrometallurgy* 2010; 103(1–4): 86–95. https: //doi.org/10.1016/j.hydromet.2010.03.003
[24] Torres CM, Ghorbani Y, Hernández PC, Justel FJ, Aravena MI, Herreros OO. Cupric and chloride ions: Leaching of chalcopyrite concentrate with low chloride concentration media. *Minerals* 2019; 9(10). https: //doi.org/10.3390/min9100639
[25] Nicol M, Basson P. The anodic behaviour of covellite in chloride solutions. *Hydrometallurgy* 2017; 172(June): 60–8. https: //doi.org/10.1016/j.hydromet.2017.06.018
[26] Pérez K, Toro N, Saldaña M, Salinas-Rodríguez E, Robles P, Torres D, Jeldres RI. Statistical Study for Leaching of Covellite in a Chloride Media. *Metals (Basel)* 2020; 10(4): 477. https: //doi.org/10.3390/met10040477
[27] Toro N, Moraga C, Torres D, Saldaña M, Pérez K, Gálvez E. Leaching Chalcocite in Chloride Media—A Review. *Minerals* 2021; 11(11): 1197. https: //doi.org/10.3390/min11111197
[28] Cisternas LA, Gálvez ED. The use of seawater in mining. *Min Proces Extract Metal Rev.* 2018; 39(1): 18–33. https: //doi.org/10.1080/08827508.2017.1389729
[29] Bogdanović GD, Petrović S, Sokić M, Antonijević MM. Chalcopyrite leaching in acid media: a review. *Metal Mat Eng* 2020; 26(2): 177–98. https: //doi.org/10.30544/526
[30] Yévenes LV, Miki H, Nicol M. The dissolution of chalcopyrite in chloride solutions: Part 2: Effect of various parameters on the rate. *Hydrometallurgy* 2010; 103(1–4): 80–5. https: //doi.org/10.1016/j.hydromet.2010.03.004
[31] Dimitrijević M, Urošević D, Milić S, Sokić M, Marković R. Dissolution of copper from smelting slag by leaching in chloride media. *J Min Metal B* 2017; 53(3): 407–12. https: //doi.org/10.2298/JMMB170425016D

[32] Petronijević N, Stanković S, Radovanović D, Sokić M, Marković B, Stopić SR, Kamberović Ž. Application of the Flotation Tailings as an Alternative Material for an Acid Mine Drainage Remediation: A Case Study of the Extremely Acidic Lake Robule (Serbia). *Metals 2020;* 10(1): 16. https: //doi.org/10.3390/MET10010016
[33] Sokić M, Marković B, Stanković S, Kamberović Ž, Štrbac N, Manojlović V, Petronijević N. Kinetics of Chalcopyrite Leaching by Hydrogen Peroxide in Sulfuric Acid. *Metals 2019;* 9(11): 1173. https: //doi.org/10.3390/MET9111173
[34] Córdoba EM, Muñoz JA, Blázquez ML, González F, Ballester A. Leaching of chalcopyrite with ferric ion. Part I: General aspects. *Hydrometallurgy* 2008; 93(3–4): 81–7. https: //doi.org/10.1016/j.hydromet.2008.04.015
[35] Molinos-Senante M, Donoso G. Water scarcity and affordability in urban water pricing: A case study of Chile. *Util Policy* 2016; 43: 107–16. https: //doi.org/10.1016/J.JUP.2016.04.014
[36] Saleth RM, Dinar A. Institutional changes in global water sector: trends, patterns, and implications. *Water Policy* 2000; 2(3): 175–99. https: //doi.org/10.1016/S1366-7017(00)00007-6
[37] Ministerio del Medio Ambiente. Informe del Estado del Medio Ambiente. *Ministerio Del Medio Ambiente.* 2020. https: //sinia.mma.gob.cl/estado-del-medio-ambiente/informe-del-estado-del-medio-ambiente-2020/. Accessed December 12, 2021.
[38] IPPC. The Working Group I contribution to the Sixth Assessment Report addresses the most up-to-date physical understanding of the climate system and climate change, bringing together the latest advances in climate science. In: Climate Change 2021: The Physical Science Basis. Cambridge University Press; 2021. ISBN 9780080967899. https: //www.ipcc.ch/report/ar6/wg1/ Accessed December 30, 2021.
[39] Bárcena A, Prado A, Samaniego J, Pérez R. La Economía del Cambio Climático en Chile. Comisión Económica para América Latina y el Caribe (CEPAL): Santiago, Chile: 2012. http: //repositorio.cepal.org/bitstream/handle/11362/35372/1/S2012058_es.pdf. Accessed November 19, 2021.
[40] Torres D, Toro N, Galvez E, Castillo D, Bermudez SA, Navarra A. Temporal Variography for the Evaluation of Atmospheric Carbon Dioxide Monitoring. *J-STARS* 2022; 15: 80–8. https: //doi.org/10.1109/JSTARS.2021.3131414
[41] Santibañez F. El cambio climático y los recursos hídricos de Chile. *Agricultura Chilena: Reflexiones y Desafíos* 2016: 147–78. https: //www.odepa.gob.cl/publicaciones/documentos-e-informes/el-cambio-climatico-y-los-recursos-hidricos-de-chile-diciembre-de-2016 Accessed July 03, 2021.
[42] Roldán F, Salazar I, González G, Roldán W, Toro N. Flow-Type Landslides Analysis in Arid Zones: Application in La Chimba Basin in Antofagasta, Atacama Desert (Chile). *Water 2022;* 14(14): 2225. https: //doi.org/10.3390/W14142225
[43] Fuentes F, García C. Ciclo económico y minería del cobre en Chile. *Revista CEPAL* 2016; Abril: 165–92. https: //repositorio.cepal.org/handle/11362/40035 Accessed September 23, 2021.
[44] Conejeros V, Pérez K, Jeldres RI, Castillo J, Hernández P, Toro N. Novel treatment for mixed copper ores: Leaching ammonia – Precipitation – Flotation (L.A.P.F.). *Min Eng.* 2020; 149 : 106242. https: //doi.org/10.1016/j.mineng.2020.106242
[45] Ortlieb L. Eventos El Niño y episodios lluviosos en el desierto de Atacama: el registro de los últimos dos siglos. *Bulletin de l'Institut Français d'Études Andines* 1995; 24(3): 519–37
[46] Vargas G, Ortlieb L, Rutllant J. Aluviones históricos en Antofagasta y su relación con eventos El Niño/Oscilación del Sur. *Revista Geológica de Chile* 2000; 27(2): 157–76. https: //doi.org/10.4067/S0716-02082000000200002
[47] Arens FL, Airo A, Feige J, Sager C, Wiechert U, Schulze-Makuch D. Geochemical proxies for water-soil interactions in the hyperarid Atacama Desert, Chile. *CATENA* 2021; 206: 105531. https: //doi.org/10.1016/J.CATENA.2021.105531
[48] Jordan TE, Kirk-Lawlor NE, Nicolás Blanco P, Rech JA, Cosentino NJ. Landscape modification in response to repeated onset of hyperarid paleoclimate states since 14 Ma, Atacama Desert, Chile. *GSA Bulletin* 2014; 126(7–8): 1016–46. https: //doi.org/10.1130/B30978.1
[49] Placzek CJ, Matmon A, Granger DE, Quade J, Niedermann S. Evidence for active landscape evolution in the hyperarid Atacama from multiple terrestrial cosmogenic nuclides. *EPSL* 2010; 295(1–2): 12–20. https: //doi.org/10.1016/J.EPSL.2010.03.006
[50] Kappes DW. Precious Metal Heap Leach Design and Practice. Mineral processing plant design, practice, and control. Vancouver, Canada: Society for Mining, Metallurgy, and Exploration; 2002; 12
[51] Schlesinger M, King M, Sole K, Davenport W. Extractive Metallurgy of Copper. Fifth Ed. Amsterdam, The Netherlands: Elsevier Ltd; 2011. ISBN 9780080967899.
[52] Saldaña M, Rodríguez F, Rojas A, Pérez K, Angulo P. Development of an empirical model for copper extraction from chalcocite in chloride media. *Hem Ind* 2020; 74(5): 285–92. https: //doi.org/10.2298/HEMIND200424031S
[53] Saldaña M, Gálvez E, Robles P, Castillo J, Toro N. Copper Mineral Leaching Mathematical Models - A Review. *Materials 2022;* 15(5): 1757. https: //doi.org/10.3390/MA15051757
[54] Saldaña M, Neira P, Gallegos S, Salinas-Rodríguez E, Pérez-Rey I, Toro N. Mineral Leaching Modeling Through Machine Learning Algorithms − A Review. *Front Earth Sci.* 2022; 10: 560. https: //doi.org/10.3389/feart.2022.816751
[55] Mellado ME, Cisternas LA, Gálvez ED. An analytical model approach to heap leaching. *Hydrometallurgy* .2009; 95(1–2): 33–8. https: //doi.org/10.1016/j.hydromet.2008.04.009
[56] Mellado ME, Casanova MP, Cisternas LA, Gálvez ED. On scalable analytical models for heap leaching. *Comput Chem Eng.* 2011; 35(2): 220–5. https: //doi.org/10.1016/j.compchemeng.2010.09.009
[57] Mellado ME, Gálvez ED, Cisternas LA. On the optimization of flow rates on copper heap leaching operations. *Int J Min Process.* 2011; 101(1–4): 75–80. https: //doi.org/10.1016/j.minpro.2011.07.011
[58] Mellado M, Cisternas L, Lucay F, Gálvez E, Sepúlveda F. A Posteriori Analysis of Analytical Models for Heap Leaching Using Uncertainty and Global Sensitivity Analyses. *Minerals* 2018; 8(2): 44. https: //doi.org/10.3390/min8020044

[59] Dixon DG, Hendrix JL. A mathematical model for heap leaching of one or more solid reactants from porous ore pellets. *Metal Trans B* 1993; 24(6): 1087–102. https: //doi.org/10.1007/BF02661000
[60] Dixon DG, Hendrix JL. Theoretical basis for variable order assumption in the kinetics of leaching of discrete grains. *AIChE J* 1993; 39(5): 904–7. https: //doi.org/10.1002/aic.690390520
[61] Dixon DG, Hendrix JL. A general model for leaching of one or more solid reactants from porous ore particles. *Metal Trans B* 1993; 24(1): 157–69. https: //doi.org/10.1007/BF02657882
[62] Torres D, Trigueros E, Robles P, Leiva WH, Jeldres RI, Toledo PG, Toro N. Leaching of pure chalcocite with reject brine and mno2 from manganese nodules. *Metals (Basel)* 2020; 10(11): 1–19. https: //doi.org/10.3390/met10111426
[63] Saldaña M, Toro N, Castillo J, Hernández P, Navarra A. Optimization of the Heap Leaching Process through Changes in Modes of Operation and Discrete Event Simulation. *Minerals* 2019; 9(7): 421. https: //doi.org/10.3390/min9070421
[64] Liu B. Uncertainty Theory. In Uncertainty Theory. 4th Ed., Springer-Verlag Berlin Heidelberg: Germany. 2007. https: //doi.org/10.1007/978-3-540-73165-8_5
[65] Jaynes ET. Probability Theory. Cambridge: Cambridge University Press; 2003. https: //doi.org/10.1017/CBO9780511790423
[66] Saldaña M, González J, Jeldres R, Villegas Á, Castillo J, Quezada G, Toro N. A Stochastic Model Approach for Copper Heap Leaching through Bayesian Networks. *Metals (Basel)* 2019; 9(11): 1198. https: //doi.org/10.3390/met9111198
[67] Taha HA. Operations Research: An Introduction. 10th Ed., Essex, England: Pearson Education Limited; 2017. ISBN 9780134444017.
[68] Petersen J. Heap leaching as a key technology for recovery of values from low-grade ores – A brief overview. *Hydrometallurgy* 2016; 165: 206–12. https: //doi.org/10.1016/j.hydromet.2015.09.001
[69] McCoy JT, Auret L. Machine learning applications in minerals processing: A review. *Min Eng.* 2019; 132: 95–109. https: //doi.org/10.1016/j.mineng.2018.12.004
[70] Peña-Graf F, Órdenes J, Wilson R, Navarra A. Discrete Event Simulation for Machine-Learning Enabled Mine Production Control with Application to Gold Processing. *Metals* 2022; 12(2): 225. https: //doi.org/10.3390/MET12020225

Razvoj analitičkog modela za iskorišćavanje bakra iz sekundarnih sulfida u hloridnim medijima u industrijskom okruženju

Manuel Saldaña[1,2], Eleazar Salinas-Rodríguez [3], Jonathan Castillo [4], Felipe Peña-Graf [5] i Francisca Roldán[6]

[1]*Faculty of Engineering and Architecture, Universidad Arturo Prat, Iquique 1110939, Chile*

[2]*Departamento de Ingeniería Química y Procesos de Minerales, Facultad de Ingeniería, Universidad de Antofagasta, Antofagasta 1240000, Chile*

[3]*Área Académica de Ciencias de la Tierra y Materiales, Universidad Autónoma del Estado de Hidalgo, Carretera Pachuca—Tulancingo km. 4.5, C.P. 42184, Mineral de la Reforma, Hidalgo C.P. 42184, Mexico*

[4]*Departamento de Ingeniería en Metalurgia, Universidad de Atacama, Copiapó 1531772, Chile*

[5]*Escuela de Ingeniería, Universidad Católica del Norte, Coquimbo 1531772, Chile*

[6]*Centro de Investigación para la Gestión Integrada del Riesgo de Desastres (CIGIDEN), Departamento de Ciencias Geológicas. Universidad Católica del Norte (UCN), Antofagasta, Chile*

(Stručni rad)

Izvod

U multivarijantnoj analizi, model predviđanja je matematičko/statistički model koji povezuje skup nezavisnih varijabli sa zavisnim ili promenljivim varijablama. Ovaj rad prezentuje opisni model koji objašnjava iskorišćavanje bakra iz sekundarnih sulfidnih minerala (halkocita) uzimajući u obzir efekte vremena, visine jalovišta, površinske brzine ispiranja, koncentracije hlorida, veličine čestica, poroznosti i efektivne difuzije rastvorene supstance unutar pora čestice. Izluživanje bakra se zatim modeluje sistemom diferencijalnih jednačina prvog reda. Rezultati su pokazali da su visina jalovišta i površinska brzina toka ispiranja najkritičnije nezavisne varijable, dok su ostale od manjeg uticaja u primenjenim uslovima rada. U ovoj studiji dobijeni su reprezentativni parametri podešavanja, tako da se model može koristiti za istraživanje izluživanja bakra u hloridnim medijima, kao deo proširenog lanca prerade bakra.

Ključne reči: ekstrakcija bakra, fenomenološko modelovanje, luženje hlorida, modelovanje, hidrometalurgija

The effect of fibre morphology on packing phenomena and bed properties in coalescers

Milica Hadnađev Kostić[1], Dunja Sokolović[2], Srđan Sokolović[3], Thomas Laminger[4,5] and Arpad Kiralj[1]

[1]*University of Novi Sad, Faculty of Technology, Bul. Cara Lazara 1, Novi Sad, Serbia*
[2]*University of Novi Sad, Faculty of Technical Sciences, Trg Dositeja Obradovića 6, Novi Sad, Serbia*
[3]*NIS a.d. Novi Sad, Serbia, Narodnog fronta 12, Novi Sad, Serbia*
[4]*Vienna University of Technology, Institute of Chemical, Environmental and Bioscience Engineering, Austria TU WIEN, Getreidemarkt 9/166, A-1060 Vienna, Austria*
[5]*AGRANA Stärke GmbH - Werk Pischelsdorf, Industriegelände, 3435 Pischelsdorf, Austria*

Abstract

In this study, fibre morphology of waste materials and its effect on packing phenomena and bed properties were investigated. Nine waste materials were used in bed coalescers. By scanning electron microscopy, it was determined that surfaces of all fibres were smooth, while cross-section differed from circular, rectangular to irregular. The fibres with circular cross-sections had diameters in the range of 12±0.8 to 40±4 μm, while the fibres of polypropylene bags and sponges appeared as strips with the widths of 452±11 and 1001±14 μm, respectively. It was also noticed that polyurethane fibres were connected forming a sponge-like structure, while polyethylene terephthalate fibres were interconnected at some points. In this work, experimental dependence of bed porosity on bed permeability was established for all investigated materials, which allows forming a fibre bed with desired permeability. The exception was the bed formed of fibres of polypropylene bags, which had the largest dimensions and yielded a different porosity-permeability dependence.

Keywords: bed permeability; bed porosity; fiber bed; coalescence filtration.

Available on-line at the Journal web address: http://www.ache.org.rs/HI/

TECHNICAL PAPER

UDC: 621.372.542-037.47+66.066.3: 539.217

Hem. Ind. **76(4)** 197-208 (2022)

1. INTRODUCTION

Fibers are often used as a filter medium in bed coalescers for liquid-liquid or gas-liquid separation. The bed formed by fibres has an extremely complex structure in which complex phenomena occur due to the two-phase flow and different surface phenomena. Fibrous filter bed could exhibit high porosity up to 98 %. In the pores of the fibre bed, the dispersed phase is in the form of a capillary-conducted phase, droplets, and globules [1-3]. Depending on the physical properties, fibres are packed in a certain way, but most often as randomly packaged free fibres. It was indicated in literature that the fibre spatial arrangement significantly influences the position of droplets in the filter bed, which affects the coalescence efficiency [4]. The droplet position at fibre intersections is particularly significant. There are numerous studies on the effect of both physical and chemical properties of fibres on the dispersed phase collected in the bed, on its transport through the bed, as well as on attachment and detachment phenomena [5-11]. However, to the best of our knowledge, in the scientific literature, there is a lack of studies on the effect of fibre morphology on the bed geometry *i.e.*, bed permeability and bed porosity. Wetting properties and solid surface phenomena are governed by the surface chemical composition (determined by molecular structure), surface geometry, and topography as well as by the properties of the fluids [6-8,11-14]. Surface geometry can be considered as either local, such as surface roughness, or global, such as different shapes of the surface like spherical or cylindrical. For curved surfaces, such as granules or fibres, an adequate method for measuring the contact angle still does not exist. Four different surface topographies can be distinguished: smooth, micro-, nano-, and micro-nano structures [15-17].

Corresponding authors: Dunja Sokolović, University of Novi Sad, Faculty of Technical Sciences, Trg Dositeja Obradovića 6, 21000 Novi Sad, Serbia
E-mail: dunjaso@uns.ac.rs
Paper received: 22 December 2021; Paper accepted: 24 August; Paper published: 21 September 2022.
https://doi.org/10.2298/HEMIND211224016K

Based on the chemical nature, fibres can be classified as metal, ceramic, glass, and polymer fibres. It can be noted that these fibres drastically differ, not only regarding the chemical nature but also regarding flexibility as fibres could be rigid or elastic. Most of the polymer fibres are very elastic, while flexibility of metal fibres differs. Ceramic and glass fibres are considered completely rigid [9]. Most fibres used in bed coalescers are elastic, which enables bed packing at different bulk densities. Different bulk density alters the properties of the bed, such as bed permeability, bed porosity, and pore size [18-20].

Fibre dimensions and the cross-section shape are extremely important properties that directly affect the behaviour of droplets in the filter bed. Several authors have studied fibres with circular cross-sections and the influence of the fibre size on the efficiency of droplet separation from the continuous liquid or gaseous phase with contradictory conclusions [21-24]. Some authors argue that the increase in the fibre diameter decreases the separation efficiency, while others claim the opposite. However, it is generally agreed that the fibre diameter is an important parameter that influences the fluid flow through the bed, affecting separation of the dispersed phase from the fluid.

Our research group extensively investigated application of different waste fibre materials as filter media in bed coalescers used for the treatment of oily wastewater [25-28]. The investigated fibre materials showed high separation efficiency of mineral oil from water. In the previous research, it was noticed that the changes in bed permeability and bed porosity due to differences in pore size, volume and connectivity, directly affected the bed coalescence efficiency [19, 25].

The scope of this study was to investigate the fibre morphology of waste materials used in our previous studies and its effect on packing phenomena, bed permeability, and bed porosity.

2. MATERIALS AND METHODS

2. 1. Properties of investigated materials

Nine waste fibre materials were investigated in this research. Materials were obtained from local stores. Polyurethane material, PU, is waste generated during furniture manufacture as the excess parts from tailoring chairs and beds. Polypropylene, PP, is waste obtained from the manufacture of carpets. Polypropylene bag material, PPDJ, is waste from used vegetable bags. Polyethylene terephthalate, BA1, is waste produced from thermal filling used for winter clothes. Polyethylene terephthalate, PE, is waste attained from excess part of filters in kitchen aspirators. Stainless steel fibres with different diameters marked as SS40, SS20, and SS12 are the waste left after the production of steel wire. Stainless steel material, SSM is the waste metal sponge used for dishwashing.

Scanning electron microscopy (JEOL, JSM-6460 LV instrument, USA) and optical microscopy (Olympus BH.2 RFCA, Netherlands) were used for investigation of the fibre morphology (surface topography, fibre dimensions) and packing phenomena of waste fibre materials. The software ImageJ was applied for the measurement of fibre dimensions. At least three measurements were performed to determine the average fibre dimensions.

Density of fibre materials was measured by the weighing method, whereas the melting point was obtained by using a differential scanning calorimeter (Q20, TA Instruments, USA). Densities and melting points of investigated materials are given in Table 1.

Table 1. *Properties of investigated materials*

Material	Density, kg m^{-3}	Melting point, °C
Polyurethane (PU)	1200	309
Polypropylene (PP)	900	168
Polypropylene bag (PPDJ)	900	168
Polyethylene terephthalate (BA1)	1400	254
Polyethylene terephthalate (PE)	1400	250
Stainless steel (SS40)	7597	1510
Stainless steel (SS20)	7597	1510
Stainless steel (SS12)	7597	1510
Stainless steel sponge (SSM)	7597	1510

2. 2. Fibre beds

The experimental setup is presented in Figure 1. It consists of two Plexiglas tubes with 5 cm diameter and two piezometers. The first Plexiglas tube is 50 cm long and filled with the fibre material, *i.e*., it represents the filter bed, while the second Plexiglas tube (1 m in length) is placed above it.

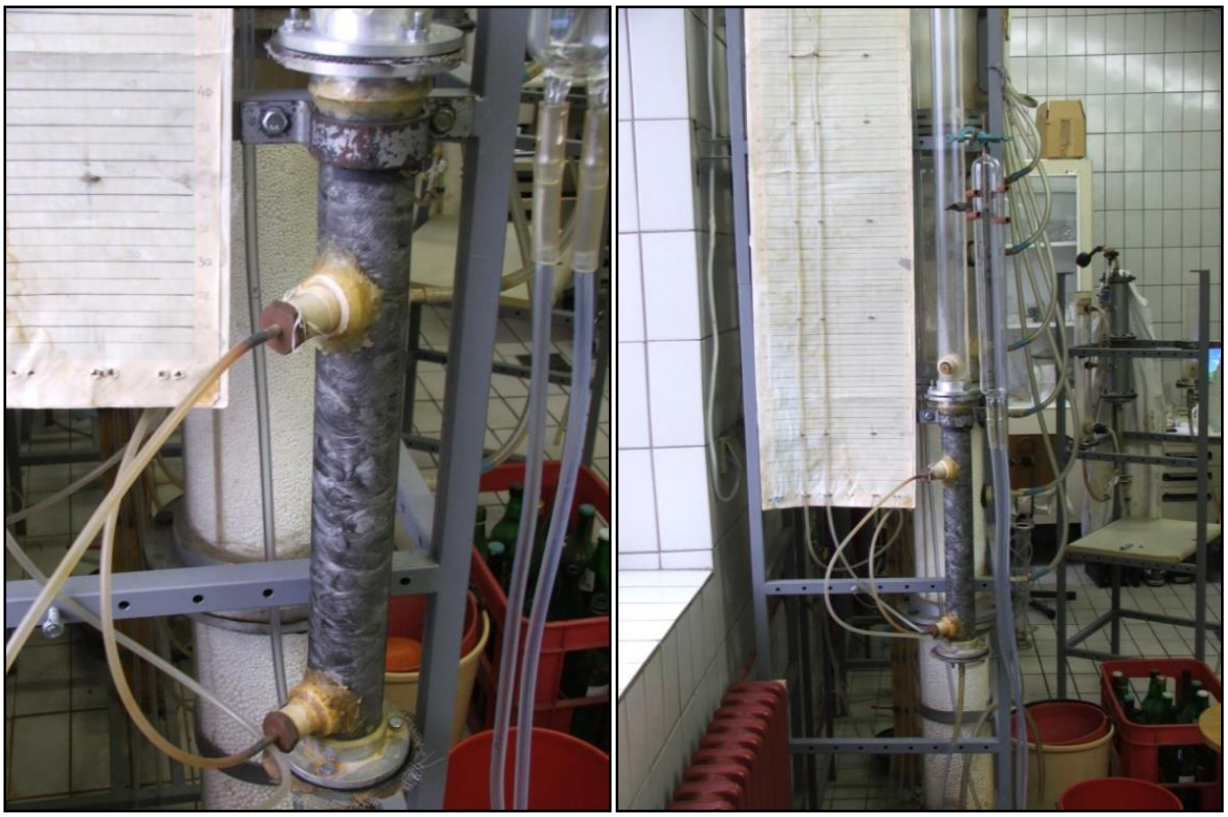

Figure 1. Experimental set up

Fibre materials applied in this research are flexible and therefore it was possible to form filter beds of different bulk densities, *i.e*. filter beds of different porosities.

The amount of fibre material, placed in the first Plexiglas tube, is determined based on the defined bed porosity. Mass of the material needed to form a filter bed of defined porosity is determined by the equation (1):

$$\varepsilon = 1 - \frac{\rho_B}{\rho} \tag{1}$$

For each new defined bed porosity, different amount of material was used, which is placed in the first Plexiglas tube. In order to ensure homogeneity of the filter bed, the measured fibre mass is divided into ten equal portions. The tube is then divided into ten segments of 5 cm in length, and filled with portions of the material, from the bottom to the top, segment by segment to ensure the bed homogeneity.

2. 3. Determination of bed porosity and bed permeability

Porosity is the fraction of empty spaces in a porous bed, *i.e*., fraction of the void volume over the total bed volume. Fluid flows through a porous bed only through connected pores. The property of porous materials that indicates an available area for fluid flow, *i.e*., the cross-sectional area available for fluid flow is called permeability [29].

Bed porosity was measured by the weighing method. The Darcy experiment was performed to determine the bed permeability for defined bed porosity.

The Darcy experiment was performed for different bed porosities, in the range from 83% to 98 % and for different fluid flowrates in the range from 30 to 600 cm^3 min^{-1}.

The pressure drop across the bed during the flow of tap water was used to determine the bed permeability for the specific bed porosity based on the Darcy law. The experiments were repeated at least three times.

3. RESULTS AND DISCUSSION

3. 1. The effect of waste fibre morphology on packing phenomena in filter beds

Fibres of cheap and free available waste materials were investigated in this study with the aim to apply these waste fibres as filter media so to contribute to sustainable development and circular economy [28].

Fibre cross-section is one of the properties that could affect geometry of the resulting packed filter bed. Fibres could have circular, triangular, rectangular, square, or irregular cross-sections. Most of the fibres used in the present investigation have circular cross-sections, that is the PP, BA1, and PE fibres. The PPDJ and SSM fibres have rectangular cross-sections, while the SS fibres, have circular or irregular cross-sections, depending on the fibre thickness (Fig. 2).

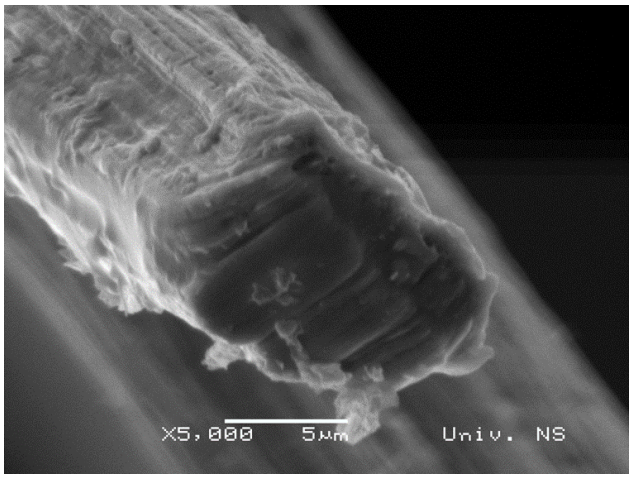

Figure 2. SEM image of the SS40 fibre cross-section (scale bar = 5 μm)

The SEM analysis has shown that most of the investigated fibres have a smooth or approximately smooth surfaces as in Figure 3 showing PU fibres clearly indicating extremely smooth surfaces and fibre interconnections. Similarly, PP fibres, exhibited smooth surfaces and uniform diameters (Fig. 4). In contrast, surfaces of stainless steel SS40 fibres are marginally wavy with slight longitudinal unevenness (Fig. 5). All other investigated materials exhibited also smooth surfaces.

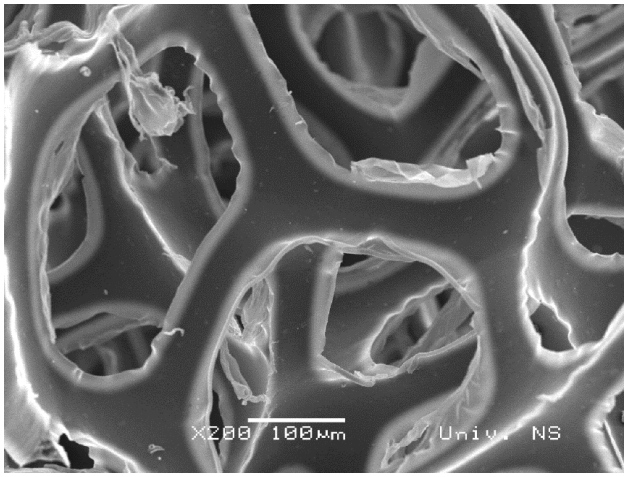

Figure 3. SEM micrograph of PU fibres (scale bar = 100 μm)

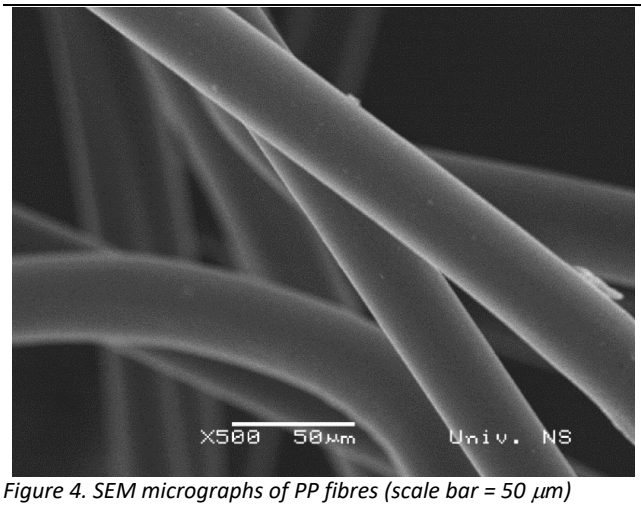

Figure 4. SEM micrographs of PP fibres (scale bar = 50 µm)

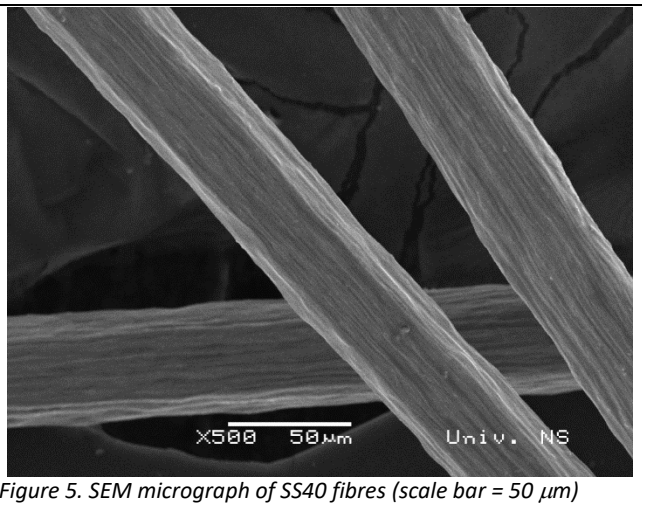

Figure 5. SEM micrograph of SS40 fibres (scale bar = 50 µm)

Diameters with SD of investigated fibre materials are presented in Table 2 showing that most of the applied fibre diameters are in the range from 12 to 44 µm. It should be noted that fibre diameters for fibres of rectangular or irregular cross-sections were approximated as circles with the same area. The exceptions are PPDJ and SSM fibres, which have much larger characteristic dimensions. As it was mentioned previously, PPDJ and SSM fibres have a rectangular cross-section, they look like wide strips, and therefore, they are defined by two characteristic lengths (Table 2). PPDJ fibres are significantly wider than SSM fibres as seen at optical micrographs of these fibres (Fig. 6).

Table 2. Fibre diameters/characteristic dimensions of investigated materials

Material	Fibre diameter ± SD, µm
Polyurethane (PU)	40 ± 4
Polypropylene (PP)	38 ± 3
Polypropylene bag (PPDJ)	1001 ± 14; 20 ± 4
Polyethylene terephthalate (BA1)	31 ± 2
Polyethylene terephthalate (PE)	38 ± 2
Stainless steel (SS40)	40 ± 2
Stainless steel (SS20)	20 ± 2
Stainless steel (SS12)	12 ± 0.8
Stainless steel sponge (SSM)	452 ± 11; 21 ± 3

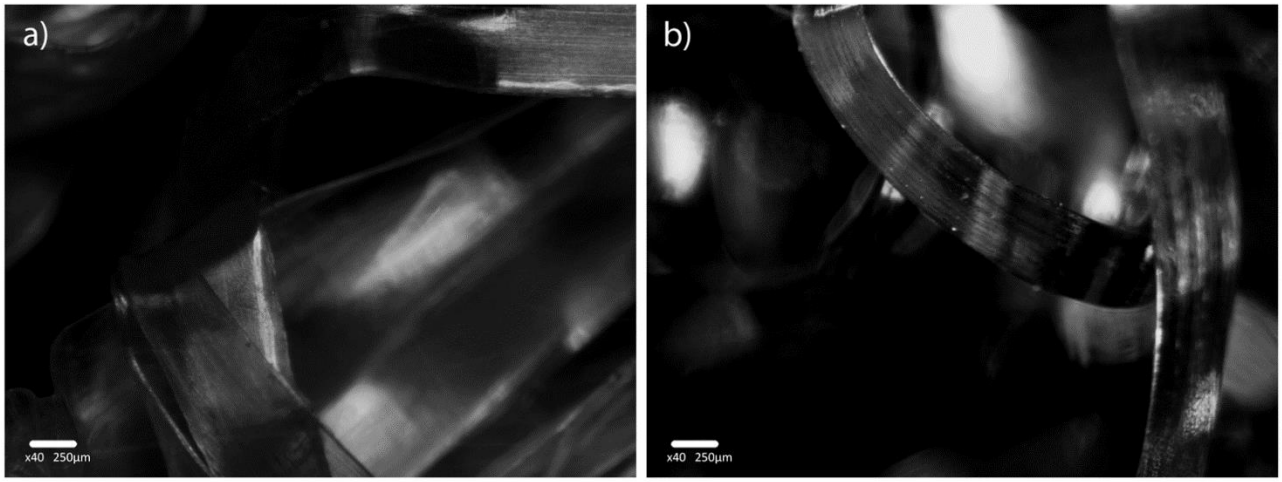

Figure 6. Optical micrographs of a) PPDJ fibres, b) SSM fibres (scale bar = 250 µm)

Visual appearance of packed fibres in filter beds with the same permeability and porosity was studied by optical microscopy. Figure 7. presents an overview of the SS40 fibre bed for permeability of 5.389×10^{-9} m^2, marked as K_{01}. Two images that are presented in this figure are taken from different angles in the fibre bed under the same conditions. It could be seen that the pores are larger in Figure 7a, than those in Figure 7b, where the fibre packing is denser. Thus, it could be concluded that the SS40 fibre material forms two different regions in the filter bed regarding the porosity and pore size due to the material rigidity.

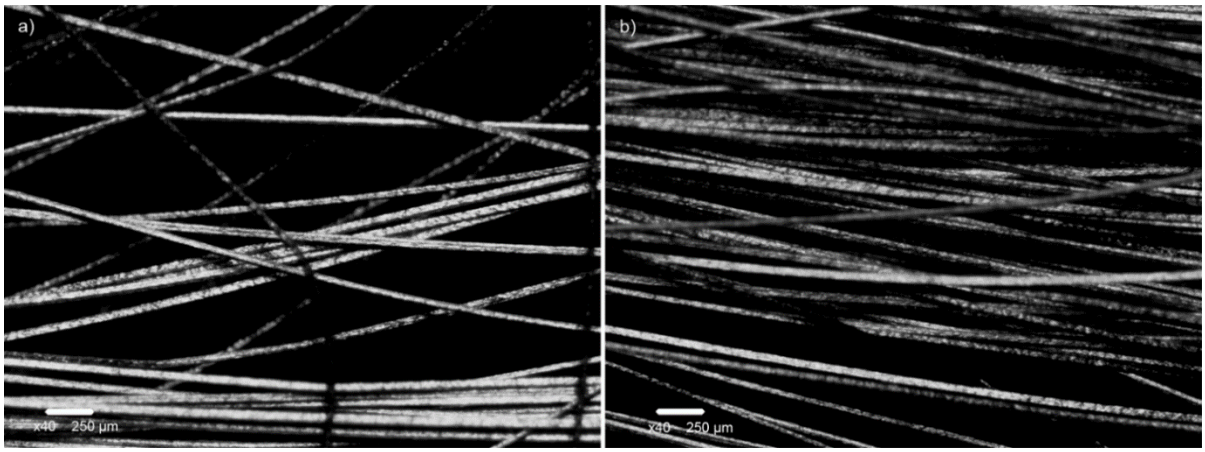

Figure 7. Optical micrographs of SS40 fibres at bed permeability K_{01}: a) region 1, b) region 2; (scale bar = 250 µm)

On the contrary, the stainless steel SS12 fibre bed at K_{01} permeability apparently has uniform pore distribution (Fig. 8). The SS12 fibres have much smaller diameters of 12 ± 0.8 µm, resulting in less rigid fibres than SS40 fibres. Therefore, the SS12 fibre bed consists of only one region, in which small and larger pores are mixed.

Figures 7 and 8 indicate that SS fibres, which differ in diameters, pack differently in the filter bed. It could be thus assumed that the diameter of stainless-steel fibres could affect their flexibility, which would directly affect fibre packing in the bed.

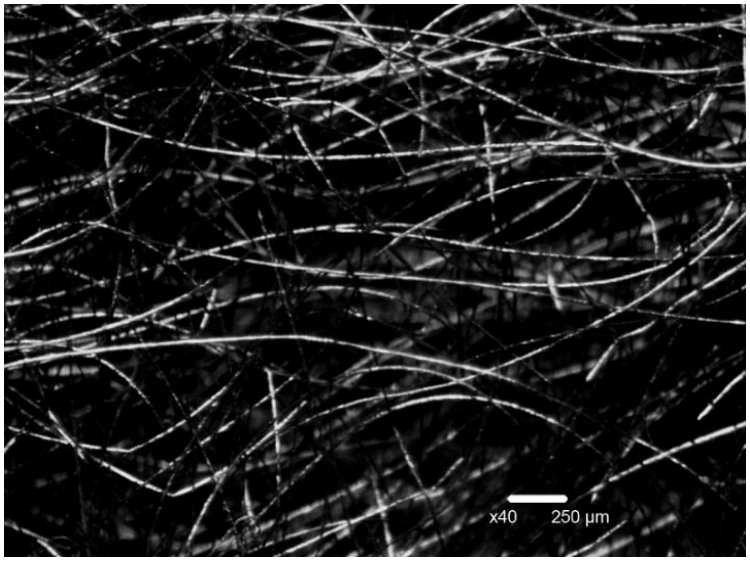

Figure 8. Optical micrograph of SS12 fibres at the permeability of K_{01} (scale bar = 250 µm)

All other investigated materials, especially polymer materials show similar pore distribution in filter bed as the SS12 filter bed (Fig. 9.)

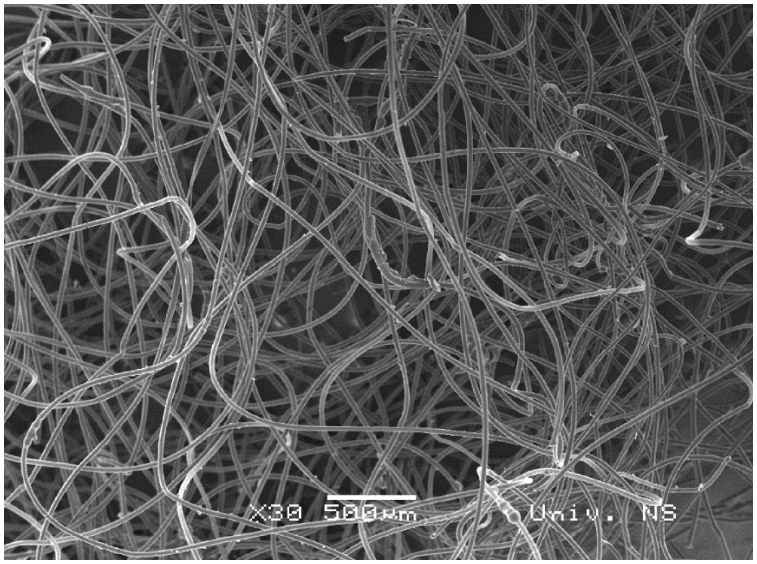

Figure 9. SEM micrograph of BA1 fibres (scale bar = 500 µm)

It should be noted that some of the investigated fibres are interconnected, such as PU fibres that form a sponge-like structure with pores in the honeycomb shape (Fig. 3). On the other hand, the PE material is composed of individual fibres that are connected at some points (Fig. 10).

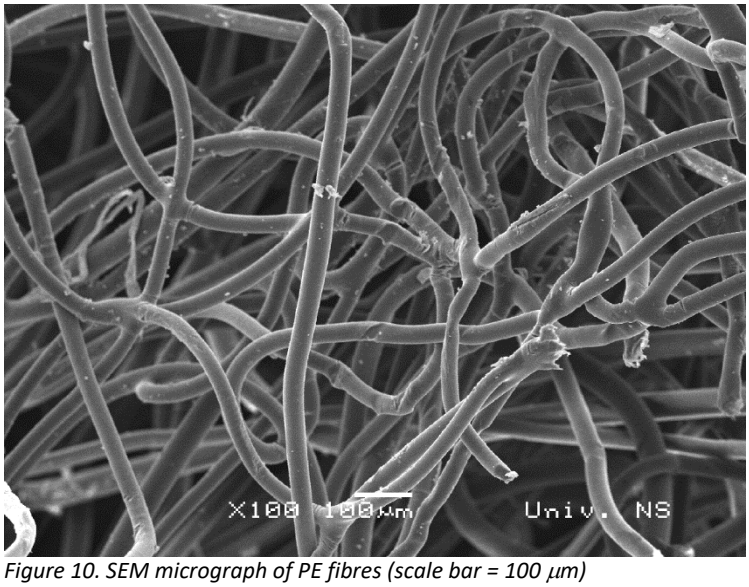

Figure 10. SEM micrograph of PE fibres (scale bar = 100 µm)

3. 2. The effect of fibre morphology on bed properties

In the previous section is seen, how different morphology influences packed bed appearance. However, the question remains whether and how these differences in the shape and dimensions of fibres reflect on the bed properties.

The investigation was conducted to define bed permeability using the Darcy's experiment for all fibre materials over different bulk densities, *i.e.* porosities. The dependence of the pressure drop per unit of bed length was linear for the entire range of investigated fluid velocities at all applied bed porosities ($R^2 \geq 0.990$). The Reynolds number was in the range from 0.01 to 0.38. The permeability values were then calculated based on the obtained slopes of the Darcy law, Eq. (2) [30]:

$$q = \frac{-kA\Delta p}{\mu L} \tag{2}$$

The pressure drop, Δp, was measured by piezometers, therefore Eq. (2) was rearranged, see Eq. (3):

$$\frac{\Delta h}{L} = \frac{b'}{\rho g} v = bv \tag{3}$$

This dependence for the PU fibre material is presented in Figure 11.

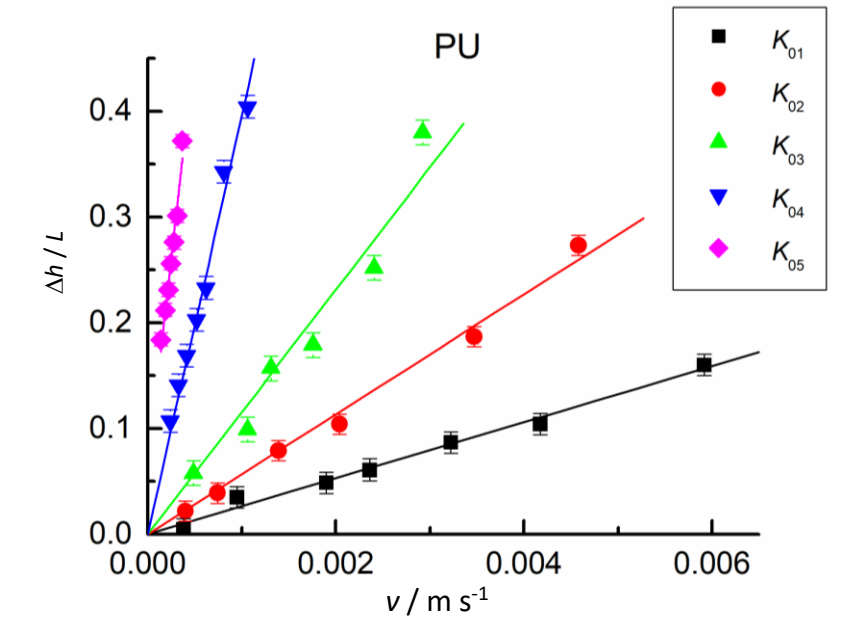

Figure 11. *Experimental data and the best linear fits of height of water column per unit of the bed length (Δh / L) dependence on the fluid velocity (v) for PU fibre beds of different permeabilities*

The obtained equations for PU filter beds and calculated values of bed permeabilities are presented in Table 3.

Table 3. The equations and R^2 values for PU fibre beds of different permeabilities

K / m^2	Equations	R^2
5.38 10^{-9} (K_{01})	$\Delta h / L$ = 26.38 ± 0.17 v	0.990
2.23 10^{-9} (K_{02})	$\Delta h / L$ = 58.60 ± 0.31 v	0.992
1.13 10^{-9} (K_{03})	$\Delta h / L$ = 125.98 ± 0.54 v	0.991
0.38 10^{-9} (K_{04})	$\Delta h / L$ = 374.23 ± 1.88 v	0.993
0.18 10^{-9} (K_{05})	$\Delta h / L$ = 791.64 ± 3.31 v	0.991

*Numbers in the equation represent slope of the line, b / s m^{-1}

Based on bed permeabilities obtained by the Darcy experiment for defined porosities, the experimental dependence of bed porosity and bed permeability for all investigated materials can be established as presented in Figure 12. This is a very beneficial result because it allows formation of a fibre bed with desired bed permeability.

It should be noted that the behaviour of all tested materials except PPDJ, fits to the same experimental curve, Eq. (4) (R^2 = 0. 9547), regardless of the studied properties of their fibres:

$$\varepsilon = 0.0366 \ln K_0 + 0.9124 \tag{4}$$

The flexibility of these fibres, their way of packaging, the connection of fibres, and their cross-section, for the investigated range, practically, do not affect the experimental dependence of porosity on permeability.

In Figure 12. it could be seen that the filter bed made of PPDJ fibres has a lower bed porosity for chosen bed permeability compared to the other investigated materials, Eq. (5). The equation for the PPDJ material (R^2 = 0.9869) is:

$$\varepsilon = 0.0393 \ln K_0 + 0.8534 \tag{5}$$

The complete set of data for PPDJ fibre beds is given in Table 4.

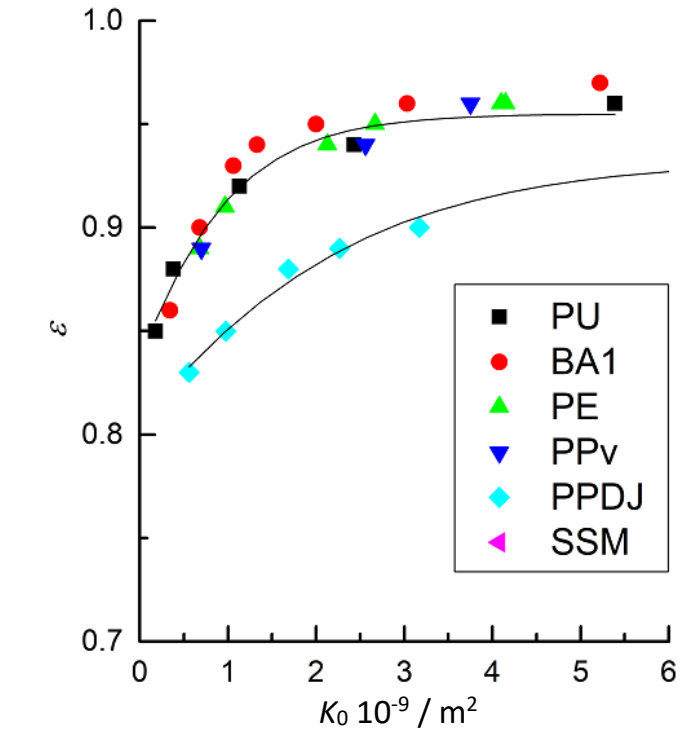

Figure 12. Experimental dependences of the bed porosity on the bed permeability for investigated materials

Table 4. Experimentally determined permeability values at different bed porosities for the PPDJ material

$K_0\,10^{-9}$ / m^2	ε
11.804	0.944
10.704	0.922
5.204	0.900
3.259	0.889
2.417	0.878
1.409	0.856
0.809	0.833

It is necessary to point out that from all investigated materials, fibres of polypropylene bags, PPDJ, have the largest dimensions. This fact can be the reason why the filter bed made of the PPDJ material has different dependence of the bed permeability on the bed porosity. Based on this result it could be concluded that the size of the fibre, has a much greater influence on bed properties than the shape of the fibre cross-section.

However, it should not be forgotten that SSM fibres are also much larger as compared to the other fibres, but still fit to the same experimental equation (4) as the other investigated materials apart from PPDJ.

4. CONCLUSION

In the investigation carried out, the studied PE, BA1, PP, and most SS fibres have circular cross-sections, the PU fibres have irregular cross-sections, while PPDJ and SSM fibres have rectangular cross-sections, which look like wide strips. The dimensions of fibres are in the range from 12 μm to 44 μm, except these of SSM and PPDJ fibres that are much larger.

The experimental dependence of the bed porosity on bed permeability was established where all investigated fibre materials yielded the same experimental equation, except for the PPDJ material, which yielded lower porosities at same permeabilities resulting in another functional dependence. The PPDJ fibres obtained from polypropylene bags have the largest dimensions, which could be the reason for the obtained differences. For all other investigated materials, the

fibre flexibility, way of packaging, the connection of fibres, and fibre cross-section, for the investigated range, practically, do not affect the experimental dependence of porosity on permeability.

The obtained experimental dependence of bed porosity on bed permeability could be used to form a bed in coalescer with predetermined, *i.e.* desired bed permeability. In this way, the bed geometry could be fixed, while the other parameters could be varied and investigated since the unknown and/or not defined bed geometry is the most common deficiency in the published literature dealing with bed coalescers, which often leads to contradictory conclusions.

NOMENCLATURE

ε - porosity
ρ_B / kg m^{-3} - bulk density
ρ / kg m^{-3} - density of material
μ / Pa·s - dynamic viscosity
Q / m^3 s^{-1} - volume flow
K / m^2 - bed permeability
A / m^2 - cross-section of filter bed
Δp / Pa - pressure drop
Δh/ cm H_20 - height of water column
L / cm - length of filter bed
b', b / s m^{-1} - the slope of the line
v / m s^{-1} - fluid velocity

Acknowledgements: The Ministry of Education, Science and Technological Development of the Republic of Serbia, Grant No. 172022, Grant No. 451-03-9/2021-14/200156, and Grant No. 451-03-9/2021-14/200134 supported the work.

We sincerely thank CEEPUS - Central European Exchange Program for University Studies for supporting the joint research by supporting the mobilities between the University of Novi Sad and TU Wien within the network "CIII-SI-0708-08-Chemistry and Chemical Engineering".

REFERENCES

[1] Spielman LA. Separation of Finely Dispersed Liquid-Liquid Suspensions by Flow through Fibrous Media. Doctoral thesis, University of California, Berkeley, United States; 1968.
[2] Spielman LA, Goren SL. Theory of Coalescence by Flow through Porous Media. *Ind Eng Chem Fundam.* 1972; 11 (1): 66-72. https://doi.org/10.1021/i160041a011
[3] Spielman LA, Goren SL. Experiments in Coalescence by Flow through Fibrous Mats. *Ind Eng Chem Fundam.* 1972; 11 (1): 73-83. https://doi.org/10.1021/i160041a012
[4] Amrei MM, Venkateshan DG, D'Souza N, Atulasimha J, Tafreshi HV. Novel Approach to Measuring the Droplet Detachment Force from Fibers. *Langmuir*. 2016; 32 (50): 13333-13339. https://doi.org/10.1021/acs.langmuir.6b03198
[5] Bhattad P, Willson CS, Thompson KE. Effect of network structure on characterization and flow modeling using X-ray micro-tomography images of granular and fibrous porous media. *Transp Porous Media.* 2011; 90 (2): 363-391. https://doi.org/10.1007/s11242-011-9789-7
[6] Bradford SA, Torkzaban S. Colloid interaction energies for physically and chemically heterogeneous porous media. *Langmuir.* 2013; 29 (11): 3668-3676. https://doi.org/10.1021/la400229f
[7] Dawar S, Chase GG. Correlations for transverse motion of liquid drops on fibers. *Sep Purif Technol.* 2010; 72 (3): 282-287. https://doi.org/10.1016/j.seppur.2010.02.018
[8] Elimelech M, Chen JY, Kuznar ZA. Particle Deposition onto Solid Surfaces with Micropatterned Charge Heterogeneity: The "Hydrodynamic Bump" Effect. *Langmuir.* 2003; 19 (17): 6594-6597. https://doi.org/10.1021/la034516j
[9] Sokolović D, Govedarica D, Šećerov-Sokolović RM. Review: Influence of fluid properties and solid surface energy on efficiency of bed coalescence. *Chem Ind Chem Eng Q.* 2018; 24 (3): 210-230. https://doi.org/10.2298/CICEQ170304034S
[10] Shou D, Fan J, Zhang H, Qian X, Ye L. Filtration Efficiency of Non-Uniform Fibrous Filters. *Aerosol Sci Technol.* 2015; 49 (10): 912-919. https://doi.org/10.1080/02786826.2015.1083092
[11] Zhu P, Kong T, Tian Y, Tang X, Tian X, Wang L. Superwettability with antithetic states: Fluid repellency in immiscible liquids. *Mater Horiz.* 2018; 5 (6): 1156-1165. DOI: 10.1039/c8mh00964c

[12] Herminghaus S. Roughness-induced non-wetting. *Europhys Lett.* 2000; 52 (2): 165-170. https://doi.org/10.1209/epl/i2000-00418-8
[13] Miwa M, Nakajima A, Fujishima A, Hashimoto K, Watanabe T. Effects of the surface roughness on sliding angles of water droplets on superhydrophobic surfaces. *Langmuir* 2000; 16 (13): 5754-5760. https://doi.org/10.1021/la991660o
[14] Xia F, Jiang L. Bio-inspired, smart, multiscale interfacial materials. *Adv Mater.* 2008; 20 (15): 2842-2858. https://doi.org/10.1002/adma.200800836
[15] Zhang P, Wang S, Wang S, Jiang L. Superwetting surfaces under different media: Effects of surface topography on wettability. *Small.* 2015; 11 (16): 1939-1946. https://doi: 10.1002/smll.201401869
[16] Yohe ST, Freedman JD, Falde EJ, Colson YL, Grinstaff MW. A Mechanistic Study of Wetting Superhydrophobic Porous 3D Meshes. *Adv Funct Mater.* 2013; 23 (29): 3628-3637. https://doi.org/10.1002/adfm.201203111
[17] Viswanadam G, Chase GG. Contact angles of drops on curved superhydrophobic surfaces. *J Colloid Interface Sci.* 2012; 367: 472-477. https://doi.org/10.1016/j.jcis.2011.11.004
[18] Davoudi M, Fang J, Chase GG. Barrel shaped droplet movement at junctions of perpendicular fibers with different orientations to the air flow direction. *Sep Purif Technol.* 2016; 162: 1-5. https://doi.org/10.1016/j.seppur.2016.02.009
[19] Šecerov Sokolović RM, Vulić TJ, Sokolović SM, Marinković-Nedučin RP. Effect of fibrous bed permeability on steady-state coalescence. *Ind Eng Chem Res.* 2003; 42 (13): 3098-3102. https://doi.org/10.1021/ie020361i
[20] Šećerov Sokolović R, Stanimirović O, Sokolović S. The influence of fibrous bed bulk density on the bed properties. *Hem Ind.* 2003; 57 (7-8): 335-340. (in Serbian) https://doi.org/10.2298/HEMIND03083355
[21] Agarwal S, von Arnim V, Stegmaier T, Planck H, Agarwal A. Role of surface wettability and roughness in emulsion separation. *Sep Purif Technol.* 2013; 107: 19-25. https://doi.org/10.1016/j.seppur.2013.01.001
[22] Agarwal S, von Arnim V, Stegmaier T, Planck H, Agarwal A. Effect of Fibrous Coalescer geometry and operating conditions on emulsion separation. *Ind Eng Chem Res.* 2013; 52 (36): 13164-13170. https://doi.org/10.1021/ie4018995
[23] Fahim M, Othman F. Coalescence of secondary dispersions in composite packed beds. *J Dispers Sci Technol.* 1987; 8 (5-6): 507-523. https://doi.org/10.1080/01932698708943620
[24] Das D, Ishtiaque SM, Das S. Influence of fibre cross-sectional shape on air permeability of nonwovens. *Fiber Polym*. 2015. 16 (1) 79-85. https://doi.org/10.1007/s12221-015-0079-9
[25] Šećerov Sokolović RM, Govedarica DD, Sokolović DS. Selection of filter media for steady-state bed coalescers. *Ind Eng Chem Res.* 2014; 53 (6): 2484-2490. https://doi.org/10.1021/ie404013e
[26] Kiralj A, Vulić T, Sokolović D, Šećerov Sokolović R, Dugić P. Separation of oil drops from water using stainless steel fiber bed. *Chem Ind Chem Eng Q.* 2017; 23 (2): 269-277. https://doi.org/10.2298/CICEQ160610041K
[27] Govedarica DD, Šećerov-Sokolović RM, Kiralj AI, Govedarica OM, Sokolović DS, Hadnađev-Kostić MS. Separation of mineral oil droplets using polypropylene fibre bed coalescence, *Hem Ind.* 2015; 69 (4): 339-346. https://doi.org/10.2298/HEMIND140322047G
[28] Srđan S. Sokolović, Arpad I. Kiralj, Dunja S. Sokolović, Aleksandar I. Jokić, Application of waste polypropylene bags as filter media in coalescers for oily water treatment, *Hem Ind*. 2019; 73 (3) 147-154 https://doi.org/10.2298/HEMIND190311013S
[29] Das, D., Ishtiaque, S.M., Das, S. Influence of fibre cross-sectional shape on air permeability of nonwovens. *Fiber Polym*. 2015; 16: 79-85. https://doi.org/10.1007/s12221-015-0079-9
[30] Cerepi A., Burlot R., Galaup S., Barde J. –P., Loisy C., Humbert L., Effects of porous solid structures on the electrical behaviour: prediction key of transport properties in sedimentary reservoir rock, *Stud Surf Sci Cat.* 2002;144: 483-490. https://doi.org/10.1016/S0167-2991(02)80171-9

Uticaj morfologije vlakana na fenomen pakovanja i svojstva sloja u koalescerima

Milica Hadnađev Kostić[1], Dunja Sokolović[2], Srđan Sokolović[3], Thomas Laminger[4, 5] i Arpad Kiralj[1]

[1]Univerzitet u Novom Sadu, Tehnološki fakultet, Bul. Cara Lazara 1, Novi Sad, Srbija
[2]Univerzitet u Novom Sadu, Fakultet tehničkih nauka, Trg Dositeja Obradovića 6, Novi Sad, Srbija
[3]NIS a.d. Novi Sad, Srbija, Narodnog fronta 12, Novi Sad, Srbija
[4]Tehnički Univerzitet u Beču, Institut za hemijsko inženjerstvo, Austrija TU WIEN, Getreidemarkt 9/166, A-1060 Beč, Austrija
[5]AGRANA Stärke GmbH - Werk Pischelsdorf, Industriegelände, 3435 Pischelsdorf, Austrija

(Stručni rad)

Izvod

U ovom radu ispitivana je morfologija vlakana otpadnih materijala i njihov uticaj na fenomen pakovanja i svojstva filtracionog sloja u koalescerima. Ispitivano je devet otpadnih materijala. Skenirajućom elektronskom mikroskopijom utvrđeno je da su površine svih vlakana glatke, dok se poprečni presek razlikuje od kružnog, pravougaonog do nepravilnog. Vlakna kružnog poprečnog preseka imala su prečnike u opsegu od 12±0,8 do 40±4 μm, dok su vlakna polipropilenskih vreća i vlakna sunđera od nerđajućeg čelika bila trake, širine 452±11 i 1001±14 μm, redom. Takođe, je primećeno da su poliuretanska vlakna povezana formirajući sunđerastu strukturu, dok su vlakna polietilen tereftalata samo na nekim mestima međusobno povezana. U ovom radu ustanovljena je eksperimentalna zavisnost poroznosti sloja od permeabilnosti sloja za sve ispitivane materijale, što omogućava formiranje sloja vlakana željene permeabilnosti. Izuzetak je sloj formiran od vlakana polipropilenskih vreća koja su najvećih dimenzija tako da je ovaj sloj pokazao različitu zavisnost poroznosti od permeabilnosti sloja u odnosu na ostale ispitivane materijale.

Ključne reči: propustljivost sloja, poroznost sloja, sloj vlakana, koalescentna filtracija

Energy plants as biofuel source and as accumulators of heavy metals

Magdalena Nikolić[1], Vladimir Tomasević[1] and Dragan Ugrinov[2]

[1]School of Engineering Management, University Union Nikola Tesla, Bulevar vojvode Mišića 43, 11000 Belgrade, Serbia
[2]Institute of Public Health, Pančevo, Pasterova 2, Pančevo, Serbia

Abstract

Fossil fuel depletion and soil and water pollution gave impetus to the development of a novel perspective of sustainable development. In addition to the use of plant biomass for ethanol production, plants can be used to reduce the concentration of heavy metals in soil and water. Due to tolerance to high levels of metals, many plant species, crops, non–crops, medicinal, and pharmaceutical energy plants are well-known metal hyperaccumulators. This paper focuses on studies investigating the potential of *Miscanthus* sp., *Beta vulgaris* L., *Saccharum* sp., *Ricinus communis* L. *Prosopis* sp. and *Arundo donax* L. in heavy metal removal and biofuel production. Phytoremediation employing these plants showed great potential for bioaccumulation of Co, Cr, Cu, Al, Pb, Ni, Fe, Cd, Zn, Hg, Se, *etc*. This review presents the potential of lignocellulose plants to remove pollutants being a valuable substrate for biofuel production. Also, pretreatments, dealing with toxic biomass, and biofuel production are discussed.

Keywords: pollutants; bioaccumulation; bioenergy.

Available on-line at the Journal web address: http://www.ache.org.rs/HI/

TECHNICAL PAPER

UDC: 620.925:58:332.368

Hem. Ind. **76(4)** 209-225 (2022)

1. INTRODUCTION

Heavy metals and metalloids present a great problem because they cannot be degraded in nature, therefore upon release they enter the natural biogeochemical cycles. The sources of these pollutants are the metallurgical and petrochemical industries, municipal landfills, wastewaters, fertilizers, pesticides, burning fossil fuels emissions, *etc*. The threat that heavy metals present causes decreased quantity and quality of crop yields and agricultural products, and loss of fertile soil, freshwater, and ecosystems [1]. Furthermore, problems related to energy and environmental protection are one of the burning issues in the 21st century [2]. Biogas/biomethane represent the future of green energy. The world's energy consumption should be taken into account the pollution caused by the use of fossil fuels accompanying the growth of total energy consumption [3]. Uncontrolled human activity, as well as energy consumption, has led to an increase in environmental pollution. Therefore, the use of energy plants in phyto and bioremediation could be a sound solution for a cleaner future [4]. Some plants have natural resistance and the ability to accumulate heavy metals in their tissues without symptoms of poisoning [5]. Phytoremediation is a green technology that is widely accepted due to its natural removal of pollutants [6]. The presence of heavy metals in the soil harms the growth and development of plants, as well as the loss of mineral balance, and thus the loss of yield and crop quality [7]. Increased interest in energy crops stems from their potential use as a carbon-neutral and environmentally friendly renewable and sustainable power resource [8]. Energy crops can be divided into two groups. The first group of annuals includes sweet and fiber sorghum, kenaf, and oilseed rape. While the second group of perennials is further classified into agricultural, such as wheat, sugar beet, cardun, reed, miscanthus, *etc.* and forest species: willows, poplars, eucalyptus, and black grasshopper [9]. Increased bioenergy demands, as well as a noticeable tendency towards renewable energy sources, have conditioned the increasing use of biomass. In line with this, sound solutions should be within the energy crops for biofuels and biomethane production [8], thus used in sustainable phytoremediation of metal-contaminated soils [10,11]. Short rotation coppice (SRC) are energy plants with a high ability to remediate heavy metals and organicpollutants. The advantage of using these plants is in their viability is up to 30 years before replanting [12].

Corresponding authors: Magdalena Nikolić, School of Engineering Management, University Union Nikola Tesla, Bulevar vojvode Misica 43, 11000 Belgrade, Serbia
E-mail: magdalena.nikolic@fim.rs
Paper received: 2 April 2022; Paper accepted: 7 November; Paper published: 5 December 2022
https://doi.org/10.2298/HEMIND220402017N

1. 1. Phytoremediation capacities of energy plants

The synergy of potential energy crops in phytoremediation programs is a new direction in obtaining energy sustainability. It includes the creation of new bioenergy resources and the phytoremediation of contaminated land. The reason for the use of some energy crops is reflected in their high phytoremediation potential. These are primarily *Miscanthus* sp.*, Ricinus* sp.*, Jatropha* sp. and *Populus* sp. Furthermore, the popularization of phytoremediation has contributed to a better insight into the process of removing pollutants from the environment. A wide range of physical, chemical, and biological remediating processes such as soil washing, chemical, and physical solidification/stabilization, chemical oxidation or reduction, *etc*. are used but marked as invasive. Due to resource and financial conservation strategies, environmental protection strategies such as green remediation/ phytoremediation have been recognized as promising [13]. Therefore, it is believed that energy crops would contribute not only to energy but also to environmental stability [14]. Recently, heavy metal removal by energy plants has been linked to thermochemical treatments. The method of valorizing contaminated biomass from phytoremediation and increasing metal and energy recovery are gaining attention. Biochemical conversion coupled with thermal treatment enables the extraction of Hg and Cd from biomass before further processing. Therefore, bioenergy plants are used to remove pollution and produce biofuels [15].

1. 2. Prerequisites for biofuel production

Lignocellulosic biomass (LCB) is composed of cellulose, hemicellulose, and lignin polymers, in which the ratio of the polymer depends on their origin [16]. Biochemical conversion of plant biomass into biofuels and biomaterials includes a pretreatment, via a combination of ozonolysis, alkaline, or acids, before enzymatic hydrolysis of polysaccharides into sugars [17,18]. After that step, sugars are converted to fuel molecules or other biomaterial molecules yeast or bacteria [19].

2. PHYTOREMEDIATION AND BIOFUEL PRODUCTION OF ENERGY PLANTS

2. 1. *Miscanthus.* sp

2. 1. 1. Phytoremediation

Miscanthus sp. is related to warmer regions, although one perennial species *Miscanthus gigantheus* can withstand harsh weather conditions in Central Europe [22]. *Miscanthus spp* is shown to be a promising genus for biofuel production regarding its lignocellulose content. *M* × *giganteus*, *M. sacchariflorus*, and *M. sinensis* clones were investigated by Arnoult *et a*l. [23]. *Miscanthus* is recognized as a poor heavy metal bioaccumulation plant. However, it has bioaccumulation potential for Cd, Cr, Cu, Ni, Pb, and Zn. It was reported that *M. sacchariflorus* heavy metal oncentration was 10, 2, and 20 ppm for Zn, Cd, and Pb, respectively. Furthermore, *M. sacchariflorus* biomass production was not disrupted in sewage sludge with the presence of Fe, Mn, Mo, B, Ba, Sr, As, Sn, Li, and Ti [24]. This plant, in particular, *M. × giganteus* J. M. Greef & Deuter ex Hodk. & Renvoize and *M. Sinensis* are also known as excellent phytoremediation species [12, 25-27]. The phytoremediation potential of *Miscanthus giganteus* grown on soil contaminated with Hg and Cd was reflected in resistance to cadmium (45–6758 μg kg $^{-1}$), and mercury (8.7–108.9 μg kg $^{-1}$). It was also found that in three years *Miscanthus giganteus* accumulated up to 293.8 μg Cd and 4.7 μg Hg per year in aboveground biomass, without a significant impact on biomass growth and productivity [27]. *M. giganteus* sequestrates inorganic pollutants in roots. According to Zhao *et al*. [26], *Miscanthus sinensis* is also a very suitable candidate for phytoremediation of soil contaminated with a high concentration of Hg (up to 706 mg kg^{-1}). Positive effects of *M. sinensis* on the diversity and abundance of soil microbial community are shown, also essential for phytostabilisation and phytoextraction [26]. Germaine *et al*. [28] showed the link between microbial communities (*Proteobacteria, Pseudomonas, and Acineto-bacter)* and 11 *Miscanthus*. sp rhizomes in organic pollutant removal. Moreover, the aboveground biomass (AGB) increase of *Miscanthus* species was related to the presence of endophyte bacterium. The presence of *Pseudomonas koreensis* AGB1 increased *Miscanthus sinensis* AGB by 54 %, [29]. *Miscanthus sinensis* compared with *M. × giganteus* showed a better ability to grow on soil contaminated with inorganic pollutants, and a high capacity for removal of organic pollutants. *M. × giganteus* showed a high ability to grow on soil contaminated with Cd, Zn, and Pb. Opposite

M. × giganteus, M. sinensis showed a high ability to remove organic pollutants [25]. *Miscanthus genotypes: M. x giganteus, M. sinensis,* and *M. floridulus* are good candidates for Zn, Cr, and Cd removal [30].

2. 1. 2. Biofuel production

Miscanthus cell wall contains 32.7 to 49.5 % cellulose, 21 to 34.8 % hemicellulose, and 17.8 to 27.7 % lignin [31]. According to Kricka *et a*l. [32], *Miscanthus × giganteus* with 41 % cellulose content can be used in both liquid and solid biofuel production. In a line with this Lee and Kuan, [31], determined that *Miscanthus floridulus*, *Miscanthus sinensis*, *Miscanthus sacchariflorus,* and *Miscanthus × giganteus* cellulose content of 37.2, 37.6, 38.95, 41 wt.% respectively, 0.233, 0.221, 0.213, 0.211, and 0.233 g of bioethanol, respectively. Application of 1 % NaOH at 121 °C for 60 min on *Miscanthus ×giganteus* and *M. sinensis 'Gracillimus'*, resulted in 34.1 and 30.0 % glucan and 11.3 and 13.6 % xylan contents, respectively. Interestingly, *Miscanthus* x g biomass can be used for high-quality briquettes. The method applied was the pressure agglomeration process a hydraulic briquette machine with an open hydraulic working chamber. Energy potential estimation was more than 17.5 MJ kg^{-1} [33]. Furthermore, instead of ethanol, products of fermentation can be isobutanol if fermentation is performed with *Clostridium sp*. Compared to ethanol, isobutanol has a higher energy density, and low absorption of moisture from the air, therefore it is less corrosive [34-36]. As the pretreatment thermochemical saccharification by H_2SO_4 or NaOH was used. Biological saccharification and fermentation included two anaerobic bacteria *Fibrobacter succinogenes* and *C. acetobutylicum.* Application of 100 mol m^{-3} H_2SO_4 resulted in 44.4 ± 8.5 g m^{-3} ethanol and 19.7 ± 3.5 g m^{-3} buthanol, while with 200 mol m^{-3} NaOH 39.7 ± 8.6 g m^{-3} ethanol and 4.3 ±0.33 g m^{-3} buthanol were produced [36].

2. 2. *Beta vulgaris* L.

2. 2. 1. Phytoremediation

Sugar beet (*Beta vulgaris* L.) is a plant whose wide genetic variation reflects adaptive morpho-physiological features under moderate and severe drought conditions [37] and high heavy metal presence [38,39]. Specifically, an efficient antioxidant system and redox signaling within some genotypes enable *B. vulgaris* tolerance to drought stress [37]. *Beta vulgaris* L. var. *cicla*. is a plant of large biomass with a short growth period and high Cd uptake and accumulation potential [39] Papazoglou and Fernando [38] suggest that sugar beet plants are proven to grow in soil containing diethylenetriamine pentaacetic acid, DTPA-extractable Cd and Ni concentrations up to 236 and 75.4 mg kg^{-1} respectively, given the same biomass quality as those grown in soil without high metal concentrations. Enhanced extraction of Cd can be achieved by adding organic amendments such as cornstalk biochar. Biochar at the concentration of 5 %, decrease the DTPA-extractable Cd concentration compared to *B. vulgaris* grown on soil without the presence of biochar. Results indicate growth of about 267 % of root dry mass and an increase in Cd plant accumulation of 206 %. Notably, there was an increase in matter-bound Cd and residual Cd, and a decrease of Fe–Mn oxides-bound Cd of about 40 % [39]. Furthermore, biochar increases the C / N ratio, up to 400, while a ratio of approximately 20 represents the threshold for N Immobilization in organic materials [40]. This species exposed to high concentrations of zinc sulfate in the nutrient solution (50, 100, and 300 µM) showed signs of reduction in total biomass (root and shoot) [41].

2. 2. 2. Biofuel production

Climate change has contributed to the setting of specific targets related to alternative renewable energy sources. The European Union has extended the use of energy crops such as sugar beet as raw materials to produce ethanol and methane. The high concentration of easily fermentable compounds has given the use of sugar beet a special place. Glucose fermentation is essential for ethanol production. Being placed as a part of a sugar factory, a factory for ethanol production, apart from glucose, uses raw or thick juice. To gain quality fuel, beetroot quality is crucial, the same as used in sugar production. The plant potential in biogas production is linked to the crude nutrient amount, low lignin, and the same amount of hemicellulose and pectin [42,43]. Sugar beetroots contain 23–24 %, dry matter from which the largest part is organic (easily-decomposable carbohydrates, the N-free solutes). A small part of crude fiber such as lignin does not exhibit potential for the ethanol production fermentation process, in contrast to sugar beet leaves that can be used

as a biofuel feedstock. The enzymatic liquefaction (pectinase and cellulase enzymes) was used for increased fermentable sugar recovery [44-46]. Surprisingly, investigation of sugar concentration in different species varieties to methane production to only dry matter importance, not sugar concentration. One report regarding this plant goes into reducing greenhouse effects with biofuel production. Carbon Intensity (CI) is used to measure all greenhouse gas emissions associated with the life cycle assessment (LCA) of a fuel. Additionally, CI sugar beet ethanol was 28.5 g CO_2e/ MJ_{EtOH} (Carbon Dioxide Equivalent/Conversion rates (Efficiencies)). This study presents an energy analysis of sugar beet-based ethanol production and CO_2 emissions [47]. The current production of table sugar or sucrose amounts to 160 million tons of sugar per year [48]. Sugar beet sucrose content was conditioned, therefore enabling the production of 100 to 120 L ethanol per t of sugar beet or approximately 5000 L/ha in mild climates [47-48].

2. 3. *Saccharum* sp.

2. 3. 1. Phytoremediation

According to the US Department of Agriculture *Saccharum sp.* contains thirteen species [49]. Sugarcane (*Saccharum officinarum* L.) is a recognized phytoremediation plant due to its biomass abundance, fast growth, and moderate uptake and accumulation of heavy metals such as Cu, Cd, Se, Pb, and Mn [50-52]. The *Saccharum officinarum* L. plant was found to be a good phytoremediator of lindane-rich garden soil, with degraded 600 mg L^{-1} of lindane. The efficiency of sugarcane was enhanced by root-inoculation with yeast Candida VITJzN04 because yeast produces growth hormone and solubilizes insoluble phosphates [53]. Therefore, the lindane-removal rates by sugarcane baggase bio-stimulated with yeast has the shortest $t_{1/2}$ (half-life period) for lindane degradation 7.1 days, compared with 13.3 days (yeast), 43.3 days (Saccharum) [53]. Furthermore, *Saccharum officinarum* L. is also used in fluoride (F^-), and bioaccumulation. The Sugarcane potential was estimated at 1000–1200 mg F^- kg^{-1} dry weight [55]. Furthermore, *Saccharum officinarum* L. was also able to remove fluoride from an aqueous environment [56].

The root zones of *S. officinarum* were amended with *Aspergilus flavus, Paecilomyces sp., Mucor sp., Penicillium sp.,* and *Trihoderma viride* efficiently degraded petroleum hydrocarbon from crude oil contamination [57]. Also, *S. officinarum* growth and development are influenced by the Fe soil content. Therefore, a study regarding the Fe accumulation potential of a plant showed that the addition of Fe-EDDHA (the chelate ferric-ethylenediamine-N, N'-bis(2-hydroxyphenyl acetic acid) increased accumulation of Fe [58]. Sugarcane exposure to copper-based compounds/nano-materials showed good bioaccumulation potential. The performed studies indicate an increased rate of Cu bioaccumulation. Translocation of Cu from the roots to the aerial parts enhanced to some extent with copper level. Therefore, an increase in the bioavailability of Cu in the soil treated with higher Cu levels could be a probable reason for that phenomenon [59]. Increased uptake of polychlorinated biphenyls (PCBs) and cadmium by *Saccharum officinarum* L. was achieved by adding tea saponin. Application of 0.01 % saponin significantly increased the uptake of PCB, while 0.3 % tea saponin assisted in increasing the uptake of Cd in roots, stems, and leaves by 96.9, 156.8, and 30.1 %, respectively [60]. In partially consolidated bioprocessing, which involved enzymes laccase (*Pleurotus djamor*) and holocellulase (*Trichoderma reseei* RUT C30), *Saccharum spontaneum* L. and *Saccharum spontaneum* biomass has been transformed into 62 g dm^{-3} ethanol.

Saccharum spontaneum L. known as wild sugarcane or kans grass showed apart from the ability to grow on heavy metal polluted sites, great efficiency to clean fly ash dumps, acid mine dumps, and sewage sludge [61,62]. *S. spontaneum* the rhizosphere amended with phosphate-solubilizing bacteria *Bacillus anthracis* strain MHR2, *Staphylococcus sp.* strain MHR3, and *Bacillus sp.* strain MHR4 showed potential in heavy metal removal from dumpsites [63]. The accumulation of Cu, Sn, and Pb/Zn are due to the adaptability of the plant to tailing environments. Exposure to different concentrations of Pb in soil (0, 100, 250, 500, and 1000 mg kg^{-1}) did not induce macro-toxicity in plants except for the highest Pb concentration used. Also, a greater amount of Pb was found in roots compared to shoots [64]. *Saccharum munja* L., a plant of the same genus, can grow on metal-contaminated coal fly ash dumps and exhibits a high capacity for heavy metal removal. Biological accumulation coefficient/factor (BAC) was defined as the concentration of heavy metals in plant shoots divided by the heavy metal concentration in soil [BAC = $c_{\text{Metal in plant shoot}}/c_{\text{Metal in soil}}$] and indicates the ability of plants to tolerate and accumulate heavy metals. In Zn, Pb, Cu, Ni, Cd, and As removal by *S. spontaneum*,

bioaccumulation factors were 8.01, 1.40, 3.02, 0.92, 1.66, and 1.47 mg dm^{-3}, respectively. *S. munja* bioaccumulation factors were higher indicating better perspectives in using this plant, amounting to 8.54, 1.66, 3.24, 0.76, 1.63, and 1.41 mg dm^{-3}, respectively [65]. Furthermore, *Saccharum arundinaceum* (Retz.) is used for cleaning the soil from heavy metal contamination around mining areas, farmland, *etc*. A mitigating circumstance in this process is the presence of sulfuric acid as a result of acid mine drainage when the mining activities expose sulfur-bearing minerals to atmospheric oxygen, moisture, *etc*. Thus, *S. arundinaceum* had the advantages of accumulating metals Cu, Zn, Pb, and Cd, with the emphasis on Cu because of the presence of strong acid in the mining soil environment [66].

2. 3. 2 Biofuel production

In a study by Kataria and Ghosh [71], *S. spontaneous* was pretreated with cellulolytic enzyme from *Trichoderma reesei*, followed by bioconversion to bioethanol performed with *Saccharomyces cerevisiae*. The total estimated bioethanol production was 0.46 g g^{-1}. Also, *Saccharum spontaneum* saccharification with *A. oryzae* enzymes with subsequent fermentation with *Pichia stipitis* NCIM3498 resulted in 0.38 g g^{-1} bioethanol production [72]. *Saccharum arundinaceum* subjected to simultaneous treatment with 3 enzymes (laccase, cellulase, and β-glucosidase) showed a great saccharification outcome of 205 ± 3.73 mg g^{-1} total reducing sugar, with the final ethanol concentration of 4.18 ± 1.14 g dm^{-3} [73].

2. 4. *Ricinus communis* L.

2. 4. 1. Phytoremediation

Ricinus communis L., commonly termed Castor, is well known for its ability to grow under harsh conditions. These include floods, extreme pH, high temperature, high salt content, harmful microorganisms, fungi, nematodes, and insects as well as smog, and SO_2 [75,76]. This plant with high oil content is not only considered an energy crop but also good wastelands remediator because of its high biomass productivity, comparable to *Brassica juncea* [77,78], as well as high antioxidant content and heavy metal bioaccumulation capacity [79]. Both stem and leaf flavonoid content enables good antioxidant activity [80]. *Ricinus communis* L. was shown in different studies to exhibit the potential to remove Cd [77], Ni, Zn, Fe [78], and Pb [81], and to tolerate Cu, Fe, Mn, and Zn [82,83]. Furthermore, *R.communis* removes organic contaminants like pesticides [84]. At places like different types of Cu-mine soils and slags rich in Cu, As, Fe, and Zn, Castor showed good bioaccumulation capacity [85]. Also, mine tailings are sources of a wide range of heavy metals (Cu, Zn, Mn, Pb, and Cd) [86]. Furthermore, Castor successfully removed Pb, Cd, and Zn at more than 70 %, and reduced BOD, and COD values in wastewater [87]

2. 4. 2 Biofuel production

Ricinus communis L. is a highly valuable plant for biofuel production [87]. The biomass carbon content is between 40 and 43 %, which nominates this plant for biogas production [88]. According to Sharma *et al.* [89], pretreatment of lignocellulosic substrates by the Dattas method enhances biogas (methane) production. For untreated and treated *R. communis* the maximum yield biogas production was 86.6 and 120.9 l kg^{-1} respectively, and methane content was 44.2 and 50.9 % respectively. Greenhouse gas (GHG) emission using compressed natural gas (CNG) as a primary fuel and castor (*Ricinus communis*) oil methyl ester (COME) was evaluated in a study by Mahla and Dhir, [90]. The study aimed to show GHG release using various blends (B10 and B20), where B20 fuel is a blend of 20 % biodiesel and 80 % conventional diesel, and B10 fuel is a blend of 10 % biodiesel and 90 % conventional diesel. Research showed increased NO_x and HC emissions, whereas CO emissions decreased by 31.6 and 37.4 % for B20-CNG and D-CNG. Also, this is a plant rich in cellulose (50 %) and hemicellulose (17 %) [89], thus promising for the use in production of biodiesel by transesterification of castor oil, shown to be up to 91 % [91]. *R. communis* biodiesel properties resemble that of diesel. Umale *et a*l. [92] compared GHG emissions using B20 and B10 castor biodiesel blends used in the engine at compression ratios (CR) of 16.5 and 17.5, respectively. The aim of the study was also to determine how efficiently the engine converts fuel supplied into useful work *via* brake-specific fuel consumption (BSFC). Results showed that the B20 castor biodiesel blend used in the engine at CR 16.5 showed lower BSFC than the B10 castor biodiesel blend and *vice versa* at CR 17.5. One more indicator is the brake thermal efficiency, which measures the efficiency of internal combustion engines. The

higher the brake thermal efficiency, the lower the fuel consumption, and greenhouse gas emissions. And in this study, both B10 and B20 had higher break thermal effects. Both blends were used in the engine at CR 17.5. Also, used B10 showed lower CO and HC emissions, and comparatively higher NOX emissions, while B 20 showed lower NOX, and comparatively higher CO and HC emissions [92].

2. 5. *Prosopis* sp

2. 5. 1. Phytoremediation

Prosopis juliflora (Sw.) DC, also known as Velvet Mesquite or simply *Prosopis. Prosopis* spp similar to *Ricinus communis* L. can tolerate and grow in arid, alkaline pH, and, saline soil, and extreme temperatures [92]. This plant is recognized to have a high ability to grow on different soil exhibiting high phytoremediation potential. Having the ability to tolerate high amounts of heavy metals, *P. juliflora* grows on the soil containing Cd, Co, Cr, Fe, Mn, Ni, Pb, and Zn up to 26, 22, 2243, 137, 9.4, 34, 18 and 14 mg kg^{-1}, respectively [93]. One of the biggest concerns in environmental protection is fluorosis, related to air pollution, caused by coal burning, and fluoride (F) related to soil contamination. However, it is found that *P. juliflora* has also the potential for tolerance and accumulation of F, yielding 4.41 mg kg^{-1} dw in the stem, 12.97 mg kg^{-1} dw in leaves, and 16.75 mg kg^{-1} dw in roots [94]. Also, it was shown that the presence of iron oxide nanoparticles (Fe_3O_4 NPs) enhanced the phytoremediation potential of this plant of F [95]. Ramírez *et a*l. [93], investigated the potential of *Prosopis laevigata* for heavy metal phytoremediation in soils polluted with a high concentration of aluminum, titanium, chromium, and zirconium up to 4.1, 14, 1.6 and 2.5 g kg^{-1}, respectively. However, at a high concentration of Cr of 435 mg kg^{-1} in the soil a lack of phytoremediation potential was observed. This study revealed that *P. laevigata* inoculated with *Bacillus* sp. showed the ability to bioaccumulate chromium Cr [93].

2. 5. 2. Biofuel production

Prosopis juliflora (Sw.) DC is rich in holocellulose (60 – 65 %), therefore, it is considered for bioethanol production [80,97-99]. In such a study, Sivarathnakumar *et al* [99] used *Kluyveromyces marxianus* leading to the increased sugar content by applying auto-hydrolysis with acid hydrolysis as a pre-treatment. Saccharification and fermentation processes resulted in 21.45 g dm^{-3} of bioethanol, produced from product and biomass yields of 0.67 and 0.28 wt.%, respectively [99].

Pasha *et a*l. [100], investigated the same process using a thermotolerant *Saccharomyces cerevisiae* VS_3 strain. As a pre-treatment strong acid and enzyme hydrolysis was applied. In this process, 80.76 % of biomass yield was converted into 84 g dm^{-3} total carbohydrates. To improve the fermentative efficiency of sugar to bioethanol production ethyl acetate extraction was employed. With 88% efficiency, *S. cerevisiae* enabled 30.0 g dm^{-3} ethanol production of 0.431±0.021 g ethanol per g sugar of utilized sugars. Thus, efficient pre-treatment induces greater production of bio-ethanol. There are some suggestions that a combination of ionic liquid (IL)-based pretreatment with pretreatment agents surfactants/salts/deep eutectic solvent [101], can be successful [102]. Ionic liquids can remove hemicellulose and lignin to some extent, also has a role in decreasing the surface tension between the two liquid phases during pretreatment and have an additive effect. Surfactant pretreatment with dodecyl benzene sulfonic acid, or dilute acid pretreatment improves lignin solubility, reduce unproductive binding to the enzyme, modifying the biomass surface. Then, pretreated biomass should be further enzymatically saccharified with cellulose or xylanase [103].

Investigating sources of important robust enzymes Vaid *et al* [102], reported that Bacillus spp, in particular, *B. amyloliquefaciens SV29* has the potential of secreting IL-stable enzymes. Furthermore, saccharification of *Prosopis juliflora* with xylanase released from *B. pumilus* strain MK001 resulted in 15.5 wt. %of sugars and reached 20.0 % saccharification efficiency. Further fermentation process with *Pichia stiptis had a* release of saccharified hydrolysates and an outcome of 0.36 wt.% ethanol yield [104]. Besides *P. juliflora, P. pallid* is also considered for bioethanol production, whereas sugar (40 %) can be converted into 18.9 % ethanol [105]. The production of bioethanol depends on the type of microorganisms. Therefore, da Silva *et al.* [97] investigated the efficiency of two microorganisms *Zymomonas mobilis* and *Saccharomyces cerevisiae* in ethanol synthesis. By cultivating Z. *mobilis* in *P. juliflora* pods after

36 h in static conditions the highest concentration of ethanol was reached (141.1 g dm^{-3}), While under the same conditions, after applying *S. cerevisiae* the highest ethanol production (44.32 g dm^{-3}) was achieved after 18 h [97].

2. 6. *Arundo donax* L.

2. 6. 1. Phytoremediation

Arundo donax L., commonly termed "giant cane" or "giant reed", is a non-food crop adapted to different kinds of environments. The phytoremediation potential of this plant in As removal has been estimated in a study conducted by Mirza *et al*. [106]. Cultivated in different hydroponics conditions with increasing doses of As (0, 50, 100, 300, 600, and 1000 μg dm^{-3}), *A. donax* showed the ability to accumulate up to 600 μg dm^{-3} [106], and good bioaccumulation potential in Zn, Cr, and Pb removal from the growing medium. In the range of 450 and 900 mg Zn kg^{-1}, 300 and 600 mg Cr kg^{-1}, and 450 and 900 mg Pb kg^{-1}, *A. donax* biomass slightly decreased, but a severe reduction was noticed at 600 mg Cr kg^{-1} [1]. Soil rich in Ni did not cause any decrease in the growth and development of A. donax. High content of Ni was found in shoots, indicating a good hyperaccumulation ability [107]. *A. donax* amended with *Trichoderma harzianum*, *Saccharomyces cerevisiae*, and *Wickerhamomyces anomalous was* individually exposed to two different concentrations of Ni, Cd, Cu, As, Zn, Pb, V, and Hg. *A. donax* and mycorrhized *A. donax* with *T. harzianum* stand out as Cd, Pb, and Hg bioaccumulators. The mean bioaccumulation percentage values were for Hg 0.60 %, for Pb 0.54 % and for Cd 0.42 % [108]. Furthermore, *A. donax* was exposed to different Cd concentrations of (0, 50, 100, 250, 500, 750, and 1000 μg dm^{-3}), in a hydroponic and soil environment. Although better performance was observed in hydroponic conditions *A. donax* is considered a Cd hyperaccumulator [109]. Additionally, grown in non-ferrous soil giant reed showed high phytoremediation potential for Cd and Pb removal [110]. Also, broad tolerance of *A. donax* to Cd, Cr, Cu, Ni, and Pb was shown in literature reporting the tolerance values of 0.5 mM, 0.2 mM, 2 mM, 0.5 mM, and 1 mM, respectively [111]. Also, a comparison between accumulating capabilities regarding some heavy metals showed that *A. donax* accumulates Zn > Ni > Cu > Cd [112]. According to Alshaal *et al.* [113], *A. donax* is strongly recommended for phytoremediation of bauxite residue or red mud being capable to accumulate and translocate heavy metals, especially Ni, but also Co, Pb, Cd, and Fe [113], As and Hg [114], Se [115], nitrate [116], Cu [117,118].

2. 6. 2. Biofuel production

Multi-applicable *A. donax* has found a place among high biomass yield energy plants, suitable for biofuel production [119-121]. Giant cane rich in cellulose is considered a good bioethanol source with pre-treatment to degrade cellulose into fermentable sugars [122]. De Bari *et al.* [119] used the steam explosion as pre-treatment and then pretreated biomass was exposed to saccharification and fermentation. After these steps, high gravity hydrolysis was applied with subsequent fermentation using *S. cerevisiae* to reach the production of ethanol concentration of 51 g dm^{-3}. *A. donax* pretreated with commercial cellulase (Multifect®) from Trichoderma reesei, produced 75 dm^3 of ethanol per ton of *Arundo* biomass [125]. Another study suggested that plants were able to produce 20 g dm^{-3} oxalic acid [126] and 8.2 g dm^{-3} ethanol [127]. Giant reed biomass pre-treated with diluted acid or liquid hot water can be converted with bacteria as a fermentative organism. Locaes *et al.* showed that the usage of commercial enzymes boosts ethanol production from 0.44 to 0.47 g dm^{-3}. Also, this study showed a great difference when ethanol production was carried out without saccharification, resulting in 7.5 g dm^{-3} of ethanol [129].

3. DISCUSSION

Recently, fossil fuel depletion brought alternative energy sources to become the "new normal" energy sources. Furthermore, energy stability is on the same level of importance as the elimination of environmental pollution. Recent studies indicate multitasking approach as phytoremediation and biofuel production from the same source - energy plants. There are a plethora of energy crops and non-crops used for this purpose. Structural properties and physiology enable these plants to clean up soil from heavy metals and then use it for biofuel production. The candidates and multiple potential plant species are presented in Table1. and Table 2.

Table 1. The bioaccumulating potential of energy plant species

Plant species	Bioaccumulation potential	References
Miscanthus × giganteus J.M. Greef & Deuterex Hodk. & Renvoize	Hg, Cd, Zn, Pb, Cu, Mn, Ti, As, Fe and Zr	[24-30]
Miscanthus sinensis	Hg, Cd, Zn, Cr	[26,30]
Miscanthus sacchariflorus	Zn, Cd, Pb, Fe, Mn, Mo, B, Ba, Sr, As, Sn, Li, and Ti	[24,30]
Miscanthus floridulus	Zn, Cr and Cd	[30]
Beta vulgaris L.	Cd	[39]
Beta vulgaris L.	DTPA-extractable Cd and Ni	[38]
Saccharum officinarum L.	Cu, Cd, Se, Pb, and Mn	[50-52]
Saccharum officinarum L.	gamma-HCH or lindane	[53,54]
Saccharum officinarum L.	F^-	[56]
Saccharum officinarum L.	Fe	[59]
Saccharum officinarum L.	PCBs and Cd	[60]
Saccharum spontaneum L.	Cu, Sn, and Pb/Zn	[11,64]
Saccharum munja	Zn, Pb, Cu, Ni, Cd, and As	[65]
Saccharum.arundinaceum	Cu, Zn, Pb, and Cd	[66]
Ricinus communis L.	Cd	[77,84]
Ricinus communis L.	Ni, Zn, and Fe	[78]
Ricinus communis L.	Pb	[81]
Ricinus communis L.	B, and tolerate Cu, Fe, Mn, and Zn	[82,83]
Ricinus communis L.	Cd, Pb, Ni, As, Cu	[84]
Ricinus communis L.	Pesticides	[84]
Prosopis juliflora (Sw.) DC	Cd, Co, Cr, Fe, Mn, Ni, Pb, and Zn	[94]
Prosopis juliflora (Sw.) DC	fluoride (F)	[95]
P. laevigata	Al, Fe, Ti, and Zn	[93]
P. laevigata inoculated with *Bacillus* sp.	Cr	[93]
Arundo donax L.	As	[106]
Arundo donax L.	Zn, Cr, and Pb	[1]
Arundo donax L.	Ni, Cd, Cu, As, Zn, Pb, V, Hg.	[108]
Arundo donax L.	Cd	[110]
Arundo donax L.	Cd, Cr, Cu, Ni, and Pb	[111,117,118]
Arundo donax L.	Ni, Co, Pb, Cd, and Fe	[113]
Arundo donax L.	As and Hg	[114]
Arundo donax L.	Se	[115]
Arundo donax L.	Nnitrates	[116]

As presented, there is a strong bioaccumulation potential in all selected plants. Silvergrass plants are recognized as heavy metal bio accumulators. *Miscanthus × giganteus* J.M. Greef & Deuter ex Hodk. & Renvoize, chiefly removes Hg, Cd, Zn, and Pb, Cu, Mn, Ti, As, Fe, and Zr, and *Miscanthus sacchariflorus* besides Zn, Cd, Pb, Fe, removes Mn, Mo, B, Ba, Sr, As, Sn, Li, and Ti. Moreover, this plant gave good results in bioethanol production. *Miscanthus × giganteus J.M. Greef & Deuter*, *ex Hodk. & Renvoize* under biological saccharification and fermentation with anaerobic bacteria *F. succinogenes* and *C. acetobutylicum* yielded 44.4 ± 8.5 g m^{-3} ethanol and 19.7 ± 3.5 g m^{-3}buthanol. Sugar beet, *Beta vulgaris* L. is suitable for Cd, DTPA-extractable cadmium, and Ni removal. An excellent result was achieved with enzymatic liquefaction (pectinase and cellulase enzymes) to produce 100-120 dm^{-3} ethanol/sugar beet.

Table 2. Biofuel production from energy plants

Plant species	Pretreatment/ Treatment applied	Biofuel produced	Ref.
Miscanthus × giganteus J.M. Greef & Deuter ex Hodk. & Renvoize	100 mol m^{-3} H_2SO_4	9572 g m^{-3} saccharides from acid treatment yielded 44.4 ± 8.5 g m^{-3} of ethanol 19.7 ± 3.5 g m^{-3} of buthanol	[36,37]
Miscanthus × giganteus J.M. Greef & Deuter ex Hodk. & Renvoize	200 mol m^{-3} NaOH	4054 g m^{-3} saccharides from alkali treatment yielded 39.7 ± 8.6 g m^{-3} of ethanol 4.3 ± 0.33 g m^{-3} of buthanol	[36,37]
Miscanthus × giganteus J.M. Greef & Deuter ex Hodk. & Renvoize	Biological saccharification and fermentation with anaerobic bacteria *F. succinogenes and C. acetobutylicum*	2504 g m^{-3} saccharides yielded 0.091 g m^{-3} of ethanol	[36,37]
Miscanthus sinensis	1 % NaOH at 121 °C for 60 min/ozonolysis	From 37.6 wt.% of cellulose, 0.221 g of ethanol was produced	[31]
Miscanthus sacchariflorus	1 % NaOH at 121 °C for 60 min/ozonolysis	From 38.95 wt.% of cellulose, 0.213 g ethanol was produced	[31]
Miscanthus floridulus	1 % NaOH at 121 °C for 60 min/ozonolysis	From 41 wt.% of cellulose, 0.233 g ethanol was produced	[31]
Beta vulgaris L.	Enzymatic liquefaction (pectinase and cellulase enzymes)	103.5 dm^3 per tonne (wet weight)	[47-48]
Beta vulgaris L.	Enzymatic liquefaction (pectinase and cellulase enzymes)	Enhanced bioethanol production-from 10 wt.% fermented sugars	[47-48]
Saccharum officinarum L.	Steam pretreatment with SO_2 and H_2O_2	Bioethanol 0.95 g dm^{-3} (ethyl alcohol)	[67,68]
Saccharum officinarum L.	Saccharification, fermentation, and rectification	10.9 g dm^{-3} ethanol	[69]
Saccharum officinarum L.	*S. cerevisiae*, *P. stipitis* and oxalic acid (2-8 wt.%).	7.9 g dm^{-3} butanol	[67,70]
Saccharum officinarum L.	Dilute acid, then fermented with *Clostridium beijerinckii* DSM 6423	62 g dm^{-3} ethanol	[74]
Saccharum officinarum L.	Partially consolidated bioprocessing (PCBP) / laccase (*Pleurotus djamor*) and holocellulase (*Trichoderma reseei* RUT C30),	0.46 g g^{-1} bioethanol / biomass	[131]
Saccharum spontaneum L.	The cellulolytic enzyme (CMCase) from *Trichoderma reesei* / bioconversion in bioethanol with *Saccharomyces cerevisiae*	21.82 ± 0.15 g L^{-1} hydrolysate / 0.40 ± 0.01 g g^{-1} ethanol	[71]
Saccharum spontaneum L.	*A. oryzae* enzymes and then fermented with *Pichia stipitis* NCIM3498	62 g dm^{-3} ethanol	[72]
Saccharum spontaneum L.	Partially consolidated bioprocessing (PCBP) / laccase (*Pleurotus djamor*) and holocellulase (*Trichoderma reseei* RUT C30)	30.78 g dm^{-3} and 31.56 g dm^{-3} of bioethanol	[131]

Plant species	Pretreatment/ Treatment applied	Biofuel produced	Ref.
Saccharum munja	Enzymatic hydrolysate fermented by the co-culture *Saccharomyces cerevisiae* and *Pichia stipitis*	4.18 ± 1.14 g dm^{-3} ethanol	[67]
Saccharum.arundinaceum	Co-immobilized tri-enzyme biocatalytic system for one-pot pretreatment (Laccase, cellulas and β-glucosidase)	biodiesel	[73]
Ricinus communis L	Pre-treatment (Heating of oil and esterification); main treatment (Transesterification) + catalyst (acid / alkaline)	99.07 % of biodiesel (methyl ester) yield	[92]
Ricinus communis L	Esterification-neutralization-transesterification (ENT) process	21.45 g dm^{-3} of bioethanol	[130]
Prosopis juliflora (Sw.) DC	Auto-hydrolysis with acid-hydrolysis, *Kluyveromyces marxianus* enzymes	30.0 g dm^{-3} of bioethanol	[99]
Prosopis juliflora (Sw.) DC	Strong acid and enzyme hydrolysis, *Saccharomyces cerevisiae*	36 wt.% ethanol yield	[100]
Prosopis juliflora (Sw.) DC	Ionic liquid based pretreatment, *Pichia stiptis* release of saccharified hydrolysates	141.1 g dm^{-3}	[104]
Prosopis juliflora (Sw.) DC	*Zymomonas mobilis* enzymes	51 g dm^{-3} bioethanol	[97]
Arundo donax L.	Steam explosion as pre-treatment than *S. cerevisiae* amendment saccharification and fermentation	4.8 g dm^{-3} bioethanol	[119]
Arundo donax L.	pretreatment by 2 vol.% of H_2SO_4, followed by enzyme hydrolysis by *Zymomonas mobilis*	8.20 g dm^{-3} of ethanol	[123]
Arundo donax L.	Dilute oxalic acid as a pretreatment, Scheffersomyces (Pichia) stipitis CBS6054 enzyme hydrolysis	75 dm^{-3} ethanol per t of biomass	[124]
Arundo donax L.	Commercial cellulase (Multifect®) from *Trichoderma reesei*	19.8 g dm^{-3} ethanol	[125]
Arundo donax L.	Dilute oxalic acid	7.5 g dm^{-3} ethanol	[126,127]
Arundo donax L.	Enzymatic hydrolysis of cellulose	Ethanol	[128]
Arundo donax L.	Pre-treated with diluted acid or liquid hot water, *Escherichia coli* amendment	9572 g m^{-3} saccharides from acid treatment yielded 44.4 ± 8.5 g m^{-3} of ethanol 19.7 ± 3.5 g m^{-3} of buthanol	[129]
Arundo donax L.	Process of sonication, aqueous solution amended with copper ($CuSO_4.5H_2O$ or $CuH_{10}O_9S$), manganese ($MnSO_4{\cdot}H_2O$ or H_2MnO_5S), and zinc ($ZnSO_4{\cdot}7H_2O$ or $H_{14}O_{11}SZn$) ions, *T. koningii* and *A. niger*	4054 g m^{-3} saccharides from alkali treatment yielded 39.7 ± 8.6 g m^{-3} of ethanol 4.3 ± 0.33 g m^{-3} of buthanol	[122]

Furthermore, besides the already mentioned heavy metals, gamma-HCH or lindane, and F^- are bioaccumulated by *Saccharum officinarum* L. which alongside *S. spontaneum* L. produced 62 g dm^{-3} ethanol in partially consolidated bioprocessing (PCBP) / laccase (*Pleurotus djamor*) and holocellulase (*Trichoderma reseei* RUT C30) treatment. *Prosopis juliflora* (Sw.) DC. remediates soil from Cd, Co, Cr, Fe, Mn, Ni, Pb, Zn, and F. Bioethanol production of 141 g dm^{-3} is possible if applied *Zymomonas mobilis* enzymes. *Arundo donax* L. showed good As, Co, Cd, Cr, Cu, Fe, Ni, Se, Pb, Zn, V, and NO_3- bioaccumulation results, and commercial cellulase (Multifect®) from *Trichoderma reesei* gave the best results

in biofuel production, 75 dm^3 of ethanol. The future relies on sustainable techniques that will provide a cleaner environment. In summary, there are many research papers indicating the feasibility of the phytoremediation-bioenergy strategy direction, where energy plants can be used to clean the environment from heavy metals and then used for biofuel production.

4. CONCLUSION

A plethora of organic and inorganic pollutants, especially heavy metals (HMs) have caused soil and water pollution. Moreover, these metals have genotoxic, and mutagenic effects on living beings [131]. Many plant species belonging to different plant families, recognized as useful phytoremediation candidates, can accumulate different pollutants without intoxication [132,133]. Scientists and engineers are working together to explore alternative energy sources because advances will allow the removal of harmful pollutants such as heavy metals while replacing fossil fuels with biofuels. Table 1. depicts various energy plants' roles in phytoremediation and biofuel production. All presented plant species have shown exceptional importance in energy stability without endangering the environment. Plant species with multiple potentials need to be further genetically improved and researched, particularly concerning reducing the toxic effect of heavy metals on subsequent biofuel production. Therefore, the compilation of these two processes has been recognized as a future direction for sustainable energy and environmental protection.

Acknowledgements: The Ministry of Education, Science and Technological Development of the Republic of Serbia, Grant No. 172022, Grant No. 451-03-9/2021-14/200156, and Grant No. 451-03-9/2021-14/200134 supported the work. We sincerely thank CEEPUS - Central European Exchange Program for University Studies for supporting the joint research by supporting the mobilities between the University of Novi Sad and TU Wien within the network "CIII-SI-0708--08-Chemistry and Chemical Engineering".

REFERENCES

[1] Barbosa B, Boléo S, Sidella S, Costa J, Duarte MP, Mendes B, Cosentino SL, Fernando AL. Phytoremediation of heavy metal-contaminated soils using the perennial energy crops Miscanthus spp. and Arundo donax L. *BioEnergy Res.* 2015; 8(4): 1500-1511. https://doi.org/10.1007/s12155-015-9688-9

[2] Petrović J, Simić M, Mihajlović M, Koprivica M, Kojić M, Nuić I. Upgrading fuel potentials of waste biomass via hydrothermal carbonization: Original scientific paper. *Hem Ind.* 2021; 75(5): 297-305. https://doi.org/10.2298/HEMIND210507025P

[3] Vindiš P, Muršec B, Rozman Č, Čus F. A Multi-Criteria Assessment of Energy Crops for Biogas Production. *Stroj Vestn-J Mech E.* 2010; 56(1): 63-70. https://www.sv-jme.eu/article/a-multi-criteria-assessment-of-energy-crops-for-biogas-production

[4] Aziz NI, Hanafiah MM, Gheewala SH. A review on life cycle assessment of biogas production: Challenges and future perspectives in Malaysia. *Biomass Bioenergy.* 2019; 122: 361-74. https://doi.org/10.1016/j.biombioe.2019.01.047

[5] Padmavathiamma P K, Li LY. Phytoremediation technology: hyper-accumulation metals in plants. *Water Air Soil Pollut.* 2007; 184 (1), 105-126. https://doi.org/10.1007/s11270-007-9401-5.

[6] Vidican R, Mihăiescu T, Pleşa A, Crişan I. (2020). Opportunities for the utilization of phytoremediation biomass rich in heavy metals. *ProEnvironment Promediu.* 2020; 13(43): 77-81.

[7] Chibuike GU, Obiora SC. Heavy metal polluted soils: effect on plants and bioremediation methods. *Appl Environ Soil Sci* 2014; 752708. https://doi.org/10.1155/2014/752708

[8] Pandey VC, Bajpai O, Singh N. Energy crops in sustainable phytoremediation. *Renew Sust Energ Rev.* 2016; 54: 58-73. http://dx.doi.org/10.1016/j.rser.2015.09.078

[9] Sathya A, Kanaganahalli V, Rao PS, Gopalakrishnan S. Cultivation of sweet sorghum on heavy metal-contaminated soils by phytoremediation approach for production of bioethanoL. In: Prasad M N V, ed Bioremediation and Bioeconomy. Amstrdam: Elsevier; 2016: 271-292. https://doi.org/10.1016/B978-0-12-802830-8.00012-5

[10] Nikolić M, Tomašević V. Implication of the Plant Species Belonging to the Brassicaceae Family in the Metabolization of Heavy Metal Pollutants in Urban Settings. *Pol J Environ Stud.* 2020; 30(1): 523-534. https://doi.org/10.15244/pjoes/122770

Pandey VC, Pandey DN, Singh N. Sustainable phytoremediation based on naturally colonizing and economically valuable plants. *J Clean Prod*. 2015; 86: 37–39. http://dx.doi.org/10.1016/j.jclepro.2014.08.030

[11] Britt C, Bullard M, Hickman G, Johnson P, King J, Nicholson F, Nixon P, Smith N. Bioenergy crops and bioremediation–a review. *Report by ADAS for the Department for Food, Environment and Rural Affairs*. 2002: 1-34. http://randd.defra.gov.uk/Document.aspx?Document=NF0417_2072_FRP.doc

[12] Gomes HI. Phytoremediation for bioenergy: challenges and opportunities. *Environ Technol Rev.* 2012; 1(1): 59-66. https://doi.org/10.1080/09593330.2012.696715

[13] Trinh TT, Werle S, Tran KQ, Magdziarz A, Sobek S, Pogrzeba M. Energy crops for sustainable phytoremediation–Thermal decomposition kinetics. *Energy Procedia*. 2019; 158: 873-878. http://dx.doi.org/10.1016/j.egypro.2019.01.224

[14] Edgar VN, Fabián FL, Mario PC, Ileana VR. Coupling Plant Biomass Derived from Phytoremediation of Potential Toxic-Metal-Polluted Soils to Bioenergy Production and High-Value by-Products—A Review. *Appl Sci.* 2021; 11(7): 1-35. https://doi.org/10.3390/app11072982

[15] Chintagunta AD, Zuccaro G, Kumar M, Kumar SJ, Garlapati VK, Postemsky PD, Kumar NS, Chandel AK, Simal-Gandara J. Biodiesel Production from Lignocellulosic Biomass Using Oleaginous Microbes: Prospects for Integrated Biofuel Production. *Front Microbio*L. 2021; 12: 1-23. https://dx.doi.org/10.3389%2Ffmicb.2021.658284

[16] Kumar, S. P. J., Gujjala, L. K. S., Dash, A., Talukdar, B., and Banerjee, R. "Biodiesel production from lignocellulosic biomass using oleaginous microbes,". In: Kuila A and V. Sharma V, eds Lignocellulosic Biomass Production and Industrial Applications, Hoboken, NJ: Wiley; 2017: 65–92. https://dx.doi.org/10.3389%2Ffmicb.2021.658284

[17] Mohapatra S, Mishra C, Behera SS, Thatoi H. Application of pretreatment, fermentation and molecular techniques for enhancing bioethanol production from grass biomass–A review. *Renew Sust Energ Rev.* 2017; 78 : 1007-1032. http://dx.doi.org/10.1016/j.rser.2017.05.026

[18] Furtado A, Lupoi JS, Hoang NV, Healey A, Singh S, Simmons BA, Henry RJ. Modifying plants for biofuel and biomaterial production. *Plant Biotechnol J.* 2014; 12(9): 1246-1258. https://doi.org/10.1111/pbi.12300

[19] Rayburn AL, Crawford J, Rayburn CM, Juvik JA. Genome size of three Miscanthus species. *Plant Mol Biol Rep.* 2009; 27(2): 184-188. https://doi.org/10.1007/s11105-008-0070-3

[20] Wang C, Kong Y, Hu R, Zhou G. Miscanthus: A fast-growing crop for environmental remediation and biofuel production. *Glob Change Biol Bioenergy.* 2021; 13(1): 58-69. https://doi.org/10.1111/gcbb.12761

[21] Gawronski SW, Greger M, Gawronska H. Plant taxonomy and metal phytoremediation. In Sherameti I and Varma A, eds Detoxification of heavy metals. Berlin, Heidelberg: Springer; 2011: 91-109. https://doi.org/10.1007/978-3-642-21408-0_5

[22] Arnoult S, Obeuf A, Béthencourt L, Mansard MC, Brancourt-Hulmel M. Miscanthus clones for cellulosic bioethanol production: relationships between biomass production, biomass production components, and biomass chemical composition. *Ind Crops Prod.* 2015; 63: 316-28. https://doi.org/10.1016/j.indcrop.2014.10.011

[23] Pidlisnyuk V, Stefanovska T, Lewis EE, Erickson LE, Davis LC. Miscanthus as a productive biofuel crop for phytoremediation. *CRC Crit Rev Plant Sci.* 2014; 33(1): 1-9. http://dx.doi.org/10.1080/07352689.2014.847616

[24] Nurzhanova A, Pidlisnyuk V, Sailaukhanuly Y, Kenessov B, Trogl J, Aligulova R, Kalugin S, Nurmagambetova A, Abit K, Stefanovska T, Erickson L. Phytoremediation of military soil contaminated by metals and organochlorine pesticides using Miscanthus. *Comm Appl Biol Sci*. 2017; 82: 61-68. Corpus ID: 207991408

[25] Zhao A, Gao L, Chen B, Feng L. Phytoremediation potential of Miscanthus sinensis for mercury-polluted sites and its impacts on soil microbial community. *Environ Sci Pollut Res.* 2019; 26(34): 34818-34829. https://doi.org/10.1007/s11356-019-06563-3

[26] Zgorelec Z, Bilandzija N, Knez K, Galic M, Zuzul S. Cadmium and mercury phytostabilization from soil using Miscanthus × giganteus. *Sci Rep.* 2020; 10(1), 1-10. https://doi.org/10.1038/s41598-020-63488-5

[27] Germaine KJ, McGuinness M, Dowling DN. Improving phytoremediation through plant-associated bacteria. In Frans J. de Bruijn, ed. Molecular microbial ecology of the rhizosphere. 1st ed. New York, NY: John Wiley & Sons, Ltd. 2013; 1: 961-73. https://doi.org/10.1002/9781118297674.ch91

[28] Babu AG, Shea PJ, Sudhakar D, Jung IB, Oh BT. Potential use of Pseudomonas koreensis AGB-1 in association with Miscanthus sinensis to remediate heavy metal(loid)-contaminated mining site soil. *J Environ Manag.* 2015; 151: 160-166. https://doi.org/10.1016/j.jenvman.2014.12.045

[29] Fernando AL, Barbosa B, Boléo S, Duarte MP, Sidella S, Costa J, Cosentino SL. Phytoremediation potential of heavy metal contaminatated soils bz the perennial energy crops *Miscanthus* spp. And *Arundo donax* L. Under low irrigation. In: *26th European Biomass Conference and Exhibition*. Denmark, Copenhagen, 2018, pp.136-139. http://dx.doi.org/10.5071/26thEUBCE2018-1CO.9.2

[30] Lee W, Kuan W. Miscanthus as cellulosic biomass for bioethanol production. *Biotechnol J.* 2015; 10(6): 840–854. https://doi.org/10.1002/biot.201400704

[31] Krička T, Matin A, Bilandžija N, Jurišić V, Antonović A, Voća N, Grubor M. Biomass valorisation of Arundo donax L., Miscanthus× giganteus and Sida hermaphrodita for biofuel production. *Int Agrophys*. 2017; 31(4): 575-581. https://doi.org/10.1515/intag-2016-0085.

[32] Ivanyshyn V, Nedilska U, Khomina V, Klymyshena R, Hryhoriev V, Ovcharuk O, Hutsol T, Mudryk K, Jewiarz M, Wróbel M, Dziedzic K. Prospects of growing miscanthus as alternative source of biofuel. In: Mudryk K and Sebastian Werle S, eds. Renewable Energy Sources: Engineering, Technology, Inovation. Berlin: Springer Proceedings in Energy; 2018: 801-812. https://doi.org/10.1007/978-3-319-72371-6_78C

[33] Cai H, Markham J, Jones S, Benavides PT, Dunn JB, Biddy M, Tao L, Lamers P, Phillips S. Techno-economic analysis and life-cycle analysis of two light-duty bioblendstocks: isobutanol and aromatic-rich hydrocarbons. *ACS Sustain Chem Eng*. 2018; 6(7): 8790-8800. https://doi.org/10.1021/acssuschemeng.8b01152

[34] Dantas ER, Bonhivers JC, Maciel Filho R, Mariano AP. Biochemical conversion of sugarcane bagasse into the alcohol fuel mixture of isopropanol-butanol-ethanol (IBE): Is it economically competitive with cellulosic ethanol? *Bioresour Technol*. 2020; 314: 1-7. https://doi.org/10.1016/j.biortech.2020.123712

[35] Raut MP, Pham TK, Gomez LD, Dimitriou I, Wright PC. Alcoholic fermentation of thermochemical and biological hydrolysates derived from Miscanthus biomass by Clostridium acetobutylicum ATCC 824. *Biomass Bioenergy*. 2019; 130: 1-33. https://doi.org/10.1016/j.biombioe.2019.105382

[36] Romano A, Sorgona A, Lupini A, Araniti F, Stevanato P, Cacco G, Abenavoli MR. Morpho-physiological responses of sugar beet (*Beta vulgaris* L.) genotypes to drought stress. *Acta Physiol Plant.* 2013; 35(3): 853-865. https://doi.org/10.1007/s11738-012-1129-1.

[37] Papazoglou EG, Fernando AL. (2017). Preliminary studies on the growth, tolerance and phytoremediation ability of sugarbeet (Beta vulgaris L.) grown on heavy metal contaminated soil. *Ind Crops Prod.* 2017; 107: 463-471. https://doi.org/10.1016/j.indcrop.2017.06.051

[38] Gu P, Zhang Y, Xie H, Wei J, Zhang X, Huang X, Wang J, Lou X. Effect of cornstalk biochar on phytoremediation of Cd-contaminated soil by Beta vulgaris var. cicla L. EcotoxicoL. *Environ. Saf.* 2020; 205: 1-9. https://doi.org/10.1016/j.ecoenv.2020.111144

[39] Calderón FJ, Benjamin J, Vigil MF. A comparison of corn (Zea mays L.) residue and its biochar on soil C and plant growth. *PLoS One*. 2015; 10(4): 1-16. https://doi.org/10.1371/journaL.pone.0121006

[40] Sagardoy RU, Morales FE, López-Millán AF, Abadía AN, Abadía JA. Effects of zinc toxicity on sugar beet (Beta vulgaris L.) plants grown in hydroponics. *Plant Bio*L. 2009; 11(3): 339-350. https://doi.org/10.1111/j.1438-8677.2008.00153

[41] Harland JI, Jones CK, Hufford C. Co-products. In: Draycott P A, ed. Sugar beet, ed., Oxford, UK: Blackwell Publishing, Ltd. 2006: 443–46. http://books.google.com/books?id=S1OLrxYiFXEC

[42] Panella L. Sugar beet as an energy crop. *Sugar Tech.* 2010; 12(3): 288-293. https://doi.org/10.1007/s12355-010-0041-5.

[43] Zicari, S., Aramrueang, N., Asato, C., Chen, C., Zhang, R. Integrated processing of sugar beets at the lab and pilot scale for bioethanol and biogas production. In: 45th Symposium on Biomaterials for Fuels and Chemicals. Clearwater Beach, FL. 2014, 1-7.

[44] Jayani RS, Saxena S, Gupta R. Microbial pectinolytic enzymes: a review. *Process Biochem*. 2005: 40 (9), 2931-2944. https://doi.org/10.1016/j.procbio.2005.03.026

[45] Nielsen PH, Oxenbøll KM, Wenzel H. Cradle-to-gate environmental assessment of enzyme products produced industrially in Denmark by Novozymes A/S. *Int J Life Cycle Assess.* 2007; 12(6): 432-438. http://dx.doi.org/10.1065/lca2006.08.265.1

[46] Alexiades A, Kendall A, Winans KS, Kaffka SR. Sugar beet ethanol (Beta vulgaris L.): A promising low-carbon pathway for ethanol production in California. *J Clean Prod***.** 2018; 172: 3907-3917. https://doi.org/10.1016/j.jclepro.2017.05.059

[47] Kaffka SR, Grantz DA. Sugar crops. In: Van Alfen N, ed. Encyclopedia of Agriculture and Food Systems. San Diego, CA: Elsevier; 2014: 240-260.

[48] Scally L, Hodkinson T, Jones MB, Origin and taxonomy of Miscanthus. In: Jones, MB, Walsh N, ed. Miscanthus for Energy and Fibre. London, UK: Earthscan Publications Ltd.; 1997: 1-45. ISBN-13: 978-1849710978, ISBN-10: 184971097X.

[49] Xia, H., Yan, Z., Chi, X., Cheng, W. Evaluation of the phytoremediation potential of Saccharum officinarum for Cd-contaminated soil. IEEE In: *2009 International Conference on Energy and Environment Technology*. Guilin, China 2009, 314-318. https://doi.org/10.1109/ICEET.2009.541

[50] Yan Z, Xia H. Evaluation of the phytoremediation potential of sugarcane for metal-contaminated soils. IEEE. In: *2010 4th International Conference on Bioinformatics and Biomedical Engineering*, Guilin, China. 2010, 1-4 https://doi.org/10.1109/ICBBE.2010.5517419

[51] Yousefi Z, Kolahi M, Majd A, Jonoubi P. Effect of cadmium on morphometric traits, antioxidant enzyme activity and phytochelatin synthase gene expression (SoPCS) of Saccharum officinarum var. cp 48-103 in vitro*. Ecotoxico*L. *Environ. Saf.* 2018; 157: 472-481. https://scite.ai/reports/10.1016/j.ecoenv.2018.03.076.

[52] Salam J A, Hatha M A, Das N. Microbial-enhanced lindane removal by sugarcane (*Saccharum officinarum*) in doped soil-applications in phytoremediation and bioaugmentation. *J Environ Manag*. 2017; 193: 394-399. https://doi.org/10.1016/j.jenvman.2017.02.006

[53] Salam JA, Das N. Lindane degradation by Candida VITJzN04, a newly isolated yeast strain from contaminated soil: kinetic study, enzyme analysis and biodegradation pathway. *World J Microbiol Biotechnol*. 2014; 30(4): 1301-1313. https://doi.org/10.1007/s11274-013-1551-6

[54] Camarena-Rangel N, Velázquez AN, del Socorro Santos-Díaz M. Fluoride bioaccumulation by hydroponic cultures of camellia (*Camellia japonica spp*.) and sugar cane (*Saccharum officinarum spp*.). *Chemosphere.* 2015; 136: 56-62. https://doi.org/10.1016/j.chemosphere.2015.03.071

[55] Baunthiyal M, Ranghar S. Accumulation of fluoride by plants: potential for phytoremediation. *Clean-Soil Air Water***.** 2015; 43(1): 127-132. https://doi.org/10.1002/clen.201300353

[56] Ubogu M, Akponah E, Vinking GE, Loho NG. Assessment of the hydrocarbon utilizing mycoflora of the root zones of saccharum officinarum. *SF J Mycol*. 2017; 2(1): 1-10.

[57] Cavalcante VS, Prado RD, Vasconcelos RD, Campos CN. Iron concentrations in sugar cane (Saccharum officinarum L.) cultivated in nutrient solution. *Agrociencia*. 2016; 50 (7): 867-75. ISSN 2521-9766

[58] Tamez C, Molina-Hernandez M, Medina-Velo IA, Cota-Ruiz K, Hernandez-Viezcas JA, Gardea-Torresdey J. Long-term assessment of nano and bulk copper compound exposure in sugarcane (Saccharum officinarum). *Sci Total Environ.* 2020; 718: 1-7. https://doi.org/10.1016/j.scitotenv.2020.137318

[59] Xia H, Chi X, Yan, Z, Cheng W. Enhancing plant uptake of polychlorinated biphenyls and cadmium using tea saponin. *Bioresour Technol.* 2009; 100(20); 4649-4653. https://doi.org/10.1016/j.biortech.2009.04.069

[60] Pandey VC, Bajpai O, Pandey DN, Singh N. Saccharum spontaneum: an underutilized tall grass for revegetation and restoration programs. *Genet Resour Crop Ev.* 2015b; 62: 443–450. https://doi.org/10.1007/s10722-014-0208-0

[61] Kumar A, Ahirwal J, Maiti SK, Das R. An Assessment of Metal in flyAsh and Their Translocation and Bioaccumulation in Perennial Grasses Growing at the Reclaimed Opencast Mines*. Int J Environ Res.*2015; 9: 1089–1096 https://dx.doi.org/10.22059/ijer.2015.996

[62] Mukherjee P, Roychowdhury R, Roy M. Phytoremediation potential of rhizobacterial isolates from Kans grass (Saccharum spontaneum) of fly ash ponds. *Clean Technol Environ Policy* 2017; 19(5): 1373-1385 https://doi.org/10.1007/s10098-017-1336-y

[63] Xia H, Chi X, Cheng W. Uptake and Growth Response of Saccharum Officinarum to Lead Pollution in SoiL. In *2009 3rd International Conference on Bioinformatics and Biomedical Engineering*, Guilin, China, IEEE. 2009 pp.1-4. http://dx.doi.org/10.1109/ICBBE.2009.5163728

[64] Banerjee R, Jana A, De A, Mukherjee A. Phytoextraction of heavy metals from coal fly ash for restoration of fly ash dumpsites. *Bioremediat J.* 2020; 24(1): 41-49. https://doi.org/10.1080/10889868.2020.1720590

[65] Huang HY, Xu J, Bai Y, Zhang WQ, Zhu F, Li T, Wang XY, An CH. Enrichment of heavy metals in *Saccharum arundinaceum (Retz.) Jeswiet* in different soil habitats. *Chin J Eco*l. 2012; 31(4): 961-966. (In Chinese)

[66] Bala A, Singh B. Development of an environmental-benign process for efficient pretreatment and saccharification of *Saccharum* biomasses for bioethanol production. *Renew Energy.* 2019; 130: 12-24. https://doi.org/10.1016/j.renene.2018.06.033

[67] Verardi A, Blasi A, De Bari I, Calabrò V. Steam pretreatment of *Saccharum officinar*um L. bagasse by adding of impregnating agents for advanced bioethanol production. *Ecotoxicol Environ Saf.* 2016; 134: 293-300. https://doi.org/10.1016/j.ecoenv.2015.07.034

[68] Sutjahjo DH. The characteristics of bioethanol fuel made of vegetable raw materials. In: *IOP Conference Series: Materials Science and Engineering*. IOP Publishing UK, 2018 pp. 1-7. https://doi.org/10.1088/1757-899X/296/1/012019

[69] Scordia D, Cosentino SL, Jeffries TW. Second generation bioethanol production from *Saccharum spontaneum* L. *ssp. aegyptiacum* (Willd.) Hack. *Bioresour Technol*. 2010; 101(14): 5358-5365. https://doi.org/10.1016/j.biortech.2010.02.036

[70] Kataria R, Ghosh S. Saccharification of Kans grass using enzyme mixture from Trichoderma reesei for bioethanol production. *Bioresour Technol*. 2011; 102(21): 9970-9975. https://doi.org/10.1016/j.biortech.2011.08.023

[71] Chandel AK, Singh OV, Rao LV, Chandrasekhar G, Narasu ML. Bioconversion of novel substrate Saccharum spontaneum, a weedy material, into ethanol by Pichia stipitis NCIM3498. *Bioresour Techno*L. 2011; 102(2): 1709-1714. https://doi.org/10.1016/j.biortech.2010.08.016

[72] Sankar MK, Ravikumar R, Kumar MN, Sivakumar U. Development of co-immobilized tri-enzyme biocatalytic system for one-pot pretreatment of four different perennial lignocellulosic biomass and evaluation of their bioethanol production potential. *Bioresour Technol*. 2018; 269: 227-236. https://doi.org/10.1016/j.biortech.2018.08.091

[73] dos Santos Vieira CF, Codogno MC, Maugeri Filho F, Maciel Filho R, Mariano AP. Sugarcane bagasse hydrolysates as feedstock to produce the isopropanol-butanol-ethanol fuel mixture: Effect of lactic acid derived from microbial contamination on Clostridium beijerinckii DSM 6423. *Bioresour Technol*. 2021; 319: 1-8. https://doi.org/10.1016/j.biortech.2020.124140

[74] Duke JA. The quest for tolerant germplasm. In: Proceedings of ASA Special Symposium 32, Crop tolerance to suboptimal land conditions. *Am Soc Agron Madison*, WI; 1978: 1–61. ISBN: 0686517032

[75] Gana AK, Yusuf AF, Apuyor B. Castor oil plant and its potential in transformation and industrialization of under developing nations in the world. *Adv J Agric Res.* 2013; (5): 72–79. https://doi.org/10.1186/s40508-016-0055-8

[76] Bauddh K, Singh RP. Effects of organic and inorganic amendments on bio-accumulation and partitioning of Cd in Brassica juncea and Ricinus communis. *Ecol Eng.* 2015; 74: 93-100. https://doi.org/10.1016/j.ecoleng.2014.10.022

[77] Ma Y, Rajkumar M, Rocha I, Oliveira RS, Freitas H. Serpentine bacteria influence metal translocation and bioconcentration of Brassica juncea and Ricinus communis grown in multi-metal polluted soils. *Front Plant Sci.* 2015; 5: 757. https://doi.org/10.3389/fpls.2014.00757

[78] Yeboah A, Lu J, Gu S, Shi Y. Amoanimaa-Dede H, Agyenim-Boateng KG, Yin X. The utilization of Ricinus communis in the phytomanagement of heavy metal contaminated soils. *Environ Rev.* 2020; 28(4): 466-477. http://dx.doi.org/10.1139/er-2020-0016

[79] Gupta R, Sharma KK, Kuhad RC. Separate hydrolysis and fermentation (SHF) of Prosopis juliflora, a woody substrate, for the production of cellulosic ethanol by Saccharomyces cerevisiae and Pichia stipitis-NCIM 3498. *Bioresour Technol.*2009; 100: 1214–1220. https://doi.org/10.1016/j.biortech.2008.08.033

[80] Ananthi TA, Meerabai RS, Krishnasamy R. Potential of Ricinus Communis L. and Brassica Juncea (L.) Czern. under natural and induced Pb Phytoextraction. *Univers J Environ ResTechnol.* 2012; 2(5): 429-438. http://www.environmentaljournal.org/20133273869

[81] de Abreu CA, Coscione AR, Pires AM, Paz-Ferreiro J. Phytoremediation of a soil contaminated by heavy metals and boron using castor oil plants and organic matter amendments. *J Geochem Explor*. 2012; 123: 3–7. https://doi.org/10.1016/j.gexplo.2012.04.013

[82] Kiran BR, Prasad M N V. Ricinus communis L. (Castor bean), a potential multi-purpose environmental crop for improved and integrated phytoremediation. *Eurobiotech J.* 2017; 1(2): 1-16. https://doi.org/10.24190/ISSN2564-615X/2017/02.01

[83] Bauddh K, Singh K, Singh B, Singh RP. Ricinus communis: A robust plant for bio-energy and phytoremediation of toxic metals from contaminated soil. *Ecol Eng*. 2015; 84: 640-652. https://doi.org/10.1016/j.ecoleng.2015.09.038

[84] Palanivel TM, Pracejus B, Victor R. Phytoremediation potential of castor (*Ricinus communis* L.) in the soils of the abandoned copper mine in Northern Oman: implications for arid regions. *Environ Sci Pollut Res*. 2020; 27(14): 17359-17369. https://doi.org/10.1007/s11356-020-08319-w

[85] Olivares AR, Carrillo-González R, González-Chávez M D C A, Hernánde RS. Potential of castor bean (Ricinus communis L.) for phytoremediation of mine tailings and oil production. *J Environ Manag.* 2013; 114: 316-323. https://doi.org/10.1016/j.jenvman.2012.10.023

[86] Tripathi S, Sharma P, Purchase D, Chandra R. Distillery wastewater detoxification and management through phytoremediation employing *Ricinus communis* L. *Bioresour Technol*. 2021; 333: 125192. https://doi.org/10.1016/j.biortech.2021.125192

[87] González-Chávez MC, Olivares AR, Carrillo-González R, Leal ER. Crude oil and bioproducts of castor bean (Ricinus communis L.) plants established naturally on metal mine tailings. *Int J Environ Sci Technol*. 2015; 12(7): 2263-2272. https://doi.org/10.1007/s13762-014-0622-z

[88] Sharma S, Madan M, Vasudevan P. Biomethane production from fermented substrates. *J Ferment Bioeng.* 1989; 68(4): 296-297. https://doi.org/10.1016/0922-338X(89)90034-2

[89] Mahla SK, Dhir A. Performance and emission characteristics of CNG-fueled compression ignition engine with Ricinus communis methyl ester as pilot fueL. *Environ Sci Pollut Res*. 2019; 26(1): 975-985. https://doi.org/10.1007/s11356-018-3681-8

[90] Boulal A, Khelafi M, Djaber A. Quality Study of biodiesel produced from Ricinus communis L. (Kharouaa) in southwest Algeria. *Aljest.* 2021. ISSN : 2437-1114

[91] Umale NH, Ingle PB, Gore V. Experimental Investigation of Biodiesel (Caster-RICINUS COMMUNIS) using Variable Compression CI Engine. *Catalyst*. 2019; 6(05): 6977-6983. e-ISSN: 2395-0056 /p-ISSN: 2395-0072

[92] Ramírez V, Baez A, López P, Bustillos R, Villalobos MÁ, Carreño R, Munive J A. Chromium hyper-tolerant Bacillus sp. MH778713 assists phytoremediation of heavy metals by mesquite trees (Prosopis laevigata). *Front Microbio*L. 2019; 10: 1-12. https://doi.org/10.3389/fmicb.2019.01833

[93] Afzal M, Shabir G, Iqbal S, Mustafa T, Khan QM, Khalid ZM. Assessment of heavy metal contamination in soil and groundwater at leather industrial area of Kasur, Pakistan. *Clean (Weinh).* 2014; 42(8): 1133-1139. https://doi.org/10.1002/clen.201100715

[94] Saini P, Khan S, Baunthiyal M, Sharma V. Organ-wise accumulation of fluoride in Prosopis juliflora and its potential for phytoremediation of fluoride contaminated soil. *Chemosphere*. 2012; 89(5): 633-635. https://doi.org/10.1016/j.chemosphere.2012.05.034

[95] Kumari S, Khan S. (2018). Effect of Fe3O4 NPs application on fluoride (F) accumulation efficiency of Prosopis juliflora. *Ecotoxicol Environ Saf.* 2018; 166: 419-426. https://doi.org/10.1016/j.ecoenv.2018.09.103

[96] da Silva CG, Stamford TL, de Andrade SA, de Souza EL, de Araújo JM. Production of ethanol from mesquite (Prosopis juliflora (SW) DC) pods mash by Zymomonas mobilis and Saccharomyces cerevisiae. *Electron J Biotechnol*. 2010; 13(5): 12-23. http://doi.org/ 10.2225/vol 13-issue 5-fulltext-21

[97] Amdebrhan BT, Asfaw S, Assefa G. Acid hydrolysis optimization of Prosopis Juliflora stem for bioethanol production. *Science.* 2016; 4: 1–11 http://dx.doi.org/10.11648/j.sjee.20160401.11

[98] Sivarathnakumar S, Jayamuthunagai J, Baskar G, Praveenkumar R, Selvakumari IAE, Bharathiraja B. Bioethanol production from woody stem Prosopis juliflora using thermo tolerant yeast Kluyveromyces marxianus and its kinetics studies. *Bioresour Technol*. 2019; 293: 1-7. https://doi.org/10.1016/j.biortech.2019.122060

[99] Pasha C, Thabit HM, Kuhad RC, Linga VR. Bioethanol production from Prosopis juliflora using thermotolerant Saccharomyces cereviseae VS3 strain. *J Biobased Mater Bioenergy* 2008; 2(3): 204-209. https://doi.org/10.1166/jbmb.2008.406

[100] Hou XD, Feng GJ, Ye M, Huang CM, Zhang Y. Significantly enhanced enzymatic hydrolysis of rice straw via a highperformance two-stage deep eutectic solvents synergistic pretreatment. *Bioresour Technol.* 2017; 238: 139–146. https://doi.org/10.1016/j.biortech.2017.04.027

[101] Vaid S, Mishra T, Bajaj BK. (2018). Ionic-liquid-mediated pretreatment and enzymatic saccharification of Prosopis sp. biomass in a consolidated bioprocess for potential bioethanol fuel production. *Energy Ecol Environ.* 2018; 3(4): 216-228. https://doi.org/10.1007/s40974-018-0095-x

[102] Chang KL, Chen XM, Wang XQ, Han YJ, Potprommanee L, Liu JY, Liao YL, Ning XA, Sun SY, Huang Q. Impact of surfactant type for ionic liquid pretreatment on enhancing delignification of rice straw. *Bioresour Technol.* 2017; 227: 388–392. https://doi.org/10.1016/j.biortech.2016.11.085

[103] Kapoor M, Nair L M, Kuhad RC. Cost-effective xylanase production from free and immobilized Bacillus pumilus strain MK001 and its application in saccharification of Prosopis juliflora. *Biochem Eng J*. 2008; 38(1): 88-97. https://doi.org/10.1016/j.bej.2007.06.009

[104] Purohit R, Patel B, Harsh L N. Potential of Prosopis pallida and Prosopis juliflora for Bioethanol production. *Curr Bot.* 2013; 4(2): 18-20.

[105] Mirza N, Mahmood Q, Pervez A, Ahmad R, Farooq R, Shah MM, Azim MR. Phytoremediation potential of Arundo donax in arsenic-contaminated synthetic wastewater. *Bioresour Technol.* 2010; 101(15): 5815-5819. https://doi.org/10.1016/j.biortech.2010.03.012

[106] Atma W, Larouci M, Meddah B, Benabdeli K, Sonnet P. Evaluation of the phytoremediation potential of Arundo donax L. for nickel-contaminated soil. *Int J Phytoremediation*. 2017; 19(4): 377-386. https://doi.org/10.1080/15226514.2016.1225291

[107] Cristaldi A, Conti GO, Cosentino SL, Mauromicale G, Copat C, Grasso A, Zuccarello P, Fiore M, Restuccia C, Ferrante M. Phytoremediation potential of Arundo donax (Giant Reed) in contaminated soil by heavy metals. *Environ Res.* 2020; 185: 1-16. https://doi.org/10.1016/j.envres.2020.109427

[108] Sabeen M, Mahmood Q, Irshad M, Fareed I, Khan A, Ullah F, Hussain J, Hayat Y, Tabassum S. Cadmium phytoremediation by Arundo donax L. from contaminated soil and water. *Biomed Res Int*. 2013; 1: 1-10. https://doi.org/10.1155/2013/324830

[109] Liu Y.N, Xiao XY, Guo ZH. Identification of indicators of giant reed (Arundo donax L.) ecotypes for phytoremediation of metal-contaminated soil in a non-ferrous mining and smelting area in southern China. *Ecol Indic.* 2019; 101: 249-260. https://doi.org/10.1016/j.ecolind.2019.01.029

[110] Cano-Ruiz J, Galea MR, Amorós MC, Alonso J, Mauri PV, Lobo MC. Assessing Arundo donax L. in vitro-tolerance for phytoremediation purposes. *Chemosphere.* 2020; 252: 1-7. https://doi.org/10.1016/j.chemosphere.2020.126576

[111] Azizi A, Krika A, Krika F. Heavy metal bioaccumulation and distribution in Typha latifolia and Arundo donax: implication for phytoremediation. *Casp J Environ Sci.* 2020; 18(1): 21-29. https://dx.doi.org/10.22124/cjes.2020.3975

[112] Alshaal T, Domokos-Szabolcsy É, Márton L, Czakó M, Kátai J, Balogh P, Elhawat N, El-Ramady H, Fári M. Phytoremediation of bauxite-derived red mud by giant reed. *Environ Chem Lett.* 2013; 11(3): 295-302. http://dx.doi.org/10.1007/s10311-013-0406-6

[113] Mahmood NMQ. Phytoremediation of arsenic (As) and mercury (Hg) contaminated soil. *World Appl Sci J*. 2010; 8(1); 113-118.

[114] Domokos-Szabolcsy É, Fári M, Márton L, Czakó M, Veres S, Elhawat N, Antal G, El-Ramady H, Zsíros O, Garab G, Alshaal T. Selenate tolerance and selenium hyperaccumulation in the monocot giant reed (Arundo donax), a biomass crop plant with phytoremediation potential. *Environ Sci Pollut Res.* 2018; 25(31): 31368-31380. https://doi.org/10.1007/s11356-018-3127-3

[115] Xing X, Baoyu G, Yaqing Z, Suhong C, Xin T, Qinyan Y, Jianya L, YanW. Nitrate removal from aqueous solution by Arundo donax L. reed based anion exchange resin. *J Hazard Mater.* 2012; 203– 204: 86–92. https://doi.org/10.1016/j.jhazmat.2011.11.094

[116] Elhawat N, Alshaal T, Domokos-Szabolcsy É, Márton L, Czakó M, KátaiJ, Balogh P, Sztrik A, El-Ramady H, Molnár M, Fári M. Phytoaccumulation potentials of two biotechnologically propagatedecotypes of Arundo donax in copper-contaminated synthetic waste-water. *Environ Sci Pollut Res*. 2014; 21(12): 7773–7780. https://doi.org/10.1007/s11356-014-2736-8

[117] Elhawat N, Alshaal T, Domokos-Szabolcsy É, El-Ramady H, Antal G, Márton L, Czakó M, Balogh P, Fari M. Copper uptake efficiency and its distribution within bioenergy grass giant reed. *Bull Environ Contam Toxicol*. 2015; 95(4): 452–458 https://doi.org/10.1007/s00128-015-1622-5

[118] De Bari I, Liuzzi F, Ambrico A, Trupo M. Arundo donax Refining to Second Generation Bioethanol and FurfuraL. *Processes*. 2020; 8(12): 1-15. https://doi.org/10.3390/pr8121591

[119] Brusca S, Cosentino SL, Famoso F, Lanzafame R, Mauro S, Messina M, Scandura PF. Second generation bioethanol production from Arundo donax biomass: an optimization method. *Energy Procedia*. 2018; 148: 728-735. http://dx.doi.org/10.1016/j.egypro.2018.08.141

[120] Zucaro A, Forte A, Basosi R, Fagnano M, Fierro A. Life Cycle Assessment of second generation bioethanol produced from low-input dedicated crops of Arundo donax L. *Bioresour Technol*.2016; 219: 589-599. https://doi.org/10.1016/j.biortech.2016.08.022

Majeed S, Hafeez FY, Li X, Salama ES, Ji J, Malik K, Umer M. Evaluation of Fungal and Sonication Pretreatments to Improve Saccharification Yield of Arundo donax. *Int J Agric Biol* .2020; 24(6): 1449-1456. http://dx.doi.org/10.17957/IJAB/15.1582

[122] Jeon Y J, Xun Z, Rogers PL. Comparative evaluations of cellulosic raw materials for second generation bioethanol production. *Lett. Appl. Microbiol*. 2010; 51(5): 518-524. https://doi.org/10.1111/j.1472-765x.2010.02923.x

[123] Scordia D, Cosentino SL, Lee JW, Jeffries TW. Bioconversion of giant reed (Arundo donax L.) hemicellulose hydrolysate to ethanol by Scheffersomyces stipitis CBS6054. *Biomass Bioenergy* 2012; 39: 296-305. https://doi.org/10.1016/j.biombioe.2012.01.023

[124] e Silva CFL, Schirmer MA, Maeda RN, Barcelos CA, Pereira JrN. 2015. Potential of giant reed (Arundo donax L.) for second generation ethanol production. *Electron J Biotechnol.* 2015; 18(1): 10-15. http://dx.doi.org/10.1016/j.ejbt.2014.11.002

[125] Ask M, Olofsson K, Di Felice T, Ruohonen L, Penttilä M, Lidén G, Olsson L. Challenges in enzymatic hydrolysis and fermentation of pretreated Arundo donax revealed by a comparison between SHF and SSF. *Process Biochem*.2012; 47: 1452–1459 http://dx.doi.org/10.1016/j.procbio.2012.05.016

[126] Scordia D, Cosentino SL, Lee JW, Jeffries TW. Dilute oxalic acid pretreatment for biorefining giant reed (Arundo donax L.). *Biomass Bioenergy* 2011; 35: 3018–3024. https://doi.org/10.1016/j.biombioe.2011.03.046

[127] Aliberti A, Ventorino V, Robertiello A, Galasso M, Blaiotta G, Comite E, Faraco V, Pepe O. Effect of cellulase, substrate concentrations, and configuration processes on cellulosic ethanol production from pretreated Arundo donax. *Bioresources*. 2017; 12(3): 5321-5342. https://doi.org/10.15376/biores.12.3.5321-5342

[128] Loaces I, Schein S, Noya F. Ethanol production by Escherichia coli from Arundo donax biomass under SSF, SHF or CBP process configurations and in situ production of a multifunctional glucanase and xylanase. *Bioresour Technol*. 2017; 224: 307-313. https://doi.org/10.1016/j.biortech.2016.10.075

[129] Silitonga AS, Masjuki HH, Ong HC, Yusaf T, Kusumo F, Mahlia TMI. Synthesis and optimization of Hevea brasiliensis and Ricinus communis as feedstock for biodiesel production: A comparative study. *Ind Crops Prod*. 2016; 85: 274-286. https://doi.org/10.1016/j.indcrop.2016.03.017

[130] Majeed S, Hafeez FY, Li X, Salama ES, Ji J, Malik K, Umer M. Evaluation of Fungal and Sonication Pretreatments to Improve Saccharification Yield of Arundo donax. *Int J Agric Biol*. 2020; 24(6): 1449-1456. https://doi.org/10.17957/IJAB/15.1582

[131] Althuri A, Gujjala LKS, Banerjee R. Partially consolidated bioprocessing of mixed lignocellulosic feedstocks for ethanol production. *Bioresour Technol*. 2017; 245: 530-539. https://doi.org/10.1016/j.biortech.2017.08.140

[132] Nikolić M, Stevović S. Family Asteraceae as a sustainable planning tool in phytoremediation and its relevance in urban areas. *Urban For Urban Green.* 2015; 14(4): 782-789. https://doi.org/10.1016/j.ufug.2015.08.002

Energetske biljke kao izvor biogoriva i kao akumulatori teških metala

Magdalena Nikolić[1], Vladimir Tomasević[1] i Dragan Ugrinov[2]

[1]Fakultet za inženjerski menadzment, Bulevar vojvode Mišića 43,11000 Beograd, Srbija
[2]Institut za javno zdravlje, Pančevo, Pasterova 2, Pančevo, Srbija

(Stručni rad)

Izvod

Nedostatak fosilnih goriva i zagađenje zemljišta i vode motivisali su stvaranje nove perspektive održivog razvoja. Ne samo da se biljna biomasa može koristiti u proizvodnji etanola, već se ista biljka može koristiti i za minimiziranje/eliminaciju teških metala prisutnih u zemljištu i vodi. Rezistentne na visoke koncentracije metala, mnoge biljne vrste, usevi, medicinske i farmaceutske energetske biljke su dobro poznati hiperakumulatori teških metala. Ovaj rad se fokusira na studije koje istražuju potencijal *Miscanthus.sp, Beta vulgaris L, Saccharum sp., Ricinus communis* L. *Prosopis sp i Arundo donak* L. u uklanjanju teških metala i proizvodnji biogoriva. Fitoremedijacija korišćenjem ovih biljaka pokazala je veliki potencijal bioakumulacije Co, Cr, Cu, Al, Pb, Ni, Fe, Cd, Zn, Hg, Se, itd. Takodje, za pretvaranje celuloze u fermentabilne šećere, predtretmani kao što su ozonoliza, tretman bazama ili kiselinama, parom ili toplom vodom, primenjeni su pre enzimske saharifikacije mikroorganizmima. Ovaj pregled predstavlja uvid u potencijal lignocelulozних biljaka da uklone zagađujuće supstance i ujedno su vredan supstrat za proizvodnju biogoriva. Takođe, razmatrani su predtretmani, bavljenje toksičnom biomasom i proizvodnja biogoriva.

Ključne reči: polutanti; bioakumulacija; bioenergija

Physical simulation of finish rolling of microalloyed steels in isothermal conditions

Stefan Dikić[1], Dragomir Glišić[1], Abdunaser Hamza Fadel[2], Gvozden Jovanović[3] and Nenad Radović[1]

[1]*University of Belgrade, Faculty of Technology and Metallurgy, Karnegijeva 4, 11120 Belgrade, Serbia*
[2]*Al Zawia University, Faculty of Natural Resources, Department of Petroleum Engineering, P.O.BOX 16418 Al Zawia, Libya*
[3]*Institute for Technology of Nuclear and Other Mineral Raw Materials, Metallurgical and Environmental Engineering, Bulevar Franš d'Eperea 86, 11000 Belgrade, Serbia*

Abstract

The aim of this work was to establish a temperature of finish rolling stage of Nb/Ti microalloyed steel containing 0.06 wt.% C, 0.77 wt.% Mn, 0.039 wt.% Nb and 0.015 wt.% Ti, using physical simulation. Samples were subjected to laboratory simulation at a twist plastometer at high temperatures, *i.e.* between 825 and 950 °C. Five pass deformation and interpass times were selected in accordance with a processing parameters at five stand finishing hot strip mill. Restoration (recovery and/or recrystallization) behavior was evaluated by calculation of Fraction Softening (FS) and Area Softening Parameter (ASP) values. At 950 °C all individual pass stress-strain curves, FS and ASP show full recrystallization in all interpass intervals. On the other hand, with a decrease in temperature to the interval of 875-825 °C, the extent of restoration is decreasing, leading to recovery as a sole softening mechanism at 825 °C, which was confirmed by the stress-strain curve shape, and values of FS and ASP. It is assumed that, due to high supersaturation, strain-induced precipitation promoted pinning of grain and subgrain boundaries and suppressed recrystallization. Therefore, the critical temperature for finish rolling was estimated to be 825 °C.

Keywords: fraction softening; mechanical metallography; deformation; recrystallization, critical rolling temperatures, controlled rolling.

Available on-line at the Journal web address: http://www.ache.org.rs/HI/

ORIGINAL SCIENTIFIC PAPER

UDC: 669.146-034.15:620.181.5

Hem. Ind. **76(4)** 227-236 (2022)

1. INTRODUCTION

Development of microalloyed steels is an answer to a growing demand of the modern industry for steels with improved strength, toughness and weldability [1-3]. Weight reduction in structures and low-cost manufacturing processes are constant challenges in metallurgical engineering [4]. Microalloyed steels are divided into two main groups: low and medium carbon microalloyed steels. In addition to for low carbon content values, low carbon microalloyed steels contain less than 0.15 wt.% of vanadium (V), titanium (Ti) and niobium (Nb) in total.

Addition of microalloying elements combined with adequate thermomechanical treatment (TMCP) results in significantly improved mechanical properties [3], in comparison to C-Mn steels, without expensive subsequent heat treatment. Thermomechanical treatment of low carbon microalloyed steels should provide desired shape and dimensions as well as final microstructure [5]. In that regard, hot rolling does not only provide controlling the temperature, strain (ε) and strain rate to attain the final dimension and microstructures, but it is also applied to obtain a product with desired mechanical properties [3,5].

The most common hot rolling technology, known as conventional controlled rolling (CCR) of microalloyed steels consists of rough rolling, finish rolling and controlled cooling of hot rolled steel before coiling [5-7]. Therefore subsequent heat treatment is not necessary [5]. Roughing stage is performed at temperatures that should be high enough to provide a complete static recrystallization (SRX) during the interpass time. Due to short interpass time and adiabatic heating, it can be assumed that finish rolling happens under isothermal conditions [5]. As shown in Figure 1,

Corresponding authors: Stefan Dikić, University of Belgrade, Faculty of Technology and Metallurgy, Karnegijeva 4, 11120 Belgrade, Serbia
E-mail: sdikic@tmf.bg.ac.rs
Paper received: 16 August2022; Paper accepted: 12 November; Paper published: 11 December 2022.
https://doi.org/10.2298/HEMIND220816018D

the roughing stage is performed above the non-recrystallization temperature, T_{nr}, temperature above which recrystallization is still complete [8-11]. Hot rolling at a finish rolling mill, is performed between T_{nr} and A_3, temperature below which recrystallization is suppressed as can be seen in Figure 1 [5,7-9,10,12]. Suppression of the recrystallization process depends on formation of precipitates (nitrides and/or carbonitrides) based on microalloying elements [13-17]. When additional strengthening is required, finish rolling might be performed in the dual phase temperature region (between A_1 and A_3), where ferrite grains are deformed as well as austenitic grains, which results in formation of substructure in deformed ferrite grains. Finish rolling is followed by controlled cooling or even accelerated cooling, which results in even finer grained microstructure. The non-recrystallization temperature, T_{nr} [8,9,16,18] is determined based on the Boratto test [7,16-18], while the T_{rl} (the lowest temperature for full recrystallization) and T_{rs} (the highest temperature for suppression of recrystallization) are also reported [8-11]. the non-recrystallization temperature, T_{nr}, is usually considered to be close to the T_{rl}, or temperature for 50 % of SRX, *i.e.* temperatures below which finish rolling can be performed [8-11,16,18].

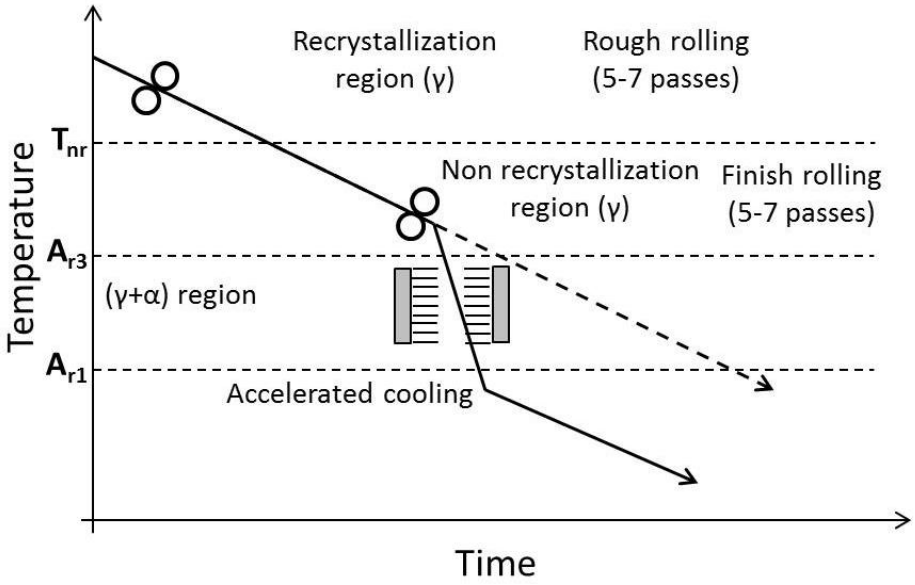

Figure 1. Schematic illustration of thermomechanical processing

Therefore, determination of critical temperatures is of great importance, to select the right temperature, which will provide large number of nucleation sites for precipitation (dislocation loops, deformation bands, subgrain boundaries, deformation twins) in microstructure during finish rolling. The proper control of critical hot rolling temperatures results in formation of un-recrystallized austenite with high nucleation sites density. In that way, a final fine grained ferritic microstructure forms during continuous cooling from hot deformation temperatures.

Evaluation of microstructural changes during plastic deformation *i.e*. during finish rolling in a hot strip mill is not possible by using traditional quenching of samples and optical microscopy, because it is not possible to quench the sample immediately after the deformation. In order to overcome this problem, it is needed to evaluate changes in microstructures on the basis of behaviour of steel during the deformation. Two opposite processes occur during hot rolling – strain hardening due to deformation and softening due to recovery/recrystallization. Therefore, the stress-strain curve or measured rolling force for each pass can be used to quantify the overall behaviour, based on comparison of yield stress, strain hardening rate and maximal stress. This approach thus quantifies changes in the microstructure based on measured stresses and forces, known as mechanical metallography. It provides accurate and reliable information and enables modelling of microstructural changes in real time on industrial scale.

The aim of this work was to establish the critical temperature for finish hot rolling of microalloyed steels by means of physical simulation.

2. EXPERIMENTAL

The low carbon microalloyed (Nb/Ti) steel tested in this work was industrially melted and casted, and subsequently pre rolled to a sheet, 30 mm thick, in a Hot Strip Mill (HSM) in the company Steelworks Smederevo, Serbia. The chemical composition was provided by the producer and is given in Table 1.

Table 1. Chemical composition of the tested steel

Elements	C	Si	Mn	P	S	Al	Nb	Ti	N	O
Content, wt.%	0.06	0.068	0.77	0.015	0.008	0.052	0.039	0.015	0.0053	0.0045

Simulation of hot rolling process during finish rolling was performed by a multi-pass isothermal torsion test, by using a Setaram-Irsid torsion tester (Irsid, France). Main advantage of torsion testing is that it enables attaining high strains without reaching plastic instability [15,19,20]. Furthermore, deformation of several rolling passes can be simulated using only one sample. During torsion, specified deformation values (Table 2) are achieved only on the outer surface of the specimen. On other hand, torsion samples could not be used for metallographic examination, due to occurrence of corrosion and porosity on the outer surface. Isothermal hot rolling simulation was performed to determine critical temperatures. The torsion test specimens were cylinders 6 mm in diameter and 50 mm in gauge length. Specimens were annealed in the testing machine at 1250 °C for 15 min in argon atmosphere, in order to provide homogeneous distribution of alloying elements and to remove the priorly existing texture. Next, the specimens were cooled down to 1000 °C at a rate of approximately 2 °C s^{-1}, at which the simulation of roughing was performed, as to provide uniform grain size distribution in all specimens before simulation of rolling at a finishing mill. Simulation of roughing in this test was performed by predeformation (PD1 and PD2 in Fig. 2) in two passes (strain 0.3), with 10 s of the interpass time. These two passes were performed to provide uniform microstructure before the finish hot rolling simulation. Subsequently, the specimens were cooled to the isothermal testing temperature (825, 850, 875 and 950 °C) and held at this temperature for 60 s to provide uniform temperature distribution. Samples were subjected to plastic deformation in five passes. To assess the reproducibility, two tests were run for each set of conditions.

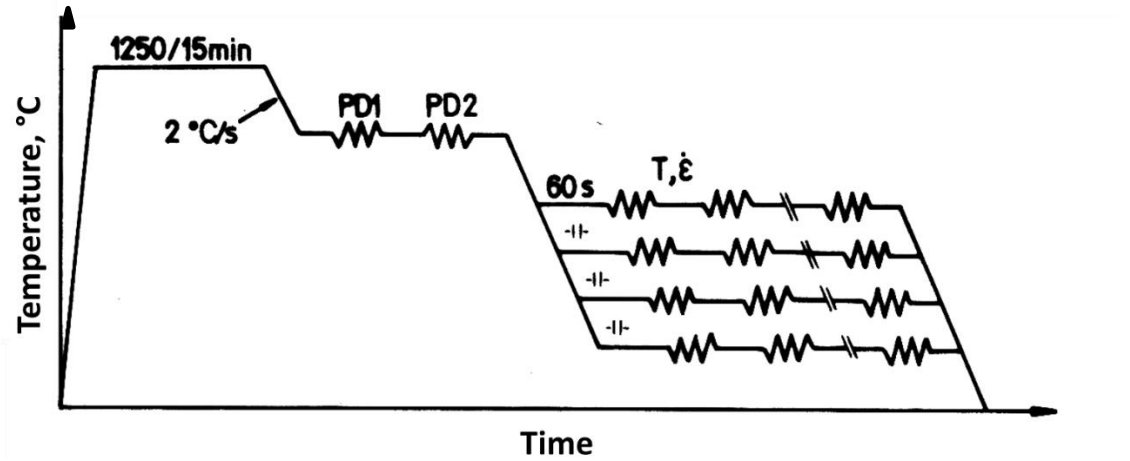

Figure 2. Schematic illustration of the simulation test of thermomechanical processing of microalloyed steel

Details/processing parameters of deformation are shown in Table 2. Strain in each pass is selected to be in accordance with five stand finish rolling schedule in the Hot Strip Mill, Steelworks Smederevo.

Table 2. Schedule of hot rolling simulation

Pass	I	II	III	IV	V
Strain	0.5	0.5	0.35	0.35	0.2
Interpass time, s	4.75	3.25	2.25	1.75	

3. RESULTS

Stress-strain curves obtained in torsion tests at specified temperatures are shown in Figure 3.

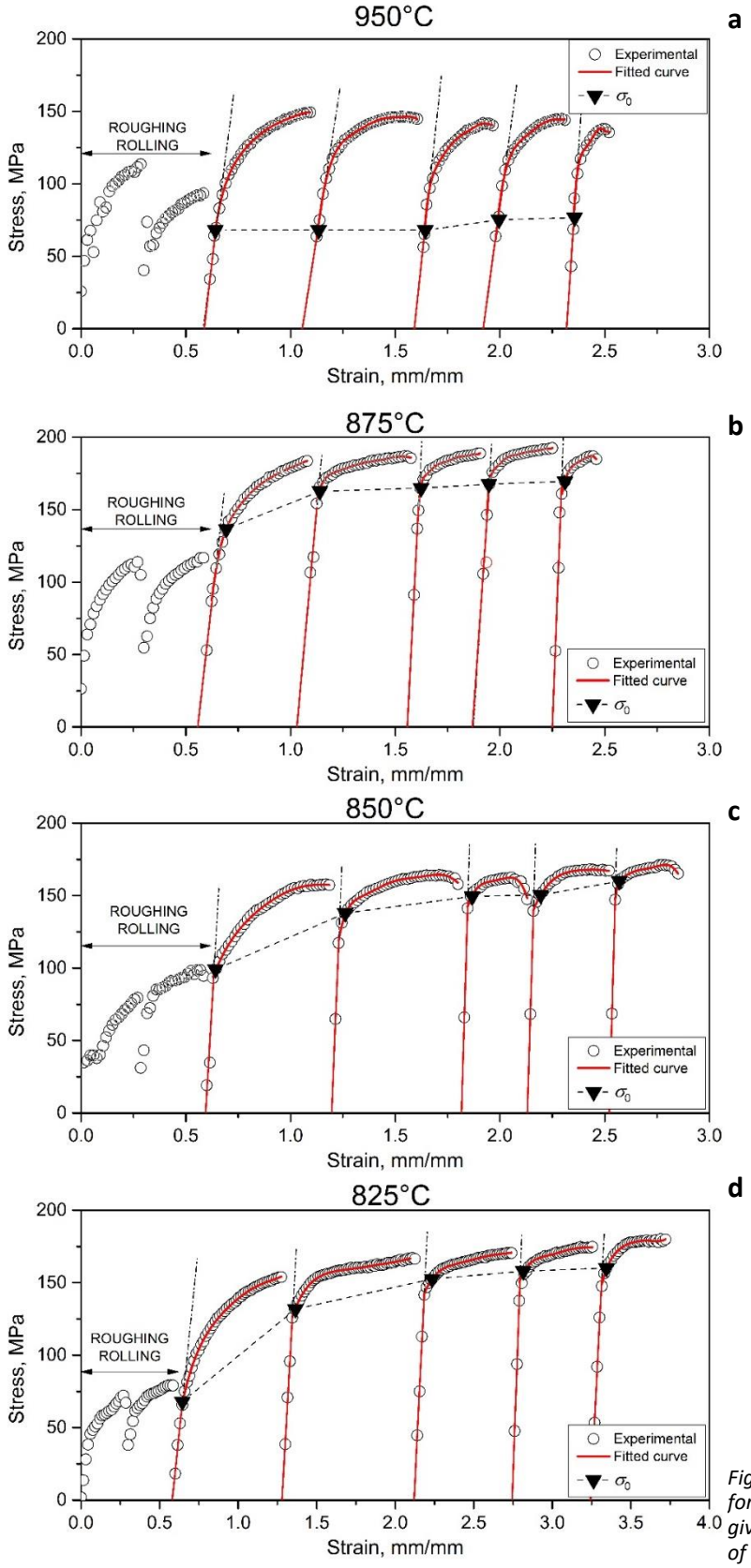

Figure 3. Experimental stress-strain curves obtained for rolling simulations according to the schedule given in Table 2 and the best linear fits in the region of plastic deformation at the testing temperatures

First two passes (0.6 strain in total) at each diagram are related to the roughing rolling stage and will not be discussed in detail. Simulation of finish rolling begins with the third pass, which represents deformation behavior of fully recrystallized samples. In that way, the third pass represents the 1st pass of the finish rolling. Stress-strain curves are represented in the graphs in Figure 3 both as experimental points and as the curves obtained by polynomial fitting. The slope of the fitted curve represents a qualitative measure for evaluation of deformation behavior (strengthening or restoration).

As can be seen in Figure 3a, at 950 °C stress-strain curves of each pass obtained during simulation exhibit the same shape, characterized by a high slope of fitted curves in the region of plastic deformation. In comparison, stress-strain curves obtained during simulations at 875 and 850°C (Fig. 3b and Fig. 3c) exhibit lower slopes of fitted curves in the region of plastic deformation while the lowest slope is obtained at 825 °C (Fig. 3d).

In order to determine yield stress (σ_0), the strain offset method (ε ~5 %) was performed, which. provides reliable results according to the literature [13,17]. The yield stress of each finish rolling pass is indicated in the graphs presented in Figure 3.

In order to evaluate and quantify recrystallization during the hot rolling simulation, mechanical metallography was applied, *i.e.* microstructural changes were evaluated on the basis of the change in deformation behavior. Stress-strain curves generated in each pass, during the isothermal torsion test, were compared to each other and analyzed in details. In order to evaluate the progress of softening (recovery and/or recrystallization) during the interpass time, fraction softening (*FS*), was calculated according to the equation [10,13,21]:

$$FS\,/\,\% = \frac{\sigma_m{}^{i} - \sigma_0{}^{i+1}}{\sigma_m{}^{i} - \sigma_0{}^{1}} 100 \quad (1)$$

where $\sigma_m{}^{i}$ is the maximum stress in the ith pass, $\sigma_0{}^{1}$ is the yield stress in the 1st pass, $\sigma_0{}^{i+1}$ is the yield stress in the (i+1) pass. All values in equation 1 are determined using the strain offset method (ε ~5 %).

According to literature [13,15], *FS* values lower than 20 % indicate recovery as a softening mechanism, *FS* values in range of 20-100 % indicate recrystallization while *FS* > 100 % indicates grain growth in the material. Furthermore, negative FS values indicate strengthening during interpass time. This strengthening can be attributed to strain induced precipitation [13,15].

An additional attempt to evaluate recrystallization behavior was performed by introducing the area softening parameter (*ASP*) [13]. Area under the curve was calculated by numerical integration. Values obtained in the 1st pass were referred as fully recrystallized and were used as a reference for comparison of the areas determined for each pass at equal strains. In order to quantify the SRX behaviour, the area softening parameter (*ASP*) was calculated by using the equation:

$$ASP\,/\,\% = \frac{A_i - A_1}{A_i} 100 \quad (2)$$

where A_i is the area under the stress-strain curve of the ith pass and $A_1$is the area under the 1st curve for the strain level of ith pass. *ASP* value lower than 0 % indicates grain growth, while those greater than 0 % indicate strengthening (incomplete static recrystallization). Complete recrystallization is indicated by *ASP* = 0 %.

The determined *FS* and *ASP* values at different temperatures are shown in Figure 4. Estimated standard deviations of calculated FS and ASP values are in the range of 2.4 to 5.7 and 1.8 to 5.1 respectively.

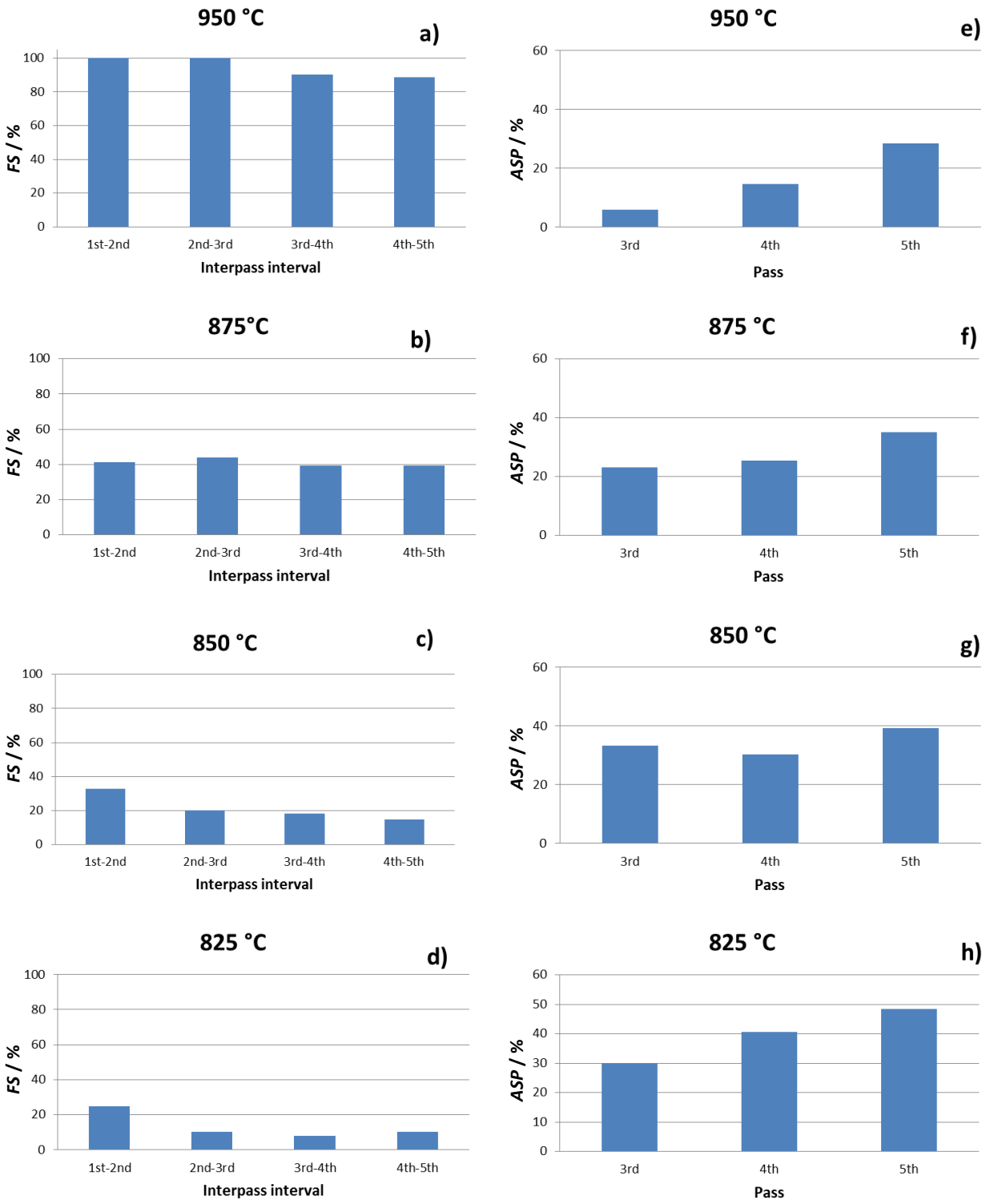

Figure 4. Changes during the interpass intervals described by: (a-d) fractional softening (FS) values between given passes (during the interpass times) and (e-h) area softening parameters (ASP) with passes, at different testing temperatures

4. DISCUSION

The aim of performed roughing rolling in this simulation test was to provide uniform grain size distribution as well as fully recrystallized microstructure before the simulation of finish rolling. It was found that after two passes and

subsequent full SRX the influence of the prior austenite grains can be neglected [3,22,23]. It could be observed that the shape of stress-strain curves for the 1st pass of finish rolling corresponds to the shape of a stress-strain curve for fully recrystallized conditions [13,16]. Therefore, it could be deduced that before finish rolling, the steel microstructure was recrystallized so that all tested samples had the same starting point in the terms of microstructure.

Shape of the stress-strain curves, strengthening and the restoration process during finish rolling are controlled by interaction of deformation, recrystallization and precipitation processes*, i.e.* by the addition of microalloying elements as well as by hot rolling parameters. Addition of Ti, V, and Nb to low carbon steels, has a great impact on the steel mechanical properties through grain refinement as well as through mechanisms of solid solution strengthening and dispersion strengthening by carbides, nitrides and/or carbonitrides in ferrite [1,8,13-16,24]. Carbides, nitrides and carbonitrides of microalloying elements precipitate at austenite grain boundaries, which cause pinning of austenite grain boundaries at temperatures just over A_3 and retardation/suppression of recrystallization.

Supersaturation ratio, k_S, of niobium carbonitride (Nb(C,N)), defined as the ratio, of actual amount of C, Nb and N in solution to the equilibrium solubility product, at specified temperature was calculated by the equation [24,25]:

$$k_s = \frac{c_{Nb}\left(c_C + \frac{12}{14}c_N\right)}{10^{2.26-\frac{6770}{T}}} \quad (3)$$

where c_{Nb}/ wt.% is the Nb concentration in steel, c_C/ wt.% is the concentration of C in steel, c_N/ wt.% is the concentration of N in steel, and T / K is the absolute temperature.

Super saturation ratios for Nb(C,N) on testing temperatures, calculated by eq. (3), are given in Table 3.

Table 3. Supersaturation ratio of Nb(C,N) at testing temperatures

Finish rolling temperature, °C	k_s	Precipitation
950	4.75	NO
875	10.92	YES
850	14.77	YES
825	20.26	YES

It is assumed that the critical supersaturation ratio for strain-induced precipitation has to be between 5.5 and 7 [8,26].

Yield stress in passes from 1st to 3rd at 950°C have similar values, which are forwarded by slight increase in 4th and 5th pass (Fig. 3a). This behaviour implicates a high share of recrystallization during the interpass times being dominant over the strengthening effect caused by plastic deformation. The obtained phenomena are quantified by calculating fraction softening *FS* values. *FS* values above 80 % obtained at 950 °C indicate almost full static recrystallization (Fig. 4a). Also, the extent of recrystallization is decreasing from 2nd to 5th pass, which can be attributed to shorter interpass times. The *ASP* values (Fig. 4e) follow the same trend, *i.e.* the increase in *ASP* indicates that SRX was impeded to same extent. Due to the low supersaturation ratio, precipitation is not expected, *i.e.* it can be assumed that the solute drag is responsible for the lower extent of recrystallization. The obtained higher *ASP* values in the last two passes might be explained by accumulation of deformation and a slightly higher level of suppression of recrystallization, which might be dominantly caused by short interpass times.

At 875 °C yield stress of each subsequent pass is higher than the yield stress of the first one (Fig.3b) but difference is not as pronounced as it is at lower temperatures. As can be seen in Figure 3c, each pass during finish rolling simulation at 850 °C has significantly higher yield stress than that obtained in the 1st pass as well as in the previous one, which indicates dominant strengthening over softening. Shapes of the obtained curves are in agreement with calculated supersaturation ratio (Table 3). In the test at 875 °C, *FS* values vary around 40 %, indicating low extent of recrystallization (Fig. 4b). Stress-strain curves from the 2nd to the final pass exhibit higher yield stress (Fig. 3b) accompanied with lower stress hardening rate which is observed as the lower slope of the fitted curves, shown in Figure 3b. This indicates suppression of recrystallization by stimulation of precipitation of Nb(C,N) [13,14]. Almost constant *FS* at 850 °C from the 1st to the last interpass interval might be related to strain-induced precipitation, which strongly affects suppression of

recrystallization [13]. During the 1st interpass time some extent of recrystallization takes part, while recovery is dominant during the interpass times between following passes (Fig. 4c). *ASP* values for simulation of hot rolling at 875 °C (Fig. 4f) imply higher strengthening effect from 3rd to 5th rolling pass compared with *ASP* values obtained at 950 °C. *ASP* results are in agreement with the obtained *FS* values. *ASP* values obtained at 850 °C (Fig. 4g) are higher than values obtained at higher temperatures which indicate suppression of recrystallization and increase in strengthening.

Further lowering of the test temperature to 850 °C (Figs 4c and 4g) and 825 °C (Figs 4d and 4h), induced similar behavior, except for more pronounced suppression of recrystallization. At 825 °C, limited restoration is observed only during the 1st interpass interval. It can be assumed that SRX is competing with precipitation, *i.e*. that SRX has a shorter incubation period. On the other hand, once precipitation started, SRX is not the governing phenomenon anymore*, i.e.* precipitation precedes recrystallization, resulting in total suppression of recrystallization. This efficient suppression of recrystallization causes strain accumulation, meaning that due to absence of recrystallization, strength at the beginning of a subsequent pass is equal to already pre-strained condition. In some cases, in the subsequent pass, the critical stress for dynamic recrystallization might be attained [6,28,29]. Results also indicate that dynamic recrystallization does not occur in this work.

Stress-strain curves for the 2nd to the 5th pass, obtained during simulation of hot rolling at 825 °C (Fig. 3d) show slightly lower values of the yield stress compared to the maximum stress of the previous pass (Fig .3d) and shows higher yield stress compared to yield stress of each previous pass as shown by σ_0^i trendline in Figure 3d. So, it is clear that strengthening is dominant over softening, which is assumed to be recovery [13,15]. Decrease in the yield stress of the 2nd pass compared to the maximum strength of the 1st pass (*FS* ~20 % Fig. 4d) is assumed to be recovery [13,15]. *FS* values are decreasing from 2nd to 5th pass (Fig. 4d). *FS* values for 3rd, 4th and 5th are lower than 20 % (Fig. 4d).

The supersaturation ratio of Nb[C,N] (Table 3) at 825 °C (20.26) is higher than 5.5, which indicates intensive strain-induced precipitation on austenite grain boundaries [13,15,24,25]. Intensive precipitation causes pinning of grain boundaries and suppression of recrystallization, which agrees with shapes of the stress-strain curves (Fig. 3d) and obtained *FS* values (Fig. 4d) as well as with the *ASP* parameter (Fig. 4h). Suppression of recrystallization causes accumulation of deformation, which results in strengthening of the hot rolled steel.

It can be assumed that due to the high supersaturation ratio, strain accumulation caused strain-induced precipitation during the interpass time, resulting in the higher volume of the precipitated phase and adequate hardening.

Based on all results, the critical temperature for the finishing stage of control rolling is estimated to be 825 °C.

5. CONCLUSION

In this paper, deformation/recrystallization behaviour of microalloyed steel at high temperatures was examined. Steel used in this research was low carbon Nb/Ti microalloyed steel and was tested in order to determine the finish rolling temperature for industrial five stand finish rolling train. Simulation was performed by a multi-pass isothermal torsion test in the temperature range of 825-950°C. Evaluation of microstructural changes during the test was performed by calculation of *FS*. A new method, area softening parameter (*ASP*), for mechanical metallography was also applied to analyse the obtained stress-strain curves.

Individual pass stress-strain curves obtained at 950°C as well as *FS* and *ASP* values indicated full recrystallization during the interpass time. At lower temperatures the extent of recrystallization during the interpass time decreased. At 825°C recrystallization is completely suppressed by strain-induced precipitation, which pins the grain boundaries. Fraction softening and *ASP* values show the same trends for each testing temperature and all the obtained results are in agreement with the shape of stress-strain curves. *ASP* as a criterion provides qualitative results, while accuracy in terms of quantitative analysis should be further developed. Finally, based on all obtained results, the critical temperature for finish rolling was estimated to be 825°C.

Funding: *This work was supported by the Ministry of Education, Science and Technological Development of the Republic of Serbia (Contract No. 451-03-68/2022-14/200135). This work was carried out as a partial fulfillment of the requirements for the PhD degree of Dikić Stefan at the University of Belgrade, Faculty of Technology and Metallurgy.*

REFERENCES

[1] Villalobos JC, Del-Pozo A, Campillo B, Mayen J, Serna S. Microalloyed steels through history until 2018: Review of chemical composition, processing and hydrogen service. *Metals (Basel)* 2018;8(5). https://doi.org/10.3390/met8050351

[2] Morrison BW. Microalloyed steels for offshore application. In: Microalloying '95. Pittsburgh, USA; 1995;105–16; ISBN 0932897983

[3] Siwecki T, Hutchinson B, Zajac S. Recrystallization controlled rolling of HSLA steels. In: Microalloying '95. Pittsburgh, USA; 1995;197–211; ISBN 0932897983

[4] Collins LE, Baragar DL, Bowker JT, Kostic MM, Subramanian SV. Steckel Mill Process Optimization for Production of X70 and X80 Gas Transmission Linepipe. In: Microalloying '95. Pittsburgh, USA: 1995;141–7; ISBN 0932897983

[5] Tanaka T. Science and technology of hot rolling process of steel. In: Microalloying '95. Pittsburgh, USA; 1995;165–81; ISBN 0932897983

[6] Drobnjak D, Radović N. A Contribution to the Study of Dynamic Recrystallization in a Nb/Ti Microalloyed Steel. *Mater Sci Forum* 1993;113–115:411–6. https://doi.org/10.4028/www.scientific.net/msf.113-115.411

[7] Siciliano F, Jonas J. Mathematical modeling of the hot strip rolling of Nb microalloyed steels. *Metall Mater Trans A* 2000; 31A: 501—530. https://doi.org/10.1007/s11661-000-0287-8

[8] Dutta B, Sellars CM. Predictions from nucleation theory. *Mater Sci Technol* 1987; 3: 197–206. https://doi.org/10.1179/mst.1987.3.3.197

[9] Yue S, Jonas JJ. The three critical temperatures of steel rolling and their experimental determination. *Mater Forum* 1990;14(4):245

[10] Ballard TJ, Speer JG, Findley KO, De Moor E. Double twist torsion testing to determine the non-recrystallization temperature. *Sci Rep* 2021;11(1). https://doi.org/10.1038/s41598-021-81139-1

[11] Felker CA, Speer JG, De Moor E, Findley KO. Hot strip mill processing simulations on a Ti-Mo microalloyed steel using hot torsion testing. *Metals (Basel)* 2020;10(3). https://doi.org/10.3390/met10030334

[12] Drobnjak D, Radovic N, Djuric B. Effect of Test Variables on QHW and Tnr. In: Mechanical Working and Steel Processing Conference. Ontario, Canada; 1995; 759–68; ISBN: 9781886362055

[13] Kwon O, DeArdo AJ. Niobium carbonitride precipitation and static softening in hot-deformed niobium microalloyed steels. In: HSLA STEELS: METALLURGY AND APPLICATION. Beijing, China; 1985;287–98; ISBN: 0-87170-299-0

[14] Palmiere EJ, Garcia CI, DeArdo AJ. Static Recrystallization and Precipitation During the Hot Deformation of Austenite. In: International Conference on Processing, Microstructure and Properties of Microalloyed and Other Modern High Strength Low Alloy Steels. Pittsburgh: Iron and Steel Society; 1991;113–33; ISBN: 0932897711

[15] Andrade HL, Akben MG, Jonas JJ. Effect of Molybdenum, Niobium, and Vanadium on Static Recovery and Recrystallization and on Solute Strengthening in Microalloyed Steels. *Metall Trans A* 1983;14A:1967–77. https://doi.org/10.1007/BF02662364

[16] F. Boratto, R. Barbosa, S. Yue, J.J. Jonas, In: THERMEC-88, Tokyo, Japan, Vol. 1 (1988) 383-389.

[17] Fernández AI, López B, Rodríguez-Ibabe JM. Relationship between the austenite recrystallized fraction and the softening measured from the interrupted torsion test technique. *Scr Mater* 1999;40(5):543–9. https://doi.org/10.1016/S1359-6462(98)00452-7

[18] Radovic N, Drobnjak D. Effect of Interpass Time and Energy for Hot Working and of Nb-microalloyed Steel Cooling Rate on Apparent Activation Critical Recrystallization Temperature. *ISIJ Int* 1999; 39(6): 575–82 https://doi.org/10.2355/isijinternational.39.575

[19] Semiatin SL, Jonas JJ. Formability and workability of metals: plastic instability and flow localization. Ohio: American Society for Metals; 1984, ISBN: 0871701839

[20] Fadel AH, Radović N. Determination of Activation Energy For Static Re-Crystallization in Nb-Ti Low Carbon Micro Alloyed Steel. *Int J Eng Inf Technol* 2017;3(2):164–9. http://mdr.misuratau.edu.ly/bitstream/handle/123456789/313/IJEIT06201615.pdf?sequence=1&isAllowed=y

[21] Rout M, Ranjan R, Pal SK, Singh SB. Study on Static Recrystallization Behavior of 304LN Stainless Steel by Two-stage Compression Test. In: All India Manufacturing Technology, Design and Research Conference (AIMTDR-2016); Maharashtra, India; 2016:1007–11; ISBN: 978-93-86256-27-0

[22] Ferreira JC, de Sousa Machado FR, Aranas C, et al. Physical Simulation Based on Dynamic Transformation Under Hot Plate Rolling of a Nb-Microalloyed Steel. *Front Mater* 2021;8. https://doi.org/10.3389/fmats.2021.716967

[23] Rodrigues SF, Siciliano F, Aranas C, Silva ES, Reis GS, Jonas JJ. High-Temperature Deformation Behaviour of High-Nb Microalloyed Steel During Plate Rolling Simulation. *Tecnol Em Metal Mater e Mineração* 2020;17(2):105–11. https://doi.org/10.4322/2176-1523.20202231

[24] Dutta B, Valdes E, Sellars CM. Mechaism and Kinetics of Strain Induced Precipitation of Nb(C,N) in Austenite. *Acta Met Mater* 1992;40(4):653–62. https://doi.org/10.1016/0956-7151(92)90006-Z

[25] Irvine K, Pickering F, Gladman T. Grain-refined C-Mn steels. *J Iron Steel Inst* 1967; 205(2): 161–82

[26] Chilton JM, Roberts MJ. Microalloying Effects in Hot-Rolled Low-Carbon Steels Finished at High Temperatures. *Metall Trans A* 1980;11A:1711–21. https://doi.org/10.1007/BF02660526

[27] Medina SF, Hernandez CA. General Expression of the Zener-Hollomon Parameter as a Function of the Chemical Composition of Low Alloy and Microalloyed Steels. *Acta Mater* 1996;44(1):137–48. https://doi.org/10.1016/1359-6454(95)00151-0
[28] Pussegoda LN, Jonas JJ. Comparison of Dynamic Recrystallization and Rolling Schedules by Laboratory Simulation Conventional Controlled. *ISIJ Int* 1991;31(3):278–88. https://doi.org/10.2355/isijinternational.31.278
[29] Jonas JJ, Ghosh C, Basabe V V. Effect of dynamic transformation on the mean flow stress. *Steel Res Int* 2013;84(3):253–8. https://doi.org/10.1002/srin.201200166

Sivimulacija završnog valjanja mikrolegiranog čelika u izotermalnim usloma

Stefan Dikić[1], Dragomir Glišić[1], Abdunaser Hamza Fadel[2], Gvozden Jovanović[3] i Nenad Radović[1]

[1]Univerzitet u Beogradu, Tehnološko-metalurški fakultet, Karnegijeva 4, 11120 Beograd, Srbija
[2]Univerzitet Al Zawia, Fakultet za prirodne resurse, Katedra za inženjerstvo nafte, 16418 Al Zawia, Libija
[3]Institut za tehnologiju nuklearnih i drugih mineralnih sirovina, Sektor za metalurgiju i zaštitu životne sredine, Bulevar Franš d'Eperea 86, 11000 Beograd, Srbija

(Naučni rad)

Izvod

Cilj ovog rada je određivanje temperature završnog valjanja Nb/Ti mikrolegiranog čelika koji sadrži 0,06 % C, 0,77 % Mn, 0,039 % Nb i 0,015 % Ti. Uzorci su ispitivani laboratorijskom simulacijom, na plastomeru - uredjaju za ispitivanje uvijanjem, na temperaturama, između 825 i 950 °C. Režim deformacije u pet provlaka i pauza između provlaka odabrani su u saglasnosti sa parametraima valjanja na petostanskoj završnoj valjačkoj pruzi valjaonice toplovaljanih traka. Udeo obnovljene mikrostrukture (oporavljanja i/ili rekristalizacije) je određivan na osnovu proračuna prekidnog omekšavanja (engl. *fraction softening*, *FS*) i parametra omekšavanja na osnovu promene površine ispod krive (engl. *area softening parameter*, *ASP*). Na 950 °C krive deformacionog ojačavanja za svaki provlak, *FS* i *ASP* pokazuju ponašanje koje odgovara potpuno rekristalisanom uzorku. Udeo obnovljene mikrostrukture se smanjuje sa sniženjem temperature do intervala 875-850°C. Pretpostavlja se da zbog velikog presićenja dolazi do pojave taloženja izazvanog deformacijom, što utiče na smanjenje pokretljivosti granica zrna/subzrna što dovodi do potiskivanja rekristalizacije. Na 825°C obnavljanje se odvija isključivo mehanizmom oporavljanja pa se ova temperatura može uzeti za kritičnu temperaturu završnog valjanja.

Ključne reči: prekidno omekšavanje; mehanička metalografija; kontrolisano valjanje; rekristalizacija, deformacija; kritične temperature

Investigation of hazardous waste
A case study of electric arc furnace dust characterization

Vanja Trifunović[1], Snežana Milić[2], Ljiljana Avramović[1], Radojka Jonović[1], Vojka Gardić[1], Stefan Đorđievski[1] and Silvana Dimitrijević[1]

[1]*Mining and Metallurgy Institute Bor, Bor, Serbia*
[2]*University of Belgrade, Technical Faculty in Bor, Bor, Serbia*

Abstract

Dust from an electric arc furnace is formed as the main by-product of the steel production process from the secondary iron-based raw materials. This dust has significant contents of Zn and Fe, as well as Pb, Cd, Ca, Mg, Cr, Mn, Si, Ni, Cu, F, Cl and other elements and is considered hazardous industrial solid waste since it contains heavy metals. In order to protect the environment and public health from the negative impact of this type of hazardous waste, it is necessary, even mandatory, to carry out its treatment in accordance with the legislation of the country where it is located. Before applying any treatment of the electric arc furnace (EAF) dust, it is necessary to perform its detailed characterization. In this paper, the following characterization of EAF dust originating in the Republic of Serbia was performed: physical-mechanical and chemical characterization, determination of granulometric composition, and mineralogical characterization. Also, the EAF dust impact on the environment and human health was assessed (Leachability and Toxicity Characteristic Leaching Procedure (TCLP) tests). The results have shown that the Zn content is in the range 32 to 35 % and that the main mineralogical phases of the dust are zincite, franklinite, magnetite, and magnesioferrite. Granulometric analysis has shown that 80 % of the sample consists of particles less than 26 μm in size. According to the leaching test results, the EAF dust is characterized as a hazardous waste due to the increased chloride content, while the TCLP test indicated dust toxicity due to the increased contents of Zn, Cd, and Pb.

Keywords: industrial waste; EAF dust; environmental impact.

Available on-line at the Journal web address: http://www.ache.org.rs/HI/

TECHNICAL PAPER

UDC: 666.952:331.461

Hem. Ind. **76(4)** 237-249 (2022)

1. INTRODUCTION

Use of the secondary raw materials, the so-called scrap iron, as a raw material, and electricity as the energy source of this process, steel production in electric arc furnaces has become more prominent than any other steel production process in the world [1,2]. The main sources of secondary raw materials for steel production are construction material waste, old cars, appliances, and household waste, which means that waste can contain a large number of different metals, plastics and rubber, glass, paint, oil, and even salts [1-8]. Due to the high process temperature (1600 °C) in the electric arc furnace, during melting of a batch, some elements evaporate and together with solid particles carried away with the gas phase, form one of the by-products - electric arc furnace dust (EAF dust) [3,8,9]. The amount of EAF dust generated during the production of 1 t of crude steel is about 10-20 kg [3,10]. A typical EAF dust has a reddish-brown or dark brown appearance, and very fine particles that can spread in the air [3,5]. Composition of EAF dust can widely vary depending on the operating conditions of the electric arc furnace, characteristics of scrap iron charged in the furnace, the working period, specifications of the steel produced, and is also specific to each plant [1,4,6,11]. EAF dust is actually the final result of a series of physical and chemical changes that the EAF dust-producing substances undergo. These phenomena, which begin in the electric arc furnace and take place within different environments along the gas path, define its physical aspect, chemical, and mineral composition. In ideal case, EAF dust should consist of iron oxide,

Corresponding authors: Vanja Trifunović, Mining and Metallurgy Institute Bor, Bor, Serbia
E-mail: vanja.trifunovic@irmbor.co.rs
Paper received: 4 June 2022; Paper accepted: 10 November; Paper published: 11 December 2022.
https://doi.org/10.2298/HEMIND220609018T

only, however, due to the presence of different types of scrap iron, containing different elements, its composition becomes complex [12].

Thus, EAE dusts usually have significant contents of Zn, Fe, and Pb, as well as variable contents of Cd, Ca, Mg, Cr, Mn, Si, Ni, Cu, F, Cl, etc. [1,4,6,12-16]. The Zn content varies from 2 to 40 wt.% [2,6,17]. Zinc present at higher concentrations in the EAF dust is most often due to its widespread use to protect steel from corrosion or it is derived from scrap brass. Since the EAF dust is formed under oxidative conditions, most of the metals are present in oxide forms. Zinc occurs in the EAF dust in the form of ZnO and $ZnFe_2O_4$, while iron mainly occurs as oxides (such as Fe_3O_4 and Fe_2O_3) [18,19].

Presence of heavy metals such as Zn, Pb, and Cd in EAF dust can pose a threat to the environment and human health due to the mobility of these toxic elements, and for this reason, EAF dust is considered hazardous industrial solid waste in many countries [20,21]. According to the United States Environmental Protection Agency (EPA), the EAF dust is listed as a hazardous solid industrial waste K061 [22], and according to the Brazilian standard ABNT 10004: 2004, the EAF dust is listed as hazardous waste from certain source K061 [23]. In the European Union Waste Catalogue [24] the EAF dust is classified as a hazardous substance with the designation 10 02 13* and 10 02 07*, depending of the gas treatment process [4]. Leachability of heavy metals such as Zn, Cu, Ni, Cd, Cr, and Pb, as well as F and Cl from waste [25] leads to significant environmental pollution and improper disposal of the EAF dust has a negative impact on the environment [5]. Thus, in the hazardous waste landfills, the EAF dust must be protected from rain, to prevent formation of leachate that could pollute the surrounding areas [25].

Zinc is an essential element needed by the human body, especially for building cells and enzymes, and it also helps wound healing. Reduced Zn content in the human body leads to negative health effects such as anorexia (loss of appetite and eating disorders), loss of taste, lethargy (fatigue and lack of energy), growth retardation, slower wound healing, *etc.* The recommended intake of zinc by the World Health Organization (WHO), through the daily diet, is 5.5 to 9.5 mg day^{-1} for men and 4.0 to 7.0 mg day^{-1} for women. Despite the great importance of Zn for human health, it should not be overlooked that it is also carcinogenic and that its excessive intake (100-500 mg day^{-1}) can be toxic. Zinc is also an important nutrient for plants. The deficiency of zinc in plants can cause chlorosis (change in leaf color) and necrosis of the root tip (death) and can also lead to reduced yields [26]. Although zinc is an important part of living organisms and the environment, this element belongs to the group of toxic metals.

In this paper, hazardous industrial waste was investigated, *i.e*. dust from an electric arc furnace originating from a steel plant in the Republic of Serbia was characterized in detail. In specific, the dust was characterized regarding physical-mechanical, chemical, and mineralogical properties as well as regarding granulometric composition and the analyses are supplemented with the assessment of the dust impact on the environment and human health.

2. EXPERIMENTAL

2. 1. Materials

Hazardous waste, which was investigated in this paper, is dust from an electric arc furnace obtained from the dry dust collecting system of a steel plant in the Republic of Serbia. Four samples (10 kg each) of the EAF dust were taken from the production process for investigating purposes. Samples were taken at random from jumbo bags from the landfill located under the canopy in the circle of the steel plant (not directly from the filter bags in which the EAF dust is collected from the electric arc furnace).

2. 2. Sample preparation

Homogenization of each of the four samples was performed by mixing the sample on foil. From the total amount of each of the EAF dust samples, representative samples were taken by the quartering procedure (Fig. 1) and marked as U1, U2, U3, and U4.

Triplicate samples from all four representative EAF dust samples (U1, U2, U3, and U4), in quantities of 0.5, 1.0, and 2.0 kg, for physical-mechanical and chemical characterization were obtained by drying in a dryer at the temperature of 105 °C, for 24 h.

Two dry representative U1 samples (5.0 g) were prepared for morphological analyses by dipping in epoxy resin after which they were ground and polished with silicon carbide and then polished with a diamond suspension. The samples were first analyzed by a polarizing microscope (JENAPOL-U, Carl Zeiss-Jena, Germany) and then coated with gold and analyzed by scanning electron microscopy with energy dispersive spectroscopy (SEM-EDS, JSM IT 300LV, JOEL, Japan).

Figure 1. Preparation of the EAF dust representative sample

Two dry representative U1 samples (1.0 g each) were prepared by comminution in an agate mortar and used for X-ray diffractometer recording.

2. 3. Characterization methods

2. 3. 1. Physico-mechanical and chemical characterization

Physico-mechanical characterization of the initial representative samples of EAF dust involves the determination of moisture, pH value of the sample, bulk density, and density of the sample.

For the determination of metals, initial EAF dust samples were dissolved in 4 acids (HCl, HNO_3, $HClO_4$, and HF), and the obtained solutions were analyzed. Concentrations of Fe, Mn, Cu, Pb, Bi, Co, Ni, Cr, Mo, P, As, Sb, Sn, Ca, Cd, Al, Si, Na, K, and Mg were measured using inductively coupled plasma atomic emission spectrometer (ICP-AES) Spectro Ciros. In addition, concentrations of metals with relatively higher content such as Zn, Fe, Mn, Cu, Pb, Ni, Ca, Na, K, and Mg were confirmed using atomic absorption spectrophotometer (AAS) PerkinElmer PinAAcle 900F. Since the concentration of Zn in EAF dust was the highest of all metals, a more accurate Zn concentration was determined by titration with ethylenediaminetetraacetic acid with methylthymol blue as an indicator. The contents of silver and gold were determined using fire assay (FA). The content of mercury was measured using flameless atomic absorption spectrophotometer AMA-254 (AAS-Hg). The content of sulfur was determined using Thermo Horiba EMIA-920V2 carbon sulfur analyser (CSA). To determine chloride (Cl^-), fluoride (F^-), and pH value, leachates were prepared by suspending initial EAF dust samples in demineralized water in a ratio of 1:10, shaking, and filtration. Concentrations of Cl^- and F^- were measured both using spectrophotometer (SF) HACH DR 3900 and ion chromatograph (IC) Thermo Dionex ICS-1600. pH values were measured by pH meter IM-23P.

2. 3. 2. Granulometric composition

Particle size distribution was determined in a representative EAF dust U1 sample without any prior preparation by using a laser device MASTERSIZER 2000 (MALVERN Instruments, UK).

2. 3. 3. Mineralogical characterization

Mineralogical characterization of a dry representative EAF dust U1 sample included analyses by using a polarization microscope (JENAPOL-U, Carl Zeiss-Jena, Germany), scanning electron microscopy with energy-dispersive X-ray spectroscopy (SEM-EDS), and X-ray diffraction analysis (XRD).

A SEM-EDS microscope (JSM IT 300LV, JOEL, Japan), with an accelerator voltage of 20 kV, was used to examine the morphology and elemental mapping of the EAF dust sample.

The XRD analysis was applied to determine the phase composition of a representative U1 EAF dust sample as a polycrystalline sample (powder) by using a PHILIPS X-ray diffractometer (PW-1710, PHILIPS, Netherlands), with a curved graphite monochromator and a scintillation counter. The measurement was carried out in the 2θ range from 4 to 70°, with a scan rate of 5° min^{-1}.

2. 3. 4. Assessment of the EAF dust impact on the environment and human health

A representative U1 EAF dust sample was assessed regarding the impact on the environment and human health after disposal, following the Rulebook on categories, testing, and classification of waste (Official Gazette of RS 93/2019, 39/2021). Laboratory tests were performed according to the accredited standard methods: SRPS EN 12457-2 for testing the leachability of materials, and EPA 1311 for testing the toxicity of materials. For Leachability test, after determining the moisture content of the sample, the EAF dust sample in the amount of 0.090 kg (calculated on dry mass) was mixed with distilled water in the liquid : solid ratio = 10 L : 1 ± 0.02 kg, in a plastic bottle. The bottle was placed on a rotary shaker and rotated at 30 rpm for 24 hours. The suspension was then filtered, the pH value and conductivity of the filtrate were measured, and a chemical analysis was performed. Based on the dry mass of the original EAF dust sample, the amount of the ingredient leached from it was calculated. To perform the TCLP test, a 100 g sample of EAF dust was mixed with 2 dm^3 of extraction liquid (acetic acid) in a plastic bottle. The plastic bottle was placed on a rotating shaker at 30 rpm for 18 hours. After the suspension was filtered, the pH value of the extract was measured, and immediately aliquot and chemical analysis of the extract was performed. The EAF dust samples for both tests were not previously additionally prepared, and both tests were performed with two samples each.

The obtained results were compared to the legislation of the Republic of Serbia, based on which the toxicity and leachability of the tested material samples were determined.

3. RESULTS AND DISCUSSION

3. 1. Characterization of the EAF dust

3. 1. 1. Physical and chemical characterization

The results of physical characterization of the representative EAF dust samples (U1, U2, U3, and U4) are presented in Table 1.

Table 1. Physical characteristics of the representative EAF dust samples

Characteristic	Sample			
	U1	U2	U3	U4
Moisture, wt.%	0.36	2.90	43.30	1.60
pH	11.42	8.05	9.10	7.15
Bulk density, kg m^{-3}	654	712	n.a.	686
Density, g cm^{-3}	4.351	4.550	n.a.	4.446

n.a. – not analyzed

The moisture contents in the EAF dust samples U1, U2, and U4 are low (below 3 wt.%), while the moisture content is higher (43.3 wt.%) in the sample U3. All EAF dust samples were taken from jumbo bags from the landfill located under the canopy. However, the sample marked as U3 was taken from a jumbo bag that stood at the very end of the canopy and was damaged (torn). For this sample, the difference in the size of EAF dust particles compared to the other taken samples could be already noticed by the visual inspection, since the EAF dust particles were in the form of larger agglomerates. The research has shown that the particle size distribution of EAF dust is closely related to the moisture content, and for this reason, dust particles will also coagulate in reaction with water [3,28].

It was shown that long-term storage of the EAF dust in conditions with increased humidity can lead to the formation of large agglomerates of the dust particles [3]. The increased humidity of the U3 sample indicates that its storage is not adequate because the EAF dust contact with water resulted in agglomeration and formation of large and solid agglomerates of the otherwise very small and powdery EAF dust particles. For this reason, bulk density was not measured for the U3 sample. The pH values of the dust samples range from 7.15 to 11.42 (Table 1), which indicates that the EAF dust is a material with basic characteristics.

Results of the chemical characterization of the four representative EAF dust samples, as well as the analytical methods used for chemical characterization, are presented in Table 2.

Table 2. Chemical composition of the representative EAF dust samples U1-U4 and analytical methods used for determination

Element	U1	U2	U3	U4	Analytical method*
	Content, wt.%				
Zn	32.44	32.95	35.21	32.38	V/AAS
Fe	18.92	21.92	22.93	28.28	ICP-AES/AAS
Mn	1.81	2.07	1.48	2.29	ICP-AES/AAS
Cu	0.19	0.20	0.23	0.19	ICP-AES/AAS
Pb	1.39	1.74	2.37	1.11	ICP-AES/AAS
Bi	0.013	<0.01	0.016	<0.01	ICP-AES
Co	0.0017	0.0013	0.0024	0.0018	ICP-AES
Ni	0.036	0.0099	0.017	0.014	ICP-AES/AAS
Cr	0.25	0.25	0.28	0.40	ICP-AES
Mo	<0.0050	0.0029	0.0053	0.0028	ICP-AES
S	0.51	0.38	0.41	0.44	CSA/ICP-AES
P	0.15	0.11	0.12	0.11	ICP-AES
As	0.0041	0.004	0.0058	0.045	ICP-AES
Sb	0.022	0.017	0.023	0.014	ICP-AES
Sn	0.037	0.044	0.055	0.035	ICP-AES
Ca	3.85	2.89	2.07	3.05	ICP-AES/AAS
Cd	0.040	0.06	0.059	0.032	ICP-AES
Ag	0.00604	0.00747	0.017	0.00730	FA/AAS
Au	0.00004	<0.00001	-	-	FA/AAS
Cl	2.85	2.23	0.16	2.50	SF/IC
Al	0.73	0.63	0.58	0.77	ICP-AES
Si	1.34	1.68	-	-	ICP-AES
Hg	0.0001	0.00006	-	-	AAS-Hg
Na	1.28	0.91	0.35	0.92	ICP-AES/AAS
K	0.87	0.69	0.22	0.74	ICP-AES/AAS
Mg	0.93	0.68	0.55	0.57	ICP-AES/AAS
F	-	-	0.52	0.023	SF/IC

**V- Volumetry; AAS – Atomic Absorption Spectrophotometry; ICP-AES - Inductively Coupled Plasma Atomic Emission Spectrometry*
CSA – Carbon/Sulfur analyzer; FA – Fire Assay; FOT – Photometry; SF – Spectrophotometry; IC – Ion Chromatography
AAS-Hg - Flameless Atomic Absorption Spectrophotometry (mercury analysis)

Comparison of the obtained results for the four dust samples from the same steel plant indicates variability of the EAF dust composition depending on the operational parameters of the melting process in the electric arc furnace and the type of charged scrap iron, which is in accordance with the literature [11,29].

Apart from the fact that treatment of EAF dust is primarily performed for environmental protection, which can be carried out by a hydrometallurgical process, for example, could be also economically viable if the EAF dust contains Zn at concentrations higher than 15 wt.%. After the treatment, returns from the obtained by-products, which can be used for production of metals could compensate the capital and operating costs of such a process [20,28]. The most significant deviations in the analyzed EAF dust samples in this work were observed in the contents of Zn, Fe, Mn, Pb, Cl,

Na, and Ca. The lowest Fe content and the highest Ca content were determined in the U1 sample. The increased Ca content in this sample is attributed to lime addition during the furnace operation, which is also the reason for the increased pH value of this sample compared to the other three analyzed samples. Zn contents in the samples can be characterized as high (32.38-35.21 wt.%), since the content of this metal varies from 2-40 wt.% in EAF dusts. For further characterization of the EAF dust, the U1 sample was selected, *i.e*. the sample with the Zn content of 32.44 wt.% and the Fe content of 18.92 wt.%.

Considering the need for EAF dust treatment, whether for environmental or economic reasons, choice of the processing methods depends on the dust chemical composition and the available quantity for exploitation. In the case of processing the investigated EAF dust, due to the limited quantities and high content of Zn, hydrometallurgical process is the most suitable in order to separate Zn and transform hazardous waste into non-hazardous waste.

3. 1. 3. Granulometric composition

Graphical presentation of particle size distribution in the U1 EAF dust sample is presented in Figure 2. Based on the obtained granulometric analysis results, it was determined that 80 vol.% of the sample consists of particles <26 μm in size. Such a fine grain distribution in the EAF dust can result in difficult filtration during the hydrometallurgical treatment.

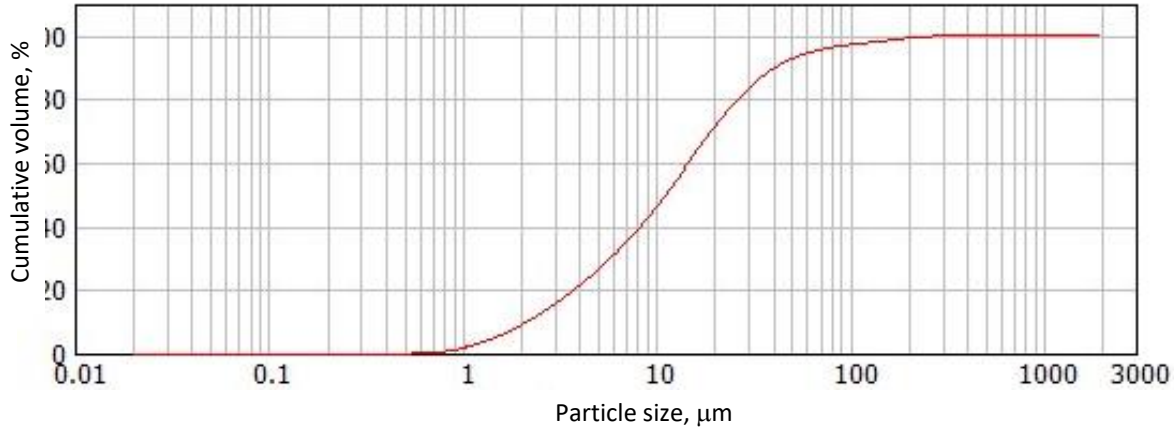

Figure 2. Granulometric composition of the representative EAF dust sample

Due to differences in methods for steel production in electric arc furnaces and methods of dust collection, physical characteristics of EAF dusts may be variable in a certain range. There are three main dust collection methods resulting in 3 EAF dust particle size intervals: 1) collection by gravity collectors, where 85 % of the particles are <10 μm in size, 2) collection in filter bags where 90 % of the particles are 50 μm in size, and 3) collection by electrostatic collectors where more than 90 % of the particles are less than 100 μm in size [3].

In this work, the investigated EAF dust was collected in filler bags, and the obtained results of the particle size distribution agree with the literature results [3,29].

3. 1. 4. Mineralogical characterization

3. 1. 4. 1. Polarized light microscopy

Table 3 presents a semi-quantitative mineralogical analysis of the U1 representative EAF dust sample.

Table 3. Presence of minerals in the U1 representative sample

Mineral	Presence	Mineral	Presence
Zinc metal	Substantial	Magnesioferrite	Low
Zincite	Substantial	Maghemite	Occurs in trace amounts
Magnetite	Substantial	Wustite	Occurs in trace amounts
Franklinite	Low	Crystalline coke	Substantial

Based on the obtained qualitative microscopic analyses in reflected light, the following composition was determined in the representative U1 dust sample: zinc metal, zincite, magnetite, franklinite, Mg-spinels, maghemite, wustite, crystalline coke (graphite), and amorphous phase. Structural-textural properties of grains containing zinc and iron minerals are presented in Table 3 and in micrographs in Figure 3. The main mineral phases of zinc in the sample are zincite (ZnO) and zinc metal (Zn). Grains with zinc (Fig. 3b) appear in the form of small white "lumps". Zinc metal is a common metal phase, mostly occurring in free grains, which are spherical with circular cross-sections (Fig. 3b-d). Zinc metal grains are sometimes surrounded by the annular franklinite ($ZnFe_2O_4$) or the central parts may be filled with Zn-Fe-Mg spinels and their eutectics (Fig. 3d). The main iron minerals that are well represented in the sample are magnetite (Fe_3O_4) and various (Fe, Mg)-spinels, which regularly occur in free spherical grains (up to 50 μm) with circular cross-sections. Other mineral phases with iron are less represented. Carbon phases are largely presented by crystalline, semi-crystalline, and amorphous coke (Fig. 3c). All coke grains (graphite) are tabular or rod-shaped, with appearance of black stripes along their foliation (glass).

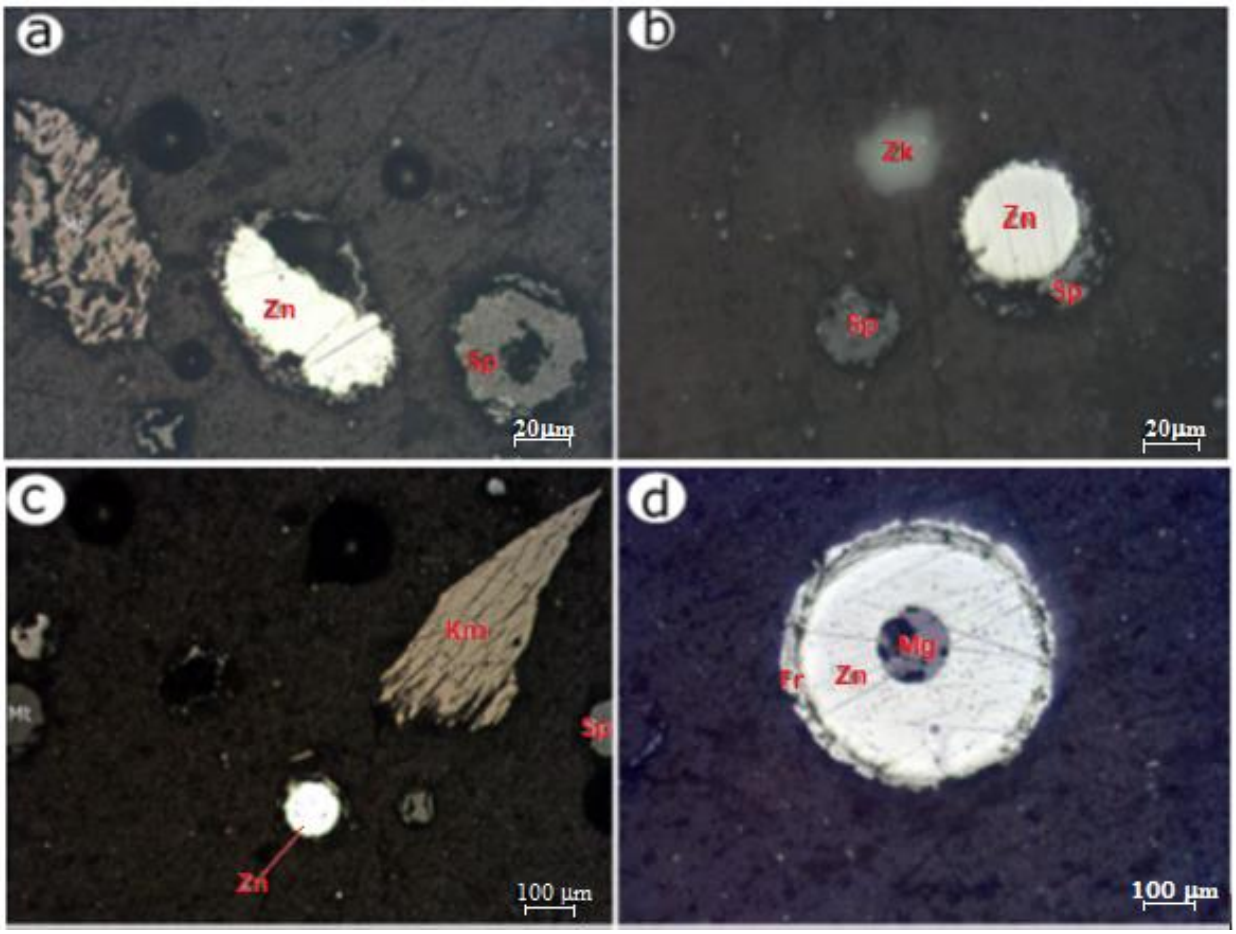

Figure 3. Micrographs of the representative EAF dust sample: a) Zn metal and spinel grains; b) zincite, spinel and Zn metal grains; c) Zn metal, crystalline coke and spinel grains; d) magnetite grain in Zn metal grain in franklinite grain
Indications of present phases: Km - crystalline coke; Mg - magnetite; Zk - zincite; Zn – zinc metal; Fr - franklinite; Sp – spinel

The obtained results are in accordance with literature data [3,4,16].

3. 1. 4. 2. SEM-EDS analysis

Figure 4 presents a SEM micrograph of the U1 EAF dust sample showing agglomerates of irregularly shaped particles, as well as agglomerates of spherical particles, which differ in size.

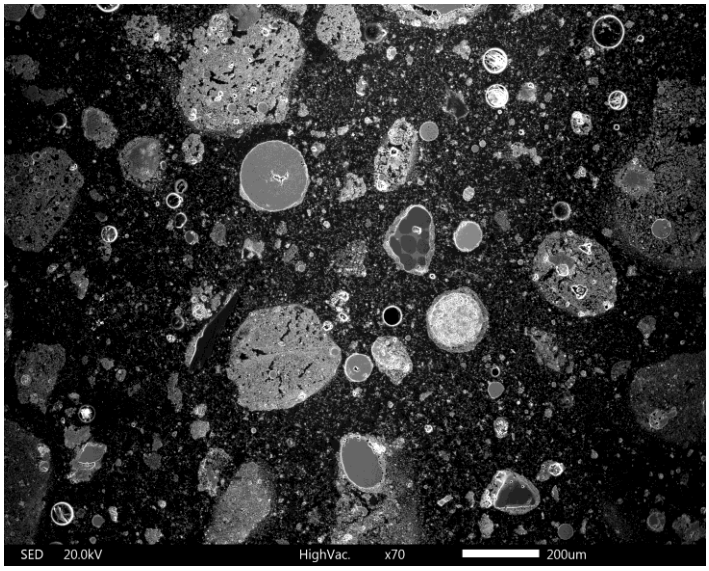

Figure 4. SEM image of the representative U1 EAF dust sample showing agglomerates of irregularly shaped as well as spherical particles

Melting of scrap iron in an electric arc furnace induces metal evaporation, resulting in EAF dust formation by two ways: by heterogeneous and homogeneous nucleation. Depending on the nucleation process, dust particles will be larger or smaller. Most of deposition of volatile metals on the surface of solid metal particles is carried out by heterogeneous nucleation, leading to formation of larger particles, *i.e.* particles with a diameter of about 200 µm. In the case that the amount of solid particles is not sufficient for agglomeration, homogeneous nucleation takes place and particle growth up to 0.02-100 µm. All interactions that occur during the formation of EAF dust make the final dust complex in terms of its chemical and physical characteristics [1, 30].

The SEM-EDS analysis has also shown an encapsulation phenomenon in the EAF dust particles, *i.e*. zinc metal particles are in some cases trapped within a sphere of magnetite and various types of glass, confirming the results obtained by polarized light microscopy. Cross-section of an EAF dust particle is presented in Figure 5, indicating that the larger particles are composed of an inner core of iron oxide (Fe_3O_4/Fe_2O_3), Zn metal, CaO, Ca-Si-Al-Ti glass, and graphite; middle layer of FeO, CaO, and graphite and a most distant layer of $ZnFe_2O_4$, leading to the assumption of heterogeneous nucleation.

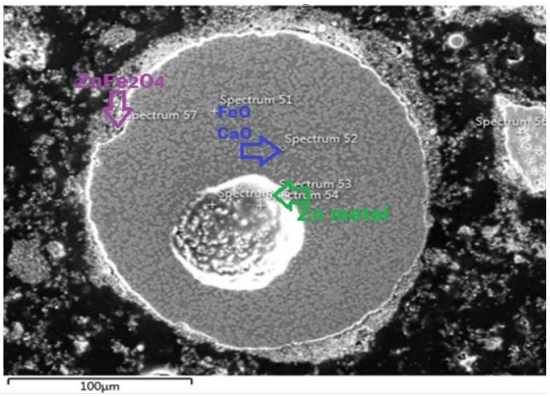

Element	Content, wt. %						
	Spectrum 51	Spectrum 52	Spectrum 53	Spectrum 54	Spectrum 55	Spectrum 56	Spectrum 57
C	20.21	23.26	12.67	12.02	11.66	20.05	21.29
O	33.82	32.15	10.37	5.91	7.98	24.41	35.44
Na						2.08	
Mg	3.01						
Al	4.69	2.66	0.45	0.20	0.48		1.53
Si		6.26	1.14	0.59	1.66		1.58
Cl						0.13	
Ca	0.45	16.91	22.81	28.81	28.92		1.11
Ti		0.52		0.93	0.92		
Cr	20.91						
Mn	2.44	1.75	4.75	3.89	3.67		1.89
Fe	14.15	16.48	45.94	43.60	42.17	41.07	34.15
Zn	0.31		1.87	1.27		12.27	3.03
Te				2.77	2.53		
Total	100.00	100.00	100.00	100.00	100.00	100.00	100.00

Figure 5. SEM-EDS analysis of a cross-section of a spherical particle

Figure 6 shows SEM-EDS analysis of the U1 EAF dust sample, which also identified the presence of ZnO, along with graphite and FeO in irregularly shaped particles.

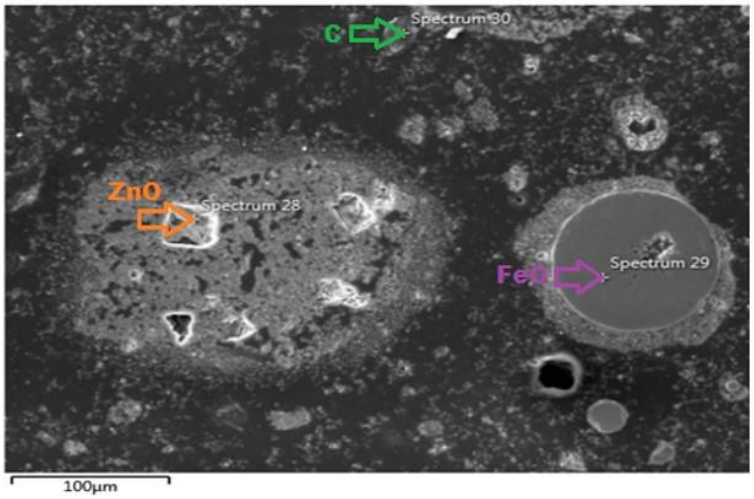

Element	Content, wt. %		
	Spectrum 28	Spectrum 29	Spectrum 30
C	62.35	17.40	69.11
O	15.48	32.90	26.15
Na	1.70		0.80
Mg		3.10	
Al		3.24	
Si		4.29	
Cl	4.72		2.67
K	0.41		0.22
Ca	0.79	13.41	0.14
Ti		0.34	
Cr		0.75	
Mn		3.13	
Fe	4.14	21.44	0.91
Zn	10.41		
Total	100.00	100.00	100.00

Figure 6. SEM-EDS analysis of the representative U1 EAF dust sample

3. 1. 4. 3. XRD analysis

In the analyzed U1 EAF dust sample, presence of the following phases was determined by the XRD analysis: zincite (ZnO), zinc metal (Zn), magnetite (Fe_3O_4), franklinite ($ZnFe_2O_4$), magnesioferrite ($MgFe_2O_4$), maghemite (Fe_2O_3), wustite (FeO) and poorly crystallized graphite (C) as shown in the diffractogram (Fig. 7). The main phases identified in the analyzed dust sample are in accordance with the results published in literature [2,3,5,10].

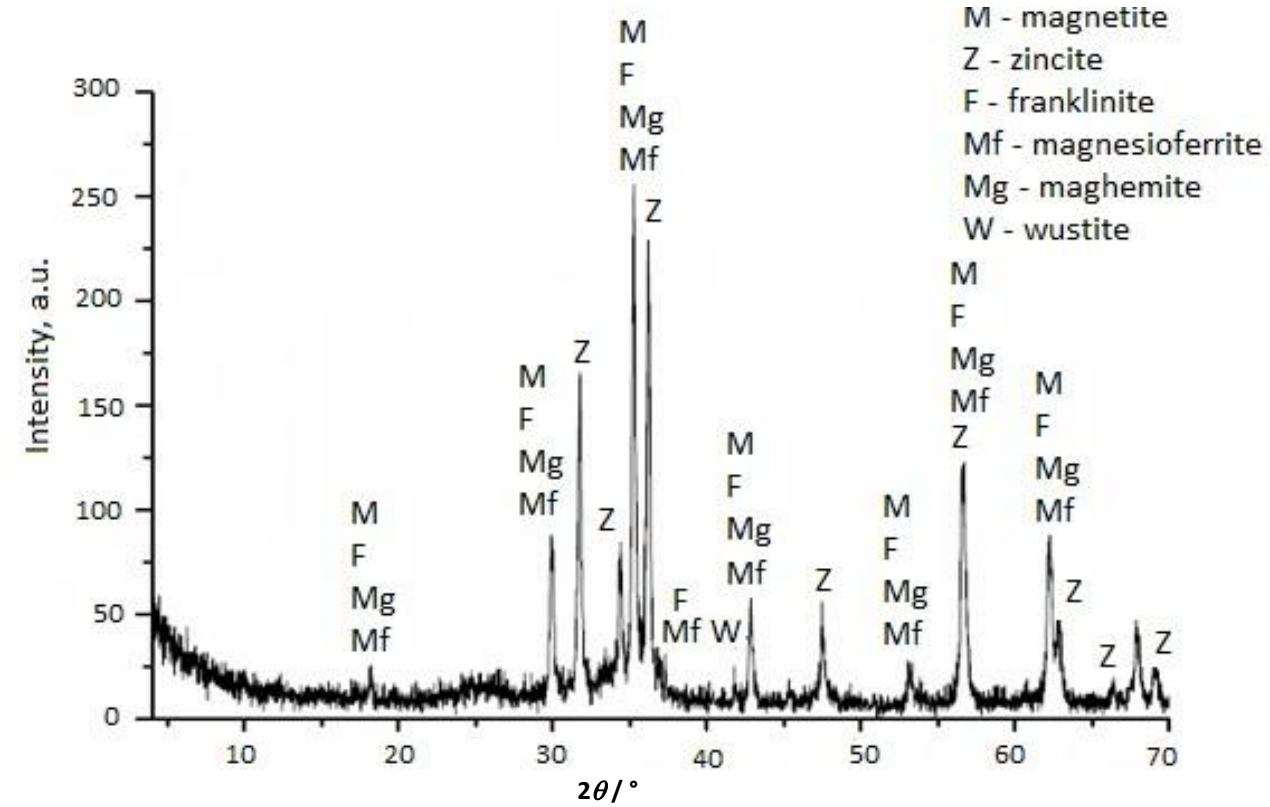

Figure 7. Diffractogram of the representative U1 EAF dust sample

Positions and relative intensity of the most intense diffraction peaks correspond to zincite, *i.e*. the most common phase, followed by the spinel phases (magnetite (Fe_3O_4), franklinite ($ZnFe_2O_4$), magnesioferrite ($MgFe_2O_4$)), while the

diffraction peaks of zinc metal (Zn), graphite (C) and maghemite (Fe_2O_3) are less expressed. Peaks of the wustite (FeO) mineral show that it appears in traces in the sample.

3. 1. 5. Assessment of the impact of EAF dust on the environment and human health

3. 1. 5. 1. Leachability test

Results of the Leachability test of the representative U1 EAF dust sample according to SRPS EN 12457-2: 2008 are presented in Table 4.

Table 4. Leachability test results for the representative U1 EAF dust sample

Parameter	Measured value	Reference value for non-hazardous waste[1]	Reference value for hazardous waste[2]
pH	11.31	6-13[3]	-
Conductivity, µS cm^{-1}	8288	-	-
		Content, mg kg^{-1} of dry matter	
Vanadium	<0.08	200	-
Chromium	<0.05	10	70
Nickel	<0.07	10	40
Copper	<0.05	50	100
Zinc	3.00	50	200
Arsenic	<0.20	2	25
Selenium	<0.33	0.5	7
Silver	<0.05	50	-
Cadmium	<0.08	1	5
Barium	2.60	100	300
Mercury	<0.005	0.2	2
Lead	10.00	10	50
Molybdenum	4.70	10	30
Antimony	<0.50	0.7	5
Chlorides, as Cl^-	**30900**	**15000**	**25000**
Fluorides, as F^-	36.30	150	500
Sulfates, as SO_4^{2-}	7400	20000	50000
Phenol index	0.24	1000	-

[1,2]Annex 10 of the Rulebook on categories, investigation and classification of waste (Official Gazette of RS 93/2019, 39/2021), Article 2, Parameters for testing waste and leachate from non-hazardous waste landfills[1] and hazardous waste[2]. Ambient temperature 21°C, humidity 52 %, pressure 970 hPa
[3]Reference value for pH according to the Rulebook 93/2019, 39/2021 Annex 7, H15- Waste that has the property of producing another substance in any way after disposal, *e.g.* leachate that has any of the following characteristics (H1-H14), is 6-13. The measured pH value is within the allowable range.

Based on the leaching test results, the EAF dust sample is categorized as a hazardous waste in terms of disposal, due to the increased chloride content in the leaching eluate (leaching solution) above the permitted limits, even for the waste disposal on a hazardous waste landfill. These results indicate that the dust has to be subjected it to the prior treatment before the final disposal.

3. 1. 5. 2. Toxicity characteristic leaching procedure

Results of the toxicity characteristic leaching procedure (TCLP) test (EPA 1311) of the representative U1 EAF dust sample intended for disposal are presented in Table 5.

The obtained results of the TCLP test show that the EAF dust sample exhibited toxic characteristics, due to the increased contents of zinc, cadmium and lead in the TCLP eluate (leaching solution), which are above the permissible limits prescribed by the regulations. This type of hazardous waste needs further attention in order to protect the environment and work conditions.

Table 5. TCLP test results for the representative U1 EAF dust sample (element contents in the extraction procedure extract)

Element	Measured content, mg dm^{-3}	Waste toxicity reference content*, mg dm^{-3}
Vanadium	<0.008	24
Chromium	<0.005	5
Nickel	0.068	20
Copper	0.050	25
Zinc	**2690.67**	**250**
Arsenic	<0.020	5
Selenium	<0.033	1
Silver	<0.005	5
Cadmium	**13.880**	**1**
Barium	0.880	100
Mercury	<0.0005	0.2
Lead	**61.160**	**5**
Molybdenum	<0.007	350
Antimony	<0.050	15

*Annex 10 of the *Rulebook* on categories, investigation and classification of waste (Official Gazette of RS *93/2019, 39/2021*), Article 1, Parameters for testing the toxic characteristics of waste intended for disposal

4. CONCLUSION

This paper presents a detailed investigation of hazardous waste, *i.e*. EAF dust from a steel production plant in Serbia. Chemical characterization has confirmed the Zn content in the dust in the range of 32 to 35 wt.%, while the main mineralogical phases were zincite, franklinite, magnetite and magnesioferrite. Granulometric analysis showed that 80 % of the sample consisted of particles less than 26 μm in size. Impact on the environment and human health was assessed by the leachability test, which characterized the EAF dust as a hazardous waste due to the increased chloride content, while the TCLP test indicated toxicity of the dust due to the increased Zn, Cd and Pb contents.

Thus, treatment of this type of hazardous waste is necessary to protect the environment and human health. With appropriate processing, it would be possible to achieve concentration and separation of valuable metals that are in the waste, which is in the present case zinc, the most abundant metal in the investigated EAF dust. In order develop hydrometallurgical processes for zinc separation and stabilization of solid residues, as well as to design safe disposal of the resulting non-hazardous waste, further experimental studies of the treatment of the investigated EAF dust are necessary.

Acknowledgments: *This work was supported by the Ministry of Education, Science and Technological Development of the Republic of Serbia, Grant No. 451-03-68/2022-14/200052 and Grant No. 451-03-68/2022-14/200131.*

REFERENCES

[1] Siame MC, Kaoma J, Hlabangana N, Danha G. An Attainable Region Approach for the Recovery of Iron and Zinc from Electric Arc Furnace Dust. *S Afr J Chem Eng*. 2019; 27: 35–42 https://doi.org/10.1016/j.sajce.2018.12.002.

[2] Wu CC, Chang FC, Chen WS, Tsai MS, Wang YN. Reduction Behavior of Zinc Ferrite in EAF-Dust Recycling with CO Gas as a Reducing Agent. *J Environ Manage*. 2014; 143: 208-213 https://doi.org/10.1016/j.jenvman.2014.04.005.

[3] Wang J, Zhang Y, Cui K, Fu T, Gao J, Hussain S, AlGarni TS. Pyrometallurgical Recovery of Zinc and Valuable Metals from Electric Arc Furnace Dust - A Review. *J Clean Prod.* 2021; 298: 126788 https://doi.org/10.1016/j.jclepro.2021.126788.

[4] Kukurugya F, Vindt T, Havlík T. Behavior of Zinc, Iron and Calcium from Electric Arc Furnace (EAF) Dust in Hydrometallurgical Processing in Sulfuric Acid Solutions: Thermodynamic and Kinetic Aspects. *Hydrometall.* 2015; 154: 20–32 https://doi.org/10.1016/j.hydromet.2015.03.008.

[5] Silvaa VS, Silvaa JS, Costaa BdS, Labesb C, Oliveira RMPB. Preparation of Glaze Using Electric-Arc Furnace Dust as Raw Material. *J Mater Res Technol*. 2019; 8(6): 5504–5514 https://doi.org/10.1016/j.jmrt.2019.09.018.

[6] Hazaveh PK, Karimia S, Rashchia F, Sheibania S. Purification of the Leaching Solution of Recycling Zinc from the Hazardous Electric Arc Furnace Dust Through an As-Bearing Jarosite. *Ecotoxicol Environ Saf*. 2020; 202: 110893 https://doi.org/10.1016/j.ecoenv.2020.110893.

[7] Čerňan M, Müller Z, Tlustý J, Valouch V. An Improved SVC Control for Electric Arc Furnace Voltage Flicker Mitigation. *Int. J. Electr. Power Energy Syst*. 2021; 129: 106831 https://doi.org/10.1016/j.ijepes.2021.106831.

[8] Bruckard WJ, Davey KJ, Rodopoulos T, Woodcock JT, Italiano J. Water Leaching and Magnetic Separation for Decreasing the Chloride Level and Upgrading the Zinc Content of EAF Steelmaking Baghouse Dusts. *Int J Miner Process*. 2005; 75: 1 – 20 https://doi.org/10.1016/j.minpro.2004.04.007.

[9] Trifunović V, Avramović Lj, Jonović R, Milić S, Đorđievski S, Jonović M. Hydrometallurgical Treatment of EAF Dust in aim of Zinc Separation, Proceedings/52nd International October Conference on Mining and Metallurgy - IOC 2021. In: *Proceedings of The 52nd International October Conference on Mining and Metallurgy*, Bor, Serbia, 2021, pp. 209-212 ISBN:978-86-6305-119-5.

[10] Halli P, Hamuyuni J, Revitzer H, Lundström M. Selection of Leaching Media for Metal Dissolution from Electric Arc Furnace Dust. *J Clean Prod*. 2017; 164: 265-276 https://doi.org/10.1016/j.jclepro.2017.06.212.

[11] Havlik T, Turzakova M, Stopic S, Friedrich B, Atmospheric Leaching of EAF Dust With Diluted Sulphuric Acid, *Hydrometall*. 2005; 77: 41–50 https://doi.org/10.1016/j.hydromet.2004.10.008.

[12] Keglevich de Buzin PJW, Heck NC, Vilela ACF. EAF dust: An Overview on the Influences of Physical, Chemical and Mineral Features in its Recycling and Waste Incorporation Routes. *J Mater Res Technol*. 2017; 6(2): 194–202 https://doi.org/10.1016/j.jmrt.2016.10.002.

[13] Halli P, Hamuyuni J, Leikola M, Lundström M. Developing a Sustainable Solution for Recycling Electric Arc Furnace Dust via Organic Acid Leaching. *Miner Eng*. 2018; 124: 1–9 https://doi.org/10.1016/j.mineng.2018.05.011.

[14] Omran M, Fabritius T. Effect of Steelmaking Dust Characteristics on Suitable Recycling Process Determining: Ferrochrome Converter (CRC) and Electric Arc Furnace (EAF) Dusts, *Powder Technol*. 2017; 308: 47–60 https://doi.org/10.1016/j.powtec.2016.11.049.

[15] Al-harahsheh M, Al-Nu'airat J, Al-Otoom A, Al-hammouri I, Al-jabali H, Al-zoubi M, Abu Al'asal S. Treatments of Electric Arc Furnace Dust and Halogenated Plastic Wastes: A Review. *J Environ Chem Eng*. 2019; 7: 102856 https://doi.org/10.1016/j.jece.2018.102856.

[16] Omran M, Fabritius T. Effect of Steelmaking Dust Characteristics on Suitable Recycling Process Determining: Ferrochrome Converter (CRC) and Electric Arc Furnace (EAF) Dusts, *Powder Technol*. 2017; 308: 47–60 https://doi.org/10.1016/j.powtec.2016.11.049.

[17] Ruiz O, Clemente C, Alonso M. Alguacil FJ. Recycling of an Electric Arc Furnace Flue Dust to Obtain High Grade Zno. *J Hazard Mater*. 2007; 141: 33–36 https://doi.org/10.1016/j.jhazmat.2006.06.079.

[18] Pickles CA, Marzoughi O. Thermodynamic Analysis of Metal Speciation During the Chlorosulphation of Electric Arc Furnace Dust. *Miner Eng*. 2019; 140: 105874 https://doi.org/10.1016/j.mineng.2019.105874.

[19] Khattab RM, El-Sayed Seleman MM, Zawrah MF. Assessment of Electric Arc Furnace Dust: Powder Characterization and its Sinterability as Ceramic Product. *Ceram Int.* 2017; 43: 12939–12947 https://doi.org/10.1016/j.ceramint.2017.06.192.

[20] Alencastro de Araújo J, Schalch V, Recycling of Electric Arc Furnace (EAF) Dust for Use in Steel Making Process, *J Mater Res Technol*. 2014; 3(3): 274–279 https://doi.org/10.1016/j.jmrt.2014.06.003.

[21] Li YC, Zhuo SN, Peng B, Min XB, Liu H, Ke Y. Comprehensive Recycling of Zinc and Iron From Smelting Waste Containing Zinc Ferrite by Oriented Transformation with SO_2. *J Clean Prod*. 2020; 263: 121468 https://doi.org/10.1016/j.jclepro.2020.121468.

[22] Environmental Protection Agency, Land Disposal Restrictions for Electric Arc Furnace Dust (K061) - Federal Register Notice, Vol. 56 No. 160, August 19, 1991 p 41164.

[23] Norma Brasileira, ABNT 10004:2004, Solid waste Classification, 2004.

[24] Commission of the European Communities, Guidance on classification of waste according toEWC-Stat categories, Supplement to the Manual for the Implementation of the Regulation (EC) No 2150/2002 on Waste Statistics, version 2, December 2010.

[25] Ledesma EF, Lozano-Lunar A, Ayuso J, Galvín AP, Fernández JM, Jiménez JR. The Role of pH on Leaching of Heavy Metals and Chlorides from Electric Arc Furnace Dust in Cement-Based Mortars. *Constr Build Mater*. 2018; 183: 365–375 https://doi.org/10.1016/j.conbuildmat.2018.06.175.

[26] Ng KS, Head I, Premier GC, Scott K, Yu E, Lloyd J, Sadhukhan J. A Multilevel Sustainability Analysis of Zinc Recovery from Wastes. *Resour Conserv Recycl*. 2016; 113: 88–105 https://doi.org/10.1016/j.resconrec.2016.05.013.

[27] Pickles CA. Thermodynamic Modelling of the Multiphase Pyrometallurgical Processing of Electric Arc Furnace Dust. *Miner Eng*. 2009; 22: 977–985 https://doi.org/10.1016/j.mineng.2009.03.007.

[28] Miki T, Chairaksa-Fujimoto R, Maruyama K, Nagasaka T. Hydrometallurgical Extraction of Zinc from CaO Treated EAF Dust in Ammonium Chloride Solution. *J Hazard Mater*. 2016; 302: 90–96 https://doi.org/10.1016/j.jhazmat.2015.09.020.

[29] Rudnik E. Investigation of Industrial Waste Materials for Hydrometallurgical Recovery of Zinc. *Miner Eng*. 2019; 139: 105871 https://doi.org/10.1016/j.mineng.2019.105871.

Ispitivanje opasnog otpada
Studija slučaja karakterizacije prašine iz elektrolučne peći

Vanja Trifunović[1], Snežana Milić[2], Ljiljana Avramović[1], Radojka Jonović[1], Vojka Gardić[1], Stefan Đorđievski[1] i Silvana Dimitrijević[1]

[1]*Institut za rudarstvo i metalurgiju Bor, Bor, Srbija*
[2]*Univerzitet u Beogradu, Tehnički fakultet u Boru, Bor, Srbija*

(Stručni rad)

Izvod

Kao međuprodukt procesa dobijanja čelika topljenjem sekundarnih sirovina na bazi gvožđa u elektrolučnoj peći, nastaje prašina. Ova prašina iz elektrolučne peći ima značajan sadržaj Zn i Fe, kao i Pb, Cd, Ca, Mg, Cr, Mn, Si, Ni, Cu, F, Cl i dr. elemenata i smatra se opasnim industrijskim čvrstim otpadom obzirom da u svom sastavu sadrži teške metale. U cilju zaštite životne sredine i javnog zdravlja od negativnog uticaja ove vrste opasnog otpada, neophodno je, čak i obavezno, sprovesti tretman otpada u skladu sa zakonodavstvom zemlje u kojoj se nalazi. Pre nego što se primeni bilo koji tretman prerade prašine iz elektrolučne peći, potrebno je izvršiti njenu detaljnu karakterizaciju. U ovom radu, izvršena je sledeća karakterizacija uzoraka prašine iz elektrolučne peći iz postrojenja u Republici Srbiji: fizička, hemijska, kao i mineraloška karakterizacija, određen je granulometrijski sastav, a određena je i procena uticaja prašine na životnu sredinu i zdravlje ljudi (testovi toksičnosti i lužljivosti). Rezultati istraživanja ove vrste opasnog otpada pokazali su da je sadržaj Zn u prašini iz elektrolučne peći iznosio od 32 mas.% do 35 mas.% i da su glavne mineraloške faze prašine cinkit, franklinit, magnetit i magnezioferit. Granulometrijska analiza je pokazala da se 80 % uzorka sastoji od čestica veličine manje od 26 μm. Što se tiče rezultata testa lužljivosti, prašina je okarakterisana kao opasan otpad zbog povećanog sadržaja hlorida, dok je testom toksičnosti utvrđeno da ispitivana prašina pokazuje toksična svojstva zbog povećanog sadržaja Zn, Cd i Pb.

Ključne reči: industrijski otpad, EAF prašina, uticaj na životnu sredinu

Biowaste composting process - comparison of a rotary drum composter and open container

Maša Buljac[1], Nediljka Vukojević Medvidović[2], Ana-Maria Šunjić[3], Zvonimir Jukić[4] and Josip Radić[1]

[1]*Department of Environmental Chemistry, Faculty of Chemistry and Technology, University of Split, Ruđera Boškovića 35, Split, Croatia*
[2]*Department of Environmental Engineering, Faculty of Chemistry and Technology, University of Split, Ruđera Boškovića 35, Split, Croatia*
[3]*Faculty of Chemistry and Technology, University of Split, Ruđera Boškovića 35, Split, Croati*
[4]*Faculty of Economics, Business and Tourism, University of Split, Cvite Fiskovića 5, Split, Croatia*

Abstract

Composting is recognized as a sustainable waste management approach in which microorganisms treat and stabilize biodegradable waste under aerobic conditions to obtain compost as a final product. In this paper, composting of biowaste in a rotary drum composter (closed system) and an open container (open system) was compared. Temperature, pH, electrical conductivity, a carbon-to-nitrogen mass ratio (C/N ratio) and contents of moisture, carbon and dry and volatile matter, were measured during composting. Results showed decreasing profiles for moisture, volatile matter, and carbon contents, as well as for the C/N ratio, while increasing profiles for the dry matter content and electrical conductivity during composting in both systems. Leachates were formed only during the first three days of composting and were characterized with high organic loads, high ammonia concentrations, low pH, and high conductivity and turbidity. The organic matter content data during the composting process were analysed according to the first order kinetic model. Results suggested that there was a difference in the rate of organic matter decomposition, which was higher when composting in the open vessel than in the rotary drum composter.

Keywords: dry content; volatile mater content; moisture content; electrical conductivity; kinetic analysis, leachate charaterization.

Available on-line at the Journal web address: http://www.ache.org.rs/HI/

ORIGINAL SCIENTIFIC PAPER

UDC: 628.473.3:628.477.4

Hem. Ind. **76(4)** 251-262 (2022)

1. INTRODUCTION

Industrialization, growing population and a high standard of living are the main causes of a significant increase in the amounts of mixed municipal waste. The usual practice of municipal waste management in many countries all over the world is based on the waste disposal on landfills, which poses a risk to human health and may cause a long-term environmental pollution [1]. Thus, primary separation of municipal waste into its main fractions (such as paper and cardboard, plastics, glass, organic biodegradable fraction, medication, batteries, *etc*.) is highly recommended [2]. There are various regulations in the European Union (Directive 1999/31/EC or Directive 2008/98/EC) that promote the relocation of biodegradable waste from landfills to reduce its impact on leachate and gases formation [3]. Namely, the organic fraction in mixed municipal waste mostly contains food waste from households. This organic fraction decomposes in landfills, and may cause groundwater pollution, production of harmful gases and unpleasant odors. Therefore, finding adequate solutions for the organic fraction is essential. Composting is a recognized technological process of biowaste management in which this type of waste is treated and stabilized with the help of microorganisms under aerobic conditions, leading to production of quality compost along with the production of heat [4, 5]. It should be noted that uncontrolled biodegradation of waste is not considered as composting [6]. In order to guarantee safety

Corresponding authors: Maša Buljac, Department of Environmental Chemistry, Faculty of Chemistry and Technology, University of Split, Ruđera Boškovića 35, Split, Croatia
E-mail: masa.buljac@ktf-split.hr
Paper received: 16 May 2022; Paper accepted: 22 November; Paper published: 11 December 2022
https://doi.org/10.2298/HEMIND220516019B

during compost use, certain quality criteria should be fulfilled such as: contents of pathogens, heavy metals, organic matter, and nutrients, as well as stability and maturity [7].

Croatia, except for a few examples, lags behind the other EU countries in separation, collection and treatment of biodegradable fractions of municipal waste. According to the data in the Waste Management Plan in the Republic of Croatia 2017-2022 [8], the quantities of recovered municipal waste in the country increased only slightly in the period 2010-2015. In 2015, the percentage of recovered waste reached fairly 18 %, compared to only 4 % reported for 2010. In addition to 18 % of the recovered waste (whereby only 2 % refers to composting and anaerobic digestion), 80 % of waste ended up in landfills, and 2 % was stored municipal waste. The reason for such devastating results is the poor system for separated collection of biowaste. Thus, it is crucial to establish separate waste collection and separation of organic waste fractions, especially since these fractions cause unpleasant odors and other environmental hazards after just a few weeks. However, as the Republic of Croatia is lagging behind in solving the problem of biowaste separation from municipal waste and disposal of untreated waste on a system level, a possible solution may be in installment of decentralized smaller devices for biowaste treatment. One of the effective and promising such devices is rotary drum composter, which provides biowaste agitation, aeration and mixing to produce a consistent and uniform compost as the end-product [9]. Also, decentralized composting ensures a sustainable and safe environment by processing smaller quantities of waste at the source [10].

There are several examples in literature describing the use of rotary drum composters such as for composting a combination of vegetable waste, cattle manure and saw dust using compost as a bulking agent [9]. It was reported that the temperature was above 55 °C for two days, nitrification occurred after the sixth day, while decreasing in the BOD/COD ratio indicates the stabilization of the compost as only the non-biodegradable parts remained [9]. In the other studies of the same group, rotary drum was investigated for composting vegetable waste and tree leaves [11] as well as sewage sludge [12]. The results suggested that composting of sewage sludge with the optimal proportion of cattle manure and saw dust, especially at carbon-to-nitrogen mass ratio (C/N) = 30, can produce stable compost within 20 days of composting [12]. In another study, rotary drum composting was investigated as a low-cost method for removal of helminths (*Ascaris lumbricoides* and *Trichuris trichiura*) in fecal sludge compost [13]. Four different rotary drums at a pilot scale were used: metal or a plastic composter with paddles or baffles, showing the composter type had a significant impact on the helminth removal so that the best results were obtained in the plastic composter with paddles [13]. Jain *et al.* investigated the efficacy of rotary drum composting of invasive aquatic weed (*Hydrilla verticillata* (L.f.) Royle), which is one of the biggest challenges in the field of solid waste management. Different mixed proportions of *H. verticillata*, cow dung and sawdust were investigated, and the results suggested that the biomass of *H. verticillata* could be utilized to produce stable compost for potential use in agricultural systems [14]. The same technique was investigated for finding a suitable inlet composition containing flower waste to obtain nutrient-enriched compost. The bulking agent (sawdust and wheat bran) helped to maintain the prolonged thermophilic conditions, adequate moisture content, leachate production and aerobic conditions during the composting process [15].

It is evident that rotary drum composting is widely applied as an efficient and decentralized technique for transforming different sources of waste and bulking agents into compost. However, none of the mentioned studies compared composting in a rotary drum composter (as a closed system) and open container (as an open system). In the present work, a pilot scale rotary drum composter was used for monitoring and analysis of biowaste composting and evaluation of the resulting compost quality. Also, the resulting compost was compared to that obtained in an open rectangular container. In addition, the organic matter content data during composting processes in both investigated systems were fitted with the first order kinetic model.

2. EXPERIMENTAL

2. 1. Composters

In order to study the composting process, a rotary drum composter and an open container were used (Figure 1.). The rotary drum composter dimensions were 95×108×50 cm while the drum dimensions were: 80 cm in length and

48 cm maximum diameter with the capacity cca 150 dm^3. Outer dimensions of the open rectangular container were 30×45×35 cm with the capacity cca 46 dm^3.

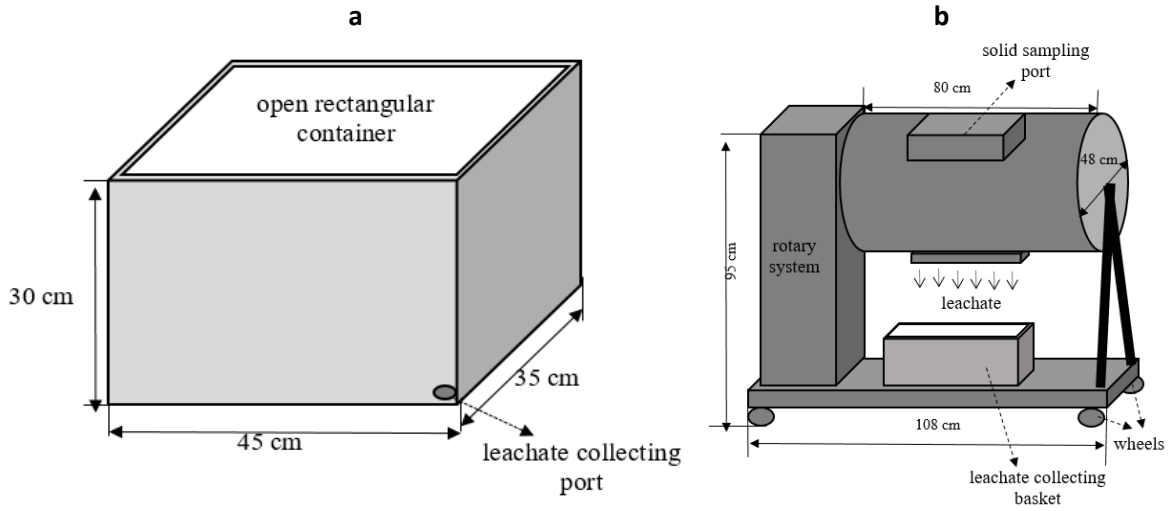

Figure. 1. Scheme of composters: a) open container; b) rotary composter

2. 2. Biowaste

The biowaste was collected in a student canteen located in the University campus of the University of Split, Croatia. Biowaste (substrate) comprised onion peels, lettuce, cucumber peels, orange peels, tomatoes, and coffee grounds. The total mass of biowaste placed in the composters was 23 kg. This biowaste was shredded using a shredder (Hurricane HMH-E 2440, iSC GmbH, Landau an der Isar, Germany), mixed with sawdust as structural material and divided into two parts of equal masses: one part was then placed in an open rectangular container (cca 12 kg) (sample A), while the other part (cca 12 kg) was placed in a rotary drum composter (sample B). The initial samples were characterized regarding the following parameters: temperature, moisture content, dry and volatile matter contents, carbon and nitrogen contents, C/N ratio, pH value and electrical conductivity.

2. 3. Composting performance

After placing the initial samples into composters, the composting process was started and investigated. During composting, sawdust was also added for better humidity regulation and a "biogarden" organic fertilizer (type Homeo-garden, HomeOgarden, Ljubljana, Slovenia) with 5 wt.% percentage of nitrogen and enriched with *mycorrhizal fungi* in order to adjust the C/N ratio containing 2 wt.% of *Endomycorrhizal fungi: Claroideoglomus etunicatum, Rhizophagus intraradices* and *Claroideoglomus claroideum;* without genetically modified organisms -GMO-free). The biogarden organic fertilizer was added during composting in both composters at day 10, 14 and 23 in the amounts of 50, 50 and 100 g, respectively. The moisture content of the compost mass was monitored daily. The composting process in both composter types lasted 25 days during which regular mixing was performed 2-3 times a day, with the addition of water, as needed (moisture content in range 60 – 80 wt.%). Sampling of the compost mass was performed manually by taking a sample) at six places (zig-zag) in amount of cca 200 g, prior mixing and homogenization. After each sampling, the following parameters were analyzed: room and compost temperatures, moisture content, dry matter content, volatile matter content, carbon content, C/N ratio, pH value and electrical conductivity, according to standard methods [16,17].

During the composting process, samples of leachate were also collected. The following water quality indicators were determined: pH value, electrical conductivity, turbidity, chemical oxygen demand (COD) and Kjeldahl nitrogen. All experimental analyses were performed by standard methods [16].

2. 4. Measurement methods

Temperature was monitored two times per day by using a digital thermometer throughout the composting period. pH value and electrical conductivity were determined in filtrate obtained by mixing 5 g of the sample with 100 cm^3 of deionized water and measured by using a pH/conductivity combimeter (Orion Star Series Meter Thermo Fischer Scientific Inc., Beverly, MA, USA). Moisture and dry matter contents were determined by drying the sample at 105 °C for 24 h, while volatile matter and carbon contents were determined by annealing in a muffle furnace at 550 °C for 4 h. Nitrogen content was measured according to the Kjeldahl method. The C/N ratio was determined by dividing the carbon content to the nitrogen content [16,17]. Chemical oxygen demand (COD) was determined by the dichromate method. All measurements were done in triplicates.

3. RESULTS AND DISCUSSION

3. 1. Analysis of the composting process

3. 1. 1. Temperature profile during the composting process

Temperature is an indicator of the progress of the composting process. The change in temperature is directly related to the biochemical activity of microorganisms, as decomposition of organic matter releases heat and causes an increase in temperature in the substrate. Change in the temperature in the compost mass causes changes in the number and types of members in the mixed culture of microorganisms involved in the decomposition of the substrate. Results of the monitored compost and room temperatures during composting are graphically shown in Figure 2.

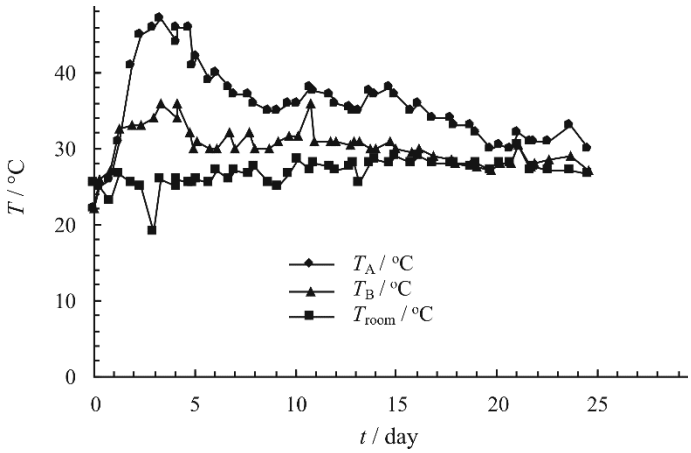

Figure 2. Results of continuous temperature monitoring of samples in the investigated open container (T_A) and rotary drum (T_B) and room temperature (T_{room}) over the course of the composting process. Note: standard deviation from the average value for temperature is in range ± (0.3-1.2).

Two phases of the aerobic process can be distinguished: a mesophilic and a thermophilic phase. Depending on the local conditions, during the aerobic mesophilic phase temperature is between 20 and 40 °C, and during the thermophilic phase temperature is in the range from 40 to 70 °C. The results show that the temperature of sample A rises sharply during the first three days, from the room temperature (22 °C) to 47 °C. This sudden rise in temperature occurred due to the activity of thermophilic microorganisms. The thermophilic phase lasted for three days followed by a cooling period up to day 11, when the temperature decreased to 38 °C. Further cooling was observed up to the end of the experiment (day 25). In sample B, during the first 3-5 days, the temperature first rose sharply from the room temperature to 36 °C and continuously declined to 30 °C. As soon as the temperature drops, it is a sign that either compost has been produced (food is exhausted) or that there is a threat to the life of microorganisms. It can be seen that the sample A has a satisfactory temperature rise (thermophilic phase), while sample B reached the temperature lower than 36 °C (mesophilic phase). This can be associated with different performances of the composting devices (open *vs*. closed). Also, we noticed that the temperature of the sample A (open container) in the core of compost mass

was significantly higher when compared to the temperature of the mass surface, whilst in case of compost in a rotating drum the temperature throughout the whole mass was uniform. The obtained results of temperature change during composting corresponded to those found in literature [9,18].

3. 1. 2. Changes in moisture and dry matter contents during composting

Moisture content is one of the critical factors influencing the effectiveness of a biological treatment and must be monitored systematically throughout the process timeline on a regular basis [19]. Moisture loss during the composting process can be viewed as an index of decomposition rate, since heat generation, which accompanies decomposition, drives vaporization (*i.e*. moisture loss) [9]. Therefore, it is necessary to monitor the dry matter content (moisture content) throughout the composting process.

The monitored dry matter content during the composting process is graphically shown in Figure 3.

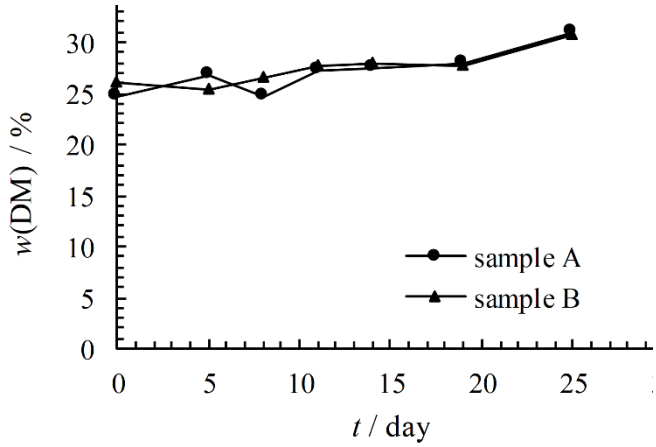

Figure 3 Dry matter content change) during the composting process . Note: standard deviation from the average value for dry matter content is in range ± (2.1-3.5)

Dry matter contents increased over time during the composting process in both devices and at the end of the process reached values of around 30 wt.%. This was expected as the compost mass becomes looser and water binding capacity decreases as the process progresses. Correspondingly, the initial moisture content was about 75.5 wt.% in both composts at the beginning of the process, while at the end it was 69 wt.%. Leachate from composting processes have to be collected and fully treated, in order to avoid pollution of underground and runoff water and detrimental effects on the environment. Interestingly, except at the beginning of the composting process, in both investigated systems there was almost no leachate generation. Similar behavior was reported in the literature [3,9,20]. The reason for such behaviour is probably connected with grinding of the collected biowaste by a shredder before filling composters in order to achieve smaller particles, which have larger surface area and can degrade more quickly. The highest amount of leachate was produced during the first three days (in sample A, total 1670 cm^3, and in sample B 1630 cm^3), after which leachate formation was not detected. According to literature [21], absence of leachate production might relate to the addition of sawdust, which preserves leaching. A very high C/N ratio achieved already in the initial stage can be associated with the leachate production in this stage, as biowaste grinding induced leaching nutrients from the biowaste. Thus, the leachate collected during the days 2 and 3 were analyzed and the results are compared with maximal allowed values according to the Croatian Regulation for discharge into surface water and public sewage system [22].

The leachate samples were cloudy and dark green in color (turbidity results shown in Table 1 are extremely high and range from 377 to 917 NTU). The increased values of electrical conductivity (in the range 5610 - 9510 µS cm^{-1}) indicate organic substances and the increased presence of salts, anions and cations. The pH values are slightly acidic (in the range of 4.62 - 5.10) which is attributed to the rapid conversion of soluble organic matter into volatile fatty acids (VFA). The low pH recorded in the leachate can accelerate the process of biological nitrification and, thus, complicate maintenance of the constant efficiency of a composting process [23].

Table 1. Results of physical and chemical characterization of leachate.

Parameter	Leachate after the 2nd day of composting		Leachate after the 3rd day of composting		Surface water	Public sewage system
	system A	system B	system A	system B		
pH	4.62±0.12	4.59±0.11	5.08±0.15	5.10±0.10	6.5-9.5	6.5 – 9.5
Conductivity, μS cm^{-1}	9230±40	5610±26	7800±32	9510±42	-	-
Turbidity, NTU	917±7.5	377±3.5	981±8.7	891±6.7	-	-
COD, mg O_2 dm^{-3}	34313 ±110.55	27410 ±101.85	24460±95.55	25380±105.95	125	700
TN_K, mg N dm^{-3}	288.54±11.55	182.09±9.85	1048.04±55.73	732.20±35.62	15*	50*

Note: system A - leachate from composting in an open container, B - leachate from composting in a rotary composter;
*values in last two columns are taken from Croatian regulations NN 26/20 [22]. However, values for total nitrogen are compared since values for Kjeldahl nitrogen are not specified in the Croatian regulation. The results are reported as the average values±standard deviation.

COD levels in the leachate are very high and in the range 24460 – 34313 mg O_2 dm^{-3}, which indicates the presence of organic and inorganic substances susceptible to oxidation with dichromate. The values significantly exceed the limit values prescribed by the Croatian regulation.

Increased concentration of ammonia indicates biodegradation of complex organic molecules and organic nitrogen, which results in the formation of ammonium ions. This is precisely why nitrogen was analyzed here as Kjeldahl nitrogen, as it includes organic and ammonium nitrogen. The resulting value is compared with the regulatory data for total nitrogen, as data for Kjeldahl nitrogen are not prescribed by the Croatian low. It can be seen that the values significantly exceed the limit values prescribed by Croatian regulations.

Phosphates, heavy metals and plasticizers in the leachate after composting were not determined in this work, although their presence has been proven in the literature [23].

3. 1. 3. Changes in volatile matter and carbon contents during composting

Experimentally determined volatile matter and carbon contents during the composting process are shown in Figure 4. The carbon content is calculated from the volatile matter content, according to the equation [24]:

$$w(\mathrm{C}) = \frac{w(\mathrm{VM})}{1.8} \quad (1)$$

where w(VM) / % is the volatile matter content and w(C) / % is the carbon content.

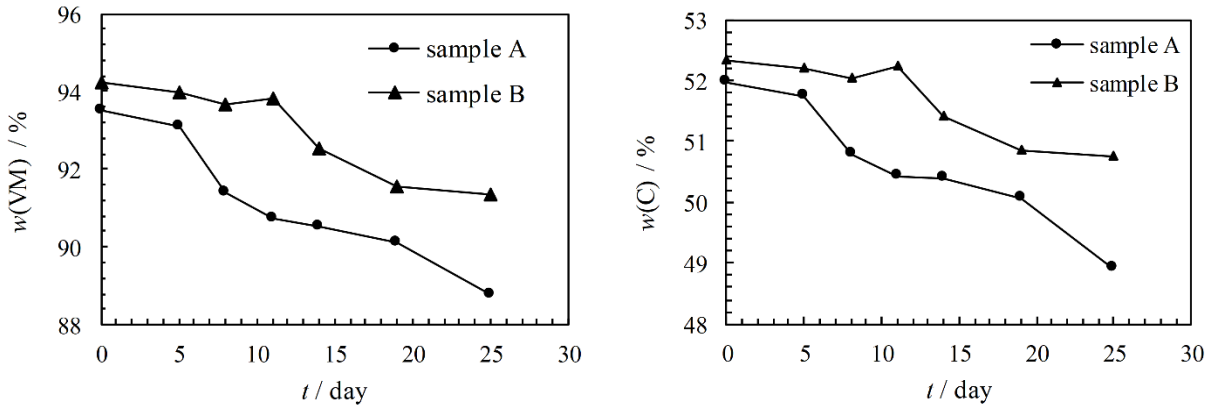

Figure 4. Contents of (a) volatile matter and (b) carbon during the composting process in the open container (sample A) and rotary drum (sample B). Note: standard deviation from the average value for volatile matter is in range ±(1.2-3.5), for carbon content in range ±(2.5-4.1)

There is a slight decrease in the volatile matter content in both samples, from the beginning to the end of the process, as is evident in Figure 4. Values ranged from ~94 to 89 % for sample A and to 91 % for the sample B indicating a more pronounced decrease in the open container as compared to that in the rotary drum. Similar results were reported in the literature [18]. Since the volatile matter content is related to the organic matter content in compost, in

addition to the influence of the system design, the reason for this finding may be the structural material (sawdust) that was added to control humidity, which causes a high C/N ratio. Therefore, it might be better to use some other material to regulate humidity.

3. 1. 4. Changes in pH and electrical conductivity values during composting

The measured pH and electrical conductivity values during the composting process are shown in Figure 5. At the beginning of the process, the initial pH value was 6.36 in sample A and 6.17 in sample B. During the process, the pH value rose slightly, which can be attributed to the activity of microorganisms. The highest pH value was observed on day 19 and was 8.56 for sample A and 8.84 for sample B, probably due to the formation of higher amounts of ammonia in the latter case. After the thermophilic phase, under conditions of good aeration, ammonia oxidized to nitrate, which gradually reduced the pH value [9,21]. The final pH value after 25 days was 7.59 in both systems.

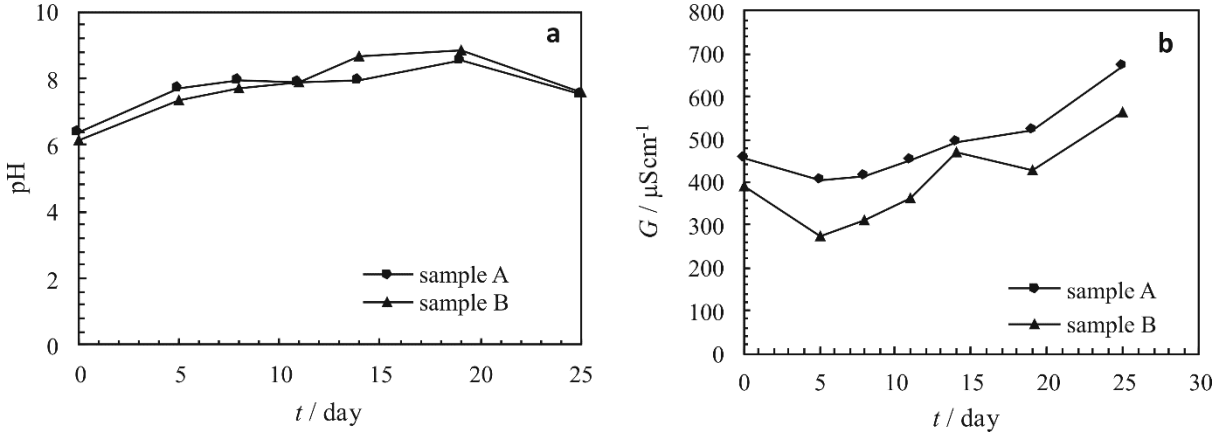

Figure 5. Measured (a) pH values and (b) electrical conductivities during composting in the open container (sample A) and rotary drum (sample B). Note: standard deviation from the average value for pH is in range ±(0.09-0.18), for electrical conductivity in range ±(8.8-32.5)

Electrical conductivity is an indicator of the contents of soluble salts in compost and it depends on the amount and type of ions in the solution. Low electrical conductivity value can induce lower fertility of a compost due to low contents of potassium, calcium, and magnesium. However, high salt concentrations may indicate potential phytotoxicity (germination arrest or slowed root work). A value of 3500 μS cm^{-1} was suggested as the upper limit for the substrate used for seed germination in container plant production [25]. According to the obtained results (Figure 5b), the values for sample A ranged from 455 to 671 μS cm^{-1}, and from 392 to 565 μS cm^{-1} for sample B.

3. 1. 5. Change in the C/N ratio during composting

The C/N ratio determines the level of the end product maturity and stability. It was therefore monitored over the composting process to monitor microbial activities in both composters. Rapid decomposition of organic matter results in a decrease in the organic carbon content, accumulation of nutrient and microbiological amounts, which leads to a decrease in the C/N ratio. As can be seen in Figure 6, in sample A, a constant decrease in the C/N ratio was observed, while in sample B the C/N ratio oscillated. The C/N ratio decrease in the former case was quite large (from 248 to 106, which represented a decrease of 60 % related to the initial value), which indicated a distinct degradation rate. However, a theoretical C/N ratio of about 30 was not achieved [26]. This result can be attributed again to the addition of sawdust whose C/N ratio was 325 and thus affected the reduced nitrogen content in the compost [27]. This result indicates that some other material (leaves, wood) would be more suitable as a structural material.

Also, a very high C/N ratio already in the initial composting stage can be associated with the higher leachate production in this stage, as grinding has leached out nutrients from biowaste.

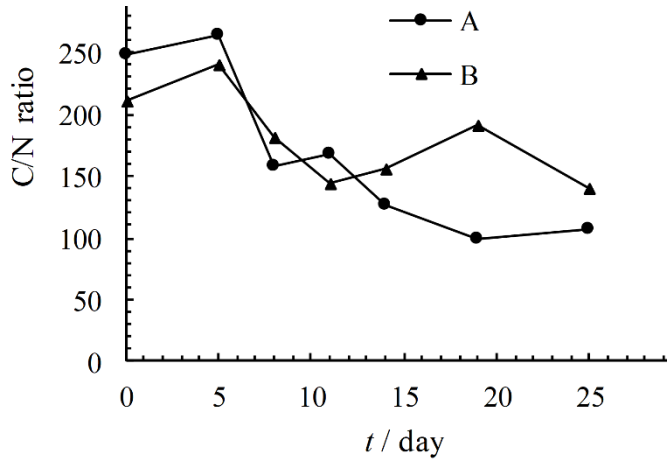

Figure 6. The C/N ratio during composting in the open container (sample A) and rotary drum (sample B). Note: standard deviation from the average value for C/N ration is in range ±(0.5-17)

3. 1. 6. Change in the nitrogen content during composting

Nitrogen contents during composting are shown in Figure 7.

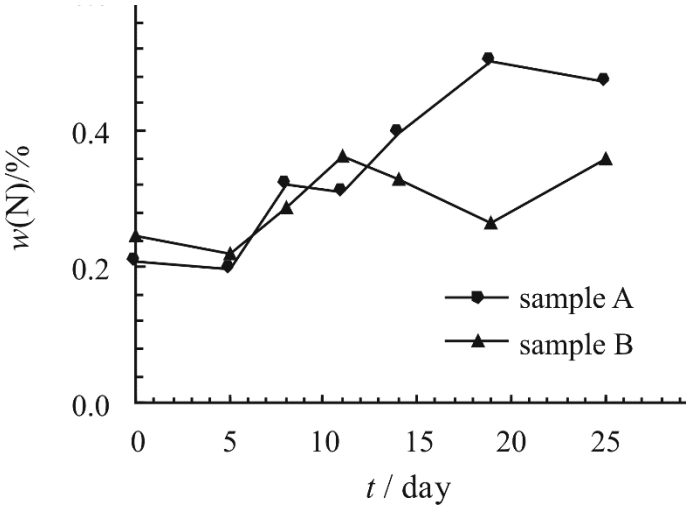

Figure 7. Nitrogen contents change during composting in the open container (sample A) and rotary drum (sample B). Note: standard deviation from the average value for nitrogen content is in range ±(0.09-0.12)

During the composting process there is a slight increase in the nitrogen content, which is attributed to the loss of mass and mineralization of organic matter. This increase is visible in sample A (from 0.21 to 0.50 %), while the nitrogen content shows oscillations in the sample B. The obtained nitrogen contents during composting are significantly lower than those reported in literature [9,25]. Obviously, the design of the reactor system affects the nitrogen content, and the open system is more favorable in this case. The open system also has its drawbacks, which are associated with gas emissions, unpleasant odors, and the appearance of insects in the compost. Also, the reason for such a low increase in the nitrogen content may be the excessive amount of sawdust in the compost, which has an increased carbon content and leads to the immobilization of the composting process.

3. 2. Comparison of physicochemical parameters of the initial sample and compost

A comparison of physicochemical parameters of the initial sample and the obtained composts after 25 days in both investigated systems are presented in Table 2.

Table 2. Comparison of physicochemical parameters of the initial sample and the obtained composts after 25 days in the open container (designation A) and rotary drum (designation B)

Parameters	A		B	
	initial sample	after 25 days	initial sample	after 25 days
T / °C	22±0.5	30±0.8	22±0.7	27±0.8
w(DM) / %	26±2.5	31±3.2	24±2.2	32±2.6
w(H_2O) / %	74±3.7	69±2.2	76±2.8	69±3.1
w(VM) / %	94±2.8	88±1.4	94±2.7	91±2.8
w(C) / %	52±1.9	49±1.8	52±2.1	51±2.0
pH	6.36±0.23	7.54±0.17	6.17±0.22	7.59±0.15
G / μS cm^{-1}	455±15.6	671±20.2	392±12.6	565±18.5
C/N mass ratio	248±12	106±8	211±9	140±11

Note: The results are reported as the average values±standard deviation

It can be seen that the examined parameters are in accordance with the literature [25], except for the C/N ratio, which is higher than the reported values. During active decomposition, a pleasant earthy odor was recorded as an indicator of proper ventilation and the absence of anaerobic conditions. Changes in the appearance of the composting material were visible in terms of color and texture as the process progressed. Already, after 20 days, both investigated composts achieved dark brown color, fine texture without any visible organic waste and typical smell of earth. A gradual decrease in the compost volume was also observed during decomposition. Changes in physicochemical parameters reflected the progress and outcome of the composting process in accordance with literature findings [28].

3. 3. Composting kinetics

Kinetic models are used as tools to optimize the composting process. By using a kinetic model and controlling the process parameters, the waste decomposition degree can be predicted. Knowing the composting kinetics is essential for design and operation of a composting plant [19]. The composting process can be mathematically described by using a first-order kinetic model according to equation [29,30]:

$$\frac{dC}{dt} = -kC \tag{2}$$

where C is the content of biodegradable substances, k is the decomposition rate constant and t is time.

The decomposition rate constant is temperature dependent and various models can be found in literature to describe this dependence [19]. The content of biodegradable organic matter corresponds to the content of volatile matter in compost. Thus, by integrating eq. (2) and assuming that $C = C_0$ for $t = 0$, it follows that:

$$\ln\frac{C}{C_0} = -kt \tag{3}$$

where C is the volatile matter content in compost at time t and C_0 is the volatile matter content in compost at the beginning of the composting process.

By the best linear fit of ln (C/C_0) *vs.* time, k is calculated from the slope of the line (Figure 8).

The model indicated that the rate of substrate decomposition was higher in the sample in the open system (k = 0.0023 day^{-1}) compared to the closed system (k = 0.0012 day^{-1}). Indeed, since the decomposition rate constant is temperature dependent, this suggests that these differences may be related to the difference in temperature rise in open and closed systems, which is to be expected given the differences in composting in an open and closed system. Good agreement of the model with the experimental data (R^2 = 0.941) in sample A is visible, which is expected since biowaste comprised easily degradable components (onion peels, lettuce, cucumbers, oranges, tomatoes, and coffee grounds). However, it should be kept in mind that the rate of decomposition of more complex substrates over time is not only a function of the substrate concentration but also of particle structure, system design (open *vs.* closed), humidity, temperature, and oxygen concentration.

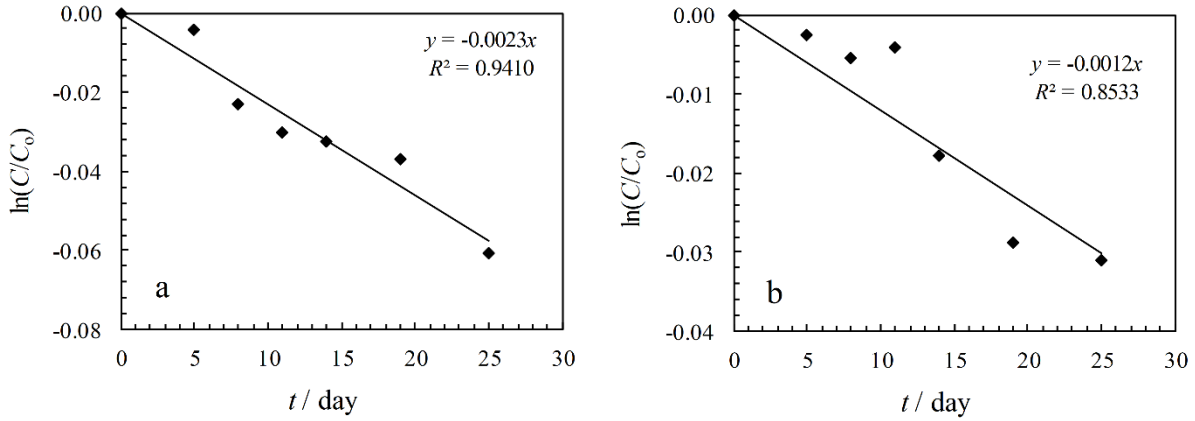

Figure 8. Interpretation of the experimental data according to the first order kinetic model (symbols) and the best linear fit (line) for composting in a) open container, b) rotary drum

4. CONCLUSION

In this work, the composting of samples of biowaste from the university canteen in a rotary drum composter and an open container was analysed. During composting in both systems, the temperature first rose sharply, followed by a continuous drop. In contrast to the open container, where a satisfactory temperature increase was observed (thermosphilic region), the sample in the rotary drum reached a temperature lower than 36 °C, which can be attributed to a different system design.

The process monitoring of the two experimental composters showed overall decreasing profiles versus composting time for parameters such as moisture content, organic carbon, volatile matter content and the C/N ratio, as well as overall increasing profiles for parameters such as electrical conductivity and the total nitrogen content.

The pH value of both initial compost materials was above 6, and after the end of the composting process, all composts had a pH value around 8, which can be attributed to the action of microorganisms.

The electrical conductivities of both samples were below the recommended upper limit of the value for the substrate used for seed germination in container plant production (3500 μS cm^{-1}). A constant decrease in the C/N ratio was observed in the open container, while it oscillated in the rotating drum. Leachate (approximately 1650 cm^3) was produced during the first three days of composting, after which period leaching was not observed. The leachate is characterized by its high organic content, high ammonia concentration, low pH, high conductivity and high turbidity. All measured values were significantly above the prescribed limit values by Croatian regulation.

A comparison of the physicochemical parameters showed that the open system exhibited better results compared to the closed system. In both systems, good compost was obtained in terms of color and texture. However, in the rotary composter temperature in the entire compost mass was uniform, which ensured uniform processing and stabilization of the compost throughout the mass.

The organic matter was reduced over time due to the microbial metabolism. Degradation rate of organic waste was modeled by the first order kinetic model. Composting in the open system exhibited higher degradation rate with the rate constant of 0.0023 day^{-1}, as compared to the closed system in which the rate constant was 0.0012 day^{-1}. These differences may be related to the difference in temperature rise in open and closed systems. Although both composting systems, the rotary drum, and the open container, can be successfully used for municipal waste composting and help to significantly reduce the amount of waste sent to landfills, the rotary composter is more suitable for urban areas because it helps to reduce the emission of unpleasant odors as well as the presence of insects in the compost. However, further research should focus on the analysis of different decentralized home composters suitable for home composting as well as for public facilities and educational institutions.

From these results, it can be concluded that the use of both rotary drum composter and open container for composting waste in community can help to significantly reduce the amount of waste and divert it from landfills.

Acknowledgements: The authors acknowledge the support European structural and investment funds under the project "BEWARE! -Practical-Active-Together-Interdisciplinary! - a program of service learning for the environment and sustainable development"

REFERENCES

[1] Panaretou V, Vakalis S, Ntolka A, Sotiropoulos A, Moustakas K, Malamis D, Loizidou, M. Assessing the alteration of physicochemical characteristics in composted organic waste in a prototype decentralized composting facility. *Environ Sci Pollut Res.* 2019; 26: 20232–20247. https://doi.org/10.1007/s11356-019-05307-7

[2] Malindzakova M, Puskas D. Biodegradable Waste Processing and Quality Control during the Composting Process. *J Manag Syst.* 2019; 20 (169): 128-133. https://www.calitatea.ro/assets/arhiva/2019/QAS_Vol.20_No.169_Apr.2019.pdf

[3] Girón-Rojas C, Gil E, Garcia-Ruiz A, Iglesias N, López M. Assessment of biowaste composting process for industrial support tool development through macro data approach. *Waste Manag.* 2020; 105: 364–372. https://doi.org/10.1016/j.wasman.2020.02.019

[4] Bruni C, Akyol Ç, Cipolletta G, Eusebi AL, Caniani D, Masi S, Colón J, Fatone F. Decentralized community composting: past, present and future aspects of Italy. *Sustainability* 2020; 12: 3319. https://doi.org/10.3390/su12083319

[5] Chen T, Zhang S, Yuan Z. Adoption of solid organic waste composting products: A critical review. *J Clean Prod.* 2020; 272: 122712. https://doi.org/10.1016/j.jclepro.2020.122712

[6] Ordinance on by-products and end-of-waste status NN 117/2014. https://narodne-novine.nn.hr/clanci/sluzbeni/2014_10_117_2217.html (in Croatian)

[7] Oviedo-Ocaña ER, Torres-Lozada P, Marmolejo-Rebellon LF, Hoyos LV, Gonzales S, Barrena R, Komilis D, Sanchez A. Stability and maturity of biowaste composts derived by small municipalities: Correlation among physical, chemical and biological indices. *Waste Manag.* 2015; 44: 63-71. http://dx.doi.org/10.1016/j.wasman.2015.07.034

[8] Waste management plan in the Republic of Croatia 2017 - 2022 NN 3/2017. https://mingor.gov.hr/UserDocsImages/UPRAVA-ZA-PROCJENU-UTJECAJA-NA-OKOLIS-ODRZIVO-GOSPODARENJE-OTPADOM/Sektor%20za%20odr%C5%BEivo%20gospodarenje%20otpadom/Ostalo/management_plan_of_the_republic_of_croatia_for_the_period_2017-2022.pdf (in Croatian)

[9] Kalamdhad AS, Kazmi A A. Rotary drum composting of different organic waste mixtures. *Waste Manag Res.* 2009; 27: 129-137. https://doi.org/10.1177/0734242X08091865

[10] Nenciu F, Stanciulescu I, Vlad H, Gabur A, Turcu OL, Apostol T, Vladut VN, Cocarta DM, Stan C. Decentralized Processing Performance of Fruit and Vegetable Waste Discarded from Retail, Using an Automated Thermophilic Composting Technology. *Sustainability* 2022; *14:* 2835. https://doi.org/10.3390/su14052835

[11] Kalamdhad AS, Singh YK, Ali M, Khwairakpam M, Kazmi AA. Rotary drum composting of vegetable waste and tree leaves. *Bioresour Technol.* 2009; 100(24): 6442-6450. https://doi.org/10.1016/j.biortech.2009.07.030

[12] Nayak AK, Kalamdhad AS. Sewage sludge composting in a rotary drum reactor: stability and kinetic analysis. *Int J Recycl Org Waste Agricult.* 2015; 4: 249–259. https://doi.org/10.1007/s40093-015-0104-4

[13] Appiah-Effah E, Nyarko KB, Awuah E, Antwi EO. Rotary drum composter as a low cost method for the removal of *Ascaris lumbricoides* and *Trichuris Trichiura* in faecal sludge compost. *Water Pract Technol.* 2018; 13(2): 237-246. https://doi.org/10.2166/wpt.2018.018

[14] Jain MS, Kalamdhad AS. Efficacy of batch mode rotary drum composter for management of aquatic weed (Hydrilla verticillata (L.f.) Royle). *J Environ Manag.* 2018; 1(221): 20-27. https://doi.org/10.1016/j.jenvman.2018.05.055

[15] Sharma D, Yadav KD. Application of rotary in-vessel composting and analytical hierarchy process for the selection of a suitable combination of flower waste. *Geol Ecol Landsc.* 2018; 2(2): 137-147. https://doi.org/10.1080/24749508.2018.1456851

[16] Standard methods for the examination of water and wastewater. 18th Edition, American Public Health Association, NW, Washington, DC 2005. https://www.standardmethods.org/doi/book/10.2105/SMWW.2882?gclid=Cj0KCQiAyracBhDoARIsACGFcS5xhJAkiLPtswQ0lFijr4XwsN46e6snKYFTCigKo_tilzMgmdTwNfQaApGNEALw_wcB

[17] Test methods for the examination of composting and compost, USDA and U.S. Composting Council. 2002. https://www.compostingcouncil.org/store/viewproduct.aspx?id=13656204

[18] Kučić Grgić D, Briški F, Ocelić Bulatović V, Vuković Domanovac M, Domanovac T, Šabić Runjavec M, Miloloža M, Cvetnić M. Composting of agroindustrial waste, biowaste and biodegradable municipal solid waste in adiabatic reactor. *Kem Ind.* 2019; 68(9-10): 381-388. https://doi.org/10.15255/KUI.2019.029 *(in Croatian).*

[19] El Houda Chaher N, Hemidat S, Chakchouk M, Nassour A, Hamdi M, Nelles M. From anaerobic to aerobic treatment: upcycling of digestate as a moisturizing agent for in-vessel composting process. *Bioresour Bioprocess*. 2020; 7(60). https://doi.org/10.1186/s40643-020-00348-0

[20] Lleó T, Albacete E, Barrena R, Font X, Artola A, Sánchez A. Home and vermicomposting as sustainable options for biowaste management. *J Clean Prod.* 2013; 47: 70-76. http://dx.doi.org/10.1016/j.jclepro.2012.08.011

[21] Varma VS, Kalamdhad AS, Effects of Leachate during Vegetable Waste Composting using Rotary Drum Composter, *Environ Eng Res.* 2014; 19(1): 67-73; https://doi.org/10.4491/eer.2014.19.1.067

[22] Croatian Regulation on Emission Limits Values in Wastewater, NN 26/2020. (In Croatian). Available online: https://narodne-novine.nn.hr/clanci /sluzbeni/2020_03_26_622.html (accessed 20 February 2022)
[23] Roy D, Azaïs A, Benkaraache S, Drogui P, Tyagi RD, Composting leachate: characterization, treatment and future perspectives, *Rev Environ Sci Biotechnol*. 2018; 17: 323-349. https://doi.org/10.1007/s11157-018-9462-5
[24] Barrena R, Pagans El, Artola A, Vázquez F, Sánchez A. Co-composting of hair waste from the tanning industry with de-inking and municipal wastewater sludges. *Biodegradation* 2006; 18(3): 257–268. https://doi:10.1007/s10532-006-9060-z
[25] Vukobratović M, Lončarić Z, Vukobratović Ž, Dadaček N. Changes in chemical properties of manure during composting (*in Croatian*). *Poljoprivreda* 2008; 14(2): 29-37. https://hrcak.srce.hr/file/49516
[26] Leśniańska A, Janowska B, Sidełko R. Immobilization of Zn and Cu in Conditions of Reduced C/N Ratio during Sewage Sludge Composting Process. *Energies* 2022: 15: 4507. https://doi.org/10.3390/en15124507
[27] Carbon-to-Nitrogen Ratio | Planet Natural, https://www.planetnatural.com/composting-101/making/c-n-ratio (Assessed 22. April 2022.
[28] ázquez MA, Sen R, Soto M. Physico-chemical and biological characteristics of compost from decentralised composting programmes. *Bioresour Technol.* 2015; 198: 520-532. http://dx.doi.org/10.1016/j.biortech.2015.09.034
[29] Kulcu R. New kinetic modeling parametars for composting process applied to composting of chicken manure. *J Mater Cycles Waste Manag.* 2016; 18: 734–741. https://doi.org/10.1007/s10163-015-0376-9
[30] Manu MK, Kumar R, Garg A. Drum composting of food waste: A kinetic study. *Procedia Environ Sci.* 2016; 5: 456–463. https://doi.org 10.1016/j.proenv.2016.07.029

Kompostiranja biootpada – usporedba rotacijskog kompostera valjkastog oblika i otvorene posude

Maša Buljac[1], Nediljka Vukojević Medvidović[2], Ana-Maria Šunjić[3], Zvonimir Jukić[4] i Josip Radić[1]

[1]Zavod za kemiju okoliša, Kemijsko-tehnološki fakultet, Sveučilište u Splitu, Ruđera Boškovića 35, Split, Hrvatska
[2]Zavod za inženjerstvo okoliša, Kemijsko-tehnološki fakultet, Sveučilište u Splitu, Ruđera Boškovića 35, Split, Hrvatska
[3]Kemijsko-tehnološki fakultet, Sveučilište u Splitu, Ruđera Boškovića 35, Split, Hrvatska
[4]Ekonomski fakultet, Sveučilište u Splitu, Cvite Fiskovića 5, Split, Hrvatska

(Naučni rad)

Izvod

Kompostiranje je prepoznato kao održiv pristup gospodarenju otpadom u kojem mikroorganizmi tretiraju i stabiliziraju biorazgradivi otpad u aerobnim uvjetima, te se dobiva kompost kao konačni proizvod. U ovom radu uspoređen je proces kompostiranja biootpada u rotacijskom komposteru valjkastog oblika (zatvoreni sustav) i otvorenoj posudi (otvoreni sustav). Tijekom kompostiranja u oba sustava su praćeni slijedeći parametri: temperatura, sadržaji suhe i hlapive tvari, vlage i ugljika, pH vrijednost i električna vodljivost te C/N omjer. Rezultati su pokazali opadajući profil sadržaja vlage, hlapive tvari, ugljika i C/N omjera te rastući profil sadržaja suhe tvari i električne vodljivosti tijekom kompostiranja kod oba sustava. Procjedne vode nastaju samo tijekom prva tri dana kompostiranja i karakterizirane su visokim organskim opterećenjem, visokom koncentracijom amonijaka, niskim pH, visokom vodljivošću i zamućenošću. Podaci o sadržaju organske tvari tijekom procesa kompostiranja analizirani su prema kinetičkom modelu prvog reda. Dobivena su dobra slaganja modela sa eksperimentalnim rezultatima, a brzina razgradnje organske tvari je veća pri kompostiranju u otvorenoj posudi, u odnosu na rotacijski komposter.

Ključne reči: sadržaj suhe tvari; sadržaj hlapljivih tvari; sadržaj vlage; električna provodljivost; kinetička analiza, karakterizacija procjedne vode

Urban chemistry as a new discipline exploring chemical and chemico-biological aspects of urban environment

Evgeny Aleksandrovich Gladkov[1] and Olga Victorovna Gladkova[2]

[1]K.A. Timiryazev Institute of Plant Physiology, Russian Academy of Sciences, IPP RAS, Botanicheskaya St., Moscow, 127276; Russia
[2]Independent scientist, Moscow, Russia

Abstract

Urban sciences can be divided into three directions: Natural, Humanities and Engineering. Within the fields of urban natural and urban engineering (technical) sciences, chemical and chemico-biological research take an important place. We propose using the new term "urban chemistry" (*i.e*. chemistry of the urban environment) focusing on the chemical aspects of the atmosphere, water bodies, and soil of cities. Urban chemistry is interconnected with urban ecology, toxicology and urban biology, and among the biological disciplines, it is particularly related to urban botany. Urban chemistry can be seen as a separate direction of urban natural sciences, which will significantly contribute to sustainable development of cities.

Keywords: chemistry of the urban environment; urban natural sciences; soil; urban air chemistry; plants; urban botany.

Available on-line at the Journal web address: http://www.ache.org.rs/HI/

LETTER TO THE EDITOR

UDC: 911.375.1+577.1

*Hem. Ind.***76(4)** 263-266 (2022)

1. URBAN NATURAL SCIENCES

In urban sciences, great importance is given to humanitarian areas. We propose to distinguish three directions in the urban sciences: Humanities (social and humanistic sciences), Natural and Engineering (technical sciences). Within the latter two areas, chemical research is particularly important so that, one of the priority directions in urban natural sciences is chemistry of the urban environment.

2. URBAN CHEMISTRY (CHEMISTRY OF THE URBAN ENVIRONMENT)

Applied chemistry aims to solve practical problems by applying principles and theories of chemistry so that various branches exist including agricultural, food, environmental, pharmaceutical, medical, and industrial chemistry. We propose using the new term "urban chemistry" (chemistry of the urban environment) specifically focusing on chemical aspects of city areas. Topics on "Urban atmospheric chemistry" or "Urban Air Chemistry" have been in focus in recent literature [1,2], while it is also important to address chemical features of the other components of environment (i.e., water and soils). Thus, we propose to use the term "urban chemistry" for the entire urban environment, *i.e*. the study of the atmosphere, water bodies, and soil of cities.

Urban air chemistry is characterized by measurements of gas and aerosol compositions [1]. Conventional knowledge of global and regional atmospheric chemistry is not sufficient to predict the behaviour of pollutants in the urban atmosphere [2] since air pollution in cities has its own specifics. Many cities record high levels of air pollution, while the degree of urban environmental pollution can vary considerably within the cities. For example, high levels of air and soil pollution can be observed along highways in roadside areas. Vehicle emissions create corridors of increased carbon and nitrogen concentrations near highways that influence surrounding ecosystems [3]. Therefore, it is of great importance to assess the frequency of urban air pollution occurrence and its influencing factors[4].

Corresponding authors: *Evgeny Aleksandrovich Gladkov, K.A. Timiryazev Institute of Plant Physiology, Russian Academy of Sciences, IPP RAS, 35 Botanicheskaya St., Moscow, 127276; Russia and **Olga Victorovna Gladkova
E-mail:*gladkovu@mail.ru and **olgav.gladkova@mail.ru
Paper received: 21 November; Paper accepted: 8 December; Paper published: 11 December 2022
https://doi.org/10.2298/HEMIND221204020G

Particulate matter concentrations are usually higher in urban areas than in rural areas [5] and most urban dwellers in the European Union were reported to be exposed to particles and fine dust levels in excess of threshold values [6].

In addition, environmental monitoring of urban soil and water pollution is equally important. For example, deicing reagents and heavy metals were shown to pose a serious threat to urban soils and plants [7,8,9] and the main features of urban soil pollution are characterized by the accumulation of copper, zinc, lead and mercury[10]. Such contamination of urban soils with heavy metals, due to the rapid urbanization and development of urban services, has become a major environmental and human health challenge [11]. Similarly, water bodies in cities, such as lakes, may be more susceptible to pollution as compared to rural areas [12].

Major impacts of human activities on urban ecosystems are demonstrated by changed degrees of environmental pollution during the COVID-19 pandemic in some cities. For example, in Volos, Greece, significant changes in metal concentrations were observed in different parts of the city during the pandemic, due to the limited movement of motorized vehicles, but also due to the long operating hours of the heating systems in the residential area [13].

In order to solve environmental problems, interdisciplinary research within urban natural and urban engineering (technical) sciences is necessary such as the use of chemical technology as well as biochemical methods for urban waste treatment and water purification. Similarly, urban chemistry is interconnected with urban ecology, toxicology, and urban biology. Among the biological disciplines, urban chemistry is particularly related to urban botany (urban plant science) since urban pollution can influence plant biodiversity. High soil heavy metal and Na concentrations, along with the pH, were reported to induce intense negative effects on plant biodiversity [14].

The impact of chemicals on the environment of cities is often assessed in regard to the maximum permissible concentrations. However, these limits do not always take into account the effects of chemicals on plants as it is the case of maximal permissible concentrations of heavy metals [8]. The task for the future is to determine these concentrations in relation to certain plant species, which can be achieved with the help of biological and chemical sciences. Thus, the development of chemico-biological directions in urban sciences is important for the sustainable functioning of urban ecosystems.

We propose that urban chemistry is considered a separate academic discipline, which can be included in the curricula of Master's degree programs in "Ecology" and "Chemistry".

Funding: Research was carried out within the state assignment of the Ministry of Science and Higher Education of the Russian Federation (theme 122042700045-3).

REFERENCES

[1] Hidy GM. Urban Air Chemistry in Changing Times. *Atmosphere*. 2022; 13(2):327. https://doi.org/10.3390/atmos13020327

[2] Harrison RM. Urban atmospheric chemistry: a very special case for study. *NPJ Clim Atmos Sci.* 2018; 1; 20175. https://doi.org/10.1038/s41612-017-0010-8

[3] Khalid N, Noman A, Masood A, Tufail A, Hadayat N, Alnusairi GSH, Alamri S, Hashem M, Aqeel M. Air pollution on highways and motorways perturbs carbon and nitrogen levels in roadside ecosystems, *Chem Ecol.* 2020; 36(9): 868-880. https://doi.org/10.1080/02757540.2020.1791102

[4] Zhou D, Lin Z, Liu L, Qi J. Spatial-temporal characteristics of urban air pollution in 337 Chinese cities and their influencing factors. *Environ Sci Pollut Res.* 2021; 28, 36234 36258. https://doi.org/10.1007/s11356-021-12825-w

[5] Patella V, Florio G, Magliacane D, Giuliano A, Crivellaro AM, Di Bartolomeo D, Genovese A, Palmieri M, Postiglione A, Ridolo E, Scaletti C, Ventura MT, Zollo A, & Air Pollution and Climate Change Task Force of the Italian Society of Allergology, Asthma and Clinical Immunology (SIAAIC). Urban air pollution and climate change: "The Decalogue: Allergy Safe Tree" for allergic and respiratory diseases care. *Clin Mol Allergy*. 2018;16, 20. https://doi.org/10.1186/s12948-018-0098-3

[6] European Environment Agency (EEA) report. EEA Report No 28/2016. https://www.eea.europa.eu/data-and-maps/figures/percentage-of-the-eu-urban

[7] Gladkov EA, Gladkova OV. Ornamental plants adapted to urban ecosystem pollution: lawn grasses tolerating deicing re-agents. *Environ Sci Pollut Res.* 2022; 29, 22947–22951. https://doi.org/10.1007/s11356-021-16355-3

[8] Gladkov EA, Gladkova OV. Plants and maximum permissible concentrations of heavy metals in soil. Archives for Technical Sciences.2021; 25(1): 77-82. http://dx.doi.org/10.7251/afts.2021.1325.077G

[9] Gladkov E.A., Gladkova, O.V. New directions of biology and biotechnology in urban environmental sciences. *Hem Ind.* 2021; 75 (6); 365-368. https://doi.org/10.2298/HEMIND211230034G

[10] Yang J-L, Zhang G-L. Formation, characteristics and eco-environmental implications of urban soils – A review. *Soil Sci Plant Nutr.* 2015;61(sup1): 30-46, https://doi.org/10.1080/00380768.2015.1035622

[11] Rezapour S, Moghaddam SS, Nouri A, Aqdam KK. Urbanization influences the distribution, enrichment, and ecological health risk of heavy metals in croplands. *Sci Rep.* 2022; 12, 3868. https://doi.org/10.1038/s41598-022-07789-x

[12] Cheng N, Liu L, Hou Z, Wu J, Wang Q, Fu Y. Pollution characteristics and risk assessment of surface sediments in the urban lakes. *Environ Sci Pollut Res*.2021; 28, 22022–22037. https://doi.org/10.1007/s11356-020-11831-8

[13] Aslanidis P-SC, Golia EE. Urban Sustainability at Risk Due to Soil Pollution by Heavy Metals—Case Study: Volos, Greece. Land. 2022; 11(7):1016. https://doi.org/10.3390/land11071016

[14] Hernández AJ, Pastor J. Relationship between plant biodiversity and heavy metal bioavailability in grasslands overlying an abandoned mine. *Environ Geochem Health*. 2008 ;30(2):127-133. https://doi.org/10.1007/s10653-008-9150-4

Urbana hemija kao nova disciplina koja istražuje hemijske i hemijsko-biološke aspekte urbane životne sredine

Evgeny Aleksandrovich Gladkov[1] i Olga Victorovna Gladkova[2]

[1]K.A. Timiryazev Institute of Plant Physiology, Russian Academy of Sciences, IPP RAS, Botanicheskaya St., Moscow, 127276; Russia
[2]Nezavisni naučnik, Moscow, Russia

(Pismo uredniku)

Izvod

Urbane nauke se mogu podeliti na tri oblasti: prirodne, humanističke i inženjerske nauke. U okviru prirodnih i inženjerskih (tehničkih) urbanih nauka, posebno su značajna hemijska i hemijsko-biološka istraživanja. Predlažemo korišćenje novog termina „urbana hemija“ (hemija urbane sredine) sa fokusom na hemijske aspekte atmosfere, vodenih sredina i zemljišta gradova. Urbana hemija je međusobno povezana sa urbanom ekologijom, toksikologijom i urbanom biologijom, a među biološkim disciplinama, ova grana hemije je posebno povezana sa urbanom botanikom. Urbana hemija se može posmatrati kao poseban pravac urbanih prirodnih nauka koji će značajno doprineti održivom razvoju gradova.

Ključne reči: hemija urbane životne sredine; urbane prirodne nauke; tlo; hemija vazduha urbane sredine; biljke; urbana botanika

Second International Conference on Electron Microscopy of Nanostructures - ELMINA2022

http://elmina.tmf.bg.ac.rs

Vuk V. Radmilović

Faculty of Technology and Metallurgy, University of Belgrade, Belgrade, Serbia

Abstract

The Second International Conference on Electron Microscopy of Nanostructures ELMINA2022 was organized by the Serbian Academy of Sciences and Arts (SASA) and the Faculty of Technology and metallurgy (FTM), University of Belgrade, Serbia and held at SASA in Belgrade, from 22 to 26 August 2022. The scope of ELMINA2022 was focused on electron microscopy methods applied to nanoscience and nanotechnology (physics, chemistry, physical metallurgy, materials science, earth, and life sciences). It highlighted recent progress in instrumentation, imaging and data analysis, large data set handling, as well as time and environment dependent processes. The scientific program contained the following topics:

- Instrumentation and New Methods
- Diffraction and Crystallography
- HRTEM and Electron Holography
- Analytical Microscopy
- In-situ Electron Microscopy
- Nanoscience and Nanotechnology
- Life Sciences

Keywords: nanoscience; nanotechnology; materials science;engineering;biology

Available on-line at the Journal web address: http://www.ache.org.rs/HI/

BOOK AND EVENT REVIEW

UDC: 005.745:77.026.34

Hem. Ind. **76(4)** 267-269 (2022)

The Second International Conference on Electron Microscopy of Nanostructures - ELMINA2022 was organized by the Serbian Academy of Sciences and Arts (SASA) and the Faculty of Technology and Metallurgy (FTM), University of Belgrade, Serbia, was held at SASA in Belgrade, from 22 to 26 August 2022. The conference was opened by Prof. Dr Velimir Radmilović, conference chair and SASA member, Prof. Dr Zoran Knežević, SASA General Secretary and Prof. Dr Robert Sinclair, Chair of the ELMINA2022 International Advisory Board. ELMINA2022 gathered over 120 participants coming from various fields related to application of electron microscopy in materials science and engineering, biology etc., out of which 92 were presenting authors. The program consisted of eight plenary, five oral and two poster sessions. Twenty-five plenary talks were given by some of the most renowned world experts in the field of theory and application of electron microscopy in characterization of nanostructures, including: **Jordi Arbiol** (Spain), **Gerhard Dehm** (Germany) **Rafal Dunin-Borkowski** (Germany), **Rolf Erni** (Switzerland), **Paulo Ferreira** (Portugal & USA), **Hamish Fraser** (USA), **Cecile Hebert** (Switzerland), **Colin Humphreys** (UK), **Thomas Kelly** (USA), **Angus Kirkland** (UK), Gerald Kothleitner (Austria), Vlado Lazarov (UK), Ivan Lazić (Netherlands), **Laurence Marks** (USA), **Joachim Mayer** (Germany), Peter Nellist (UK), **Eva Olsson (**Sweden), **Xiaoqing Pan** (USA), **Quentin Ramasse** (UK), Christina Scheu (Germany), **Robert Sinclair** (USA), **Erdmann Spiecker** (Germany), Sašo Šturm (Slovenia), and Eric Van Cappellen (USA).

Unfortunately, ELMINA2022 had a few last-minute cancellations due to COVID related issues, which is a sobering reminder that the pandemic is not behind us.

The audience could hear about the newest results in a broad range of topics, including: nanomedicine applications (*i.e.* optimizing nanoparticles for early cancer detection), energy conversion and storage (*i.e.* phenomena in Li-ion batteries and organic solar cells at the nanoscale) or just state of the art characterization methods such as *in situ*

Corresponding author: Vuk V. Radmilović, Faculty of Technology and Metallurgy, University of Belgrade
E-mail vukradmilovic@tmf.bg.ac.rs

investigation of strain induced changes in material properties or integrated Differential Phase Contrast (iDPC) STEM for beam sensitive materials.

Additionally, forty-one poster was presented. It is noteworthy that most posters were presented by PhD students as well as young researchers for whom the possibility to learn about the most recent microscopy techniques and novel nanomaterials as well as to present and discuss their research findings with the world leading scientists was indispensable.

Based on the quality of plenary talks and poster presentations as well as the fact that the conference was attended by many young researchers (more than 70), most of who were from Serbia, it was concluded that the ELMINA2022 conference was very successful. Due to the huge interest from young researchers as well as plenary speaker suggestions, it was decided that ELMINA should continue its biennial format, with ELMINA2024 planned September 9 - 13, 2024.

We would like to take this opportunity to thank first and foremost the Serbian Academy of Sciences and Arts, Faculty of Technology and Metallurgy of Belgrade University and its Innovation Center. Additionally, we would like to thank ThermoFisher Scientific as well as NanoMegas, JEOL/Scan, Analysis Ltd., Tescan Orsay/Mikrolux Ltd., Dectris, Institute for Testing Materials Serbia, European Microscopy Society, and the Federation of European Materials Societies, without whose support this conference would not have been possible.

ELMINA2022 Group Photo

Druga međunarodna konferencija o elektronskoj mikroskopiji nanostruktura ELMINA2022

http://elmina.tmf.bg.ac.rs

Vuk V. Radmilović

Tehnološko-metalurški fakultet, Univerzitet u Beogradu, Beograd, Srbija

Izvod

Druga međunarodna konferencija o elektronskoj mikroskopiji nanostruktura ELMINA2022 organizovana od strane Srpske akademije nauka i umetnosti (SANU) i Tehnološko-metalurškog fakulteta (TMF) Univerziteta u Beogradu, se održala u SANU od 22. do 26. Avgusta 2022. Fokus konferencije ELMINA2022 će biti na metodama elektronske mikroskopije primenjenim u nanonaukama i nanotehnologijama (fizika, hemija, nauka o materijalima, geologija i biomedicinske nauke). Konferencija je bila posvećena teorijskim osnovama i metodama elektronske mikroskopije koje se primenjuju u istraživanjima u oblastima nanonauka i nanotehnologija, u okviru većeg broja fakulteta i instituta koji se bave fundamentalnim i primenjenim istraživanjima.

Naučni program Konferencije je obuhvatao više oblasti, kao što su:

- Instrumentacija i nove metode
- Difrakcija i kristalografija
- Visokorezoluciona elektronska mikroskopija i elektronska holografija
- Analitičke metode
- In situ mikroskopija
- Nanonauke i nanotehnologije
- Bio-medicinske nauke (konvencionalna i krio-elektronska mikroskopija)

Ključne reči: naonauke; nanotehno-logija; nauka o metarijalima; inženjer-stvo, biologija